2021-12

Improved Bitumen Recovery Using Urea Solutions

BinDahbag, Mabkhot

UNIVERSITY OF CALGARY

Improved Bitumen Recovery Using Urea Solutions

by

Mabkhot Salama BinDahbag

A THESIS

SUBMITTED TO THE FACULTY OF GRADUATE STUDIES

IN PARTIAL FULFILMENT OF THE REQUIREMENTS FOR THE

DEGREE OF DOCTOR OF PHILOSOPHY

GRADUATE PROGRAM IN CHEMICAL AND PETROLEUM ENGINEERING

CALGARY, ALBERTA

DECEMBER, 2021

Abstract

This work presents experimental and simulation studies to design and optimize urea solutions to improve bitumen recovery. Initially, the solubility of ammonia in Athabasca bitumen was measured at vapor-liquid equilibrium (VLE) condition at different temperatures and pressures ranging from 348 to 463 K (75 to 190 ℃) and 1 to 4 MPa, respectively. The liquid phase density of ammonia-saturated bitumen was measured. The experimental solubility and density data were modeled using the Peng-Robinson equation of state (PR-EoS) by tuning the binary interaction coefficient and volume shift parameters of ammonia, respectively. The modeling results revealed that PR-EoS gives an acceptable prediction of ammonia solubility in bitumen and density of ammonia saturated-bitumen.

Additionally, 1-D sand pack flooding experiments were conducted to recover heated bitumen at 423 K and 3.447 MPa pore pressure by injecting two different concentrations of urea solutions (5 and 10 wt %) at 1 cm^3/min injection rate. Another flooding experiment was conducted by flooding sand pack with fresh water at the same flooding condition to be used as a baseline of urea solution flooding experiments. Supplementary experiments such as interfacial tension (IFT) measurements, emulsion viscosity measurements, total acid number (TAN) measurements, and Fourier-transform infrared (FTIR) measurements were conducted to prove the generation of in situ surfactants through the flooding process. The results of these flooding experiments (at 423 K) showed that flooding with urea solutions improves the oil recovery efficiency, highlighting the synergy between the reduction in viscosity of bitumen and the generation of in situ surfactants. Besides the reduction in viscosity of bitumen resulting from the heat, the generated in situ surfactants emulsify the oleic phase leading to the generation of W/O emulsion at the displacement front. This

emulsion makes the displacement front more stable due to the attenuation of the viscous fingering. The supplementary experiments confirmed the generation of in situ surfactants, as evidenced by the reduction in the interfacial tension and total acid number measurements and confirmed the results with FTIR analysis.

Along with flooding experiments, a fine grid numerical simulation was conducted to model the experimental oil recovery data to obtain relative permeability curves through history matching technique. The history matching results revealed the efficiency of urea solutions to change the rock wettability toward more water-wet and suppress viscous fingering phenomenon.

After confirming the mechanism of urea solutions in recovering bitumen, several 1-D sand pack flooding experiments were conducted by injecting hot urea solutions into cold sand packs at room temperature to optimize the injection rate, injection temperature, and urea solution concentration. Three injection rates (4, 8, and 12 cm^3/min), four injection temperatures (453, 473, 493, and 513 K), and three urea solution concentrations (5, 10, and 15 wt %) were investigated in these flooding experiments. The flooding experiments of cold sand packs revealed an optimum flow rate that leads to more efficient displacement of oil by urea solutions. The optimum flow rate is attributed to the balance between the retention time and heat delivered to the oil sands through the flooding process. The results show higher oil recovery at higher concentrations of urea. Furthermore, the results reveal that while higher injection temperature accelerates the oil recovery initially, it reduces the ultimate oil recovery.

Acknowledgments

I would like to gratefully acknowledge my supervisor, Dr. Hassan Hassanzadeh, for his unlimited support, supervision, and patience in completing my thesis. I genuinely owe him his time and supervision throughout my academic life.

I also wish to express my acknowledgment to Dr. Mingzhe Dong, Dr. Hemanta Sarma, Dr. Ke Du and the external commitee member Dr. Andy Li from University of Alberta for taking the time and accepting to be members of my defense committee, as well as for their valuable comments on my work.

My sincere gratitude extends to my parents and my wife, who supported me and encouraged me to pursue my Ph.D. study at The University of Calgary.

I wish to express my thanks to Dr. Mohsen Zirrahi, who has assisted and encouraged me while building the experimental setup for my experiments.

I very much appreciate the financial support by the Natural Sciences and Engineering Research Council of Canada (NSERC) and all member companies of the SHARP Research consortium at the University of Calgary: Cenovus Energy, Canadian Natural Resources Limited (CNRL), ConocoPhillips, CNOOC International, Devon Canada, Husky Energy, Imperial Oil Limited, Kuwait Oil Company, Osum Oil Sands, Strathcona Resources, and Suncor Energy. Also, the support of the Department of Chemical and Petroleum Engineering and the Schulich School of Engineering at the University of Calgary is appreciated. I also gratefully acknowledge Hadhramout University (HU) and Hadhramout Establishment for Human Development (HEHD) for their technical and financial supports.

My deepest and sincere gratitude also goes to all my fellow graduate students in the SHARP research group at The University of Calgary for their technical support and advice through my academic journey.

Last but not least, I would like to extend my sincere gratitude to my parents, Salama and Shaikha, my wife Mariam, my kids Abdullah, Abdulrahman, AlAnoud, Nujood, and my siblings for their unlimited support and encouragement in this journey.

"To my parents,

Salama and Shikhah,

My wife, Mariam,

my kids, Abdullah, Abdulrahman, AlAanoud, Nujood,

and my siblings"

Table of Contents

List of tables

List of Figures

Nomenclature

ASP	Alkaline-surfactant-polymer flooding
API	American petroleum institute
ASTM	American society for testing and materials
WI_o	Amott wettability index for oil phase
WI_w	Amott wettability index for water phase
AARD	Average absolute relative deviation
ρ_{avg}	Average density
k_{ij}	Binary interaction coefficient
T_b	Boiling point temperature
ω	Centric factor
CAS	Chemical abstracts society
u_c	Combined uncertainty
θ	Contact angle
CSF	Conventional steam flooding
V_{corr}^{L}	Corrected liquid molar volume
V_{corr}^{v}	Corrected vapor molar volume
P_c	Critical pressure

T_c	Critical temperature
S_{wcrit}	Critical water saturation
CSS	Cyclic steam stimulation
ρ_i	Density of component i at reference temperature
DME	Dimethyl ether
k_{eff}	Effective permeability
U	Expanded uncertainty
ES-SAGD	Expanding solvent steam-assisted gravity drainage
Y_i	Experimental value
FTIR	Fourier-transform infrared spectroscopy
GHME	Global history matching error
S_{oi}	Initial oil saturation
IFT	Interfacial tension
IUPAC	International Union of Pure and Applied Chemistry
S_{oirw}	Irreducible oil saturation
S_{wirr}	Irreducible water saturation
JBN	Johnson, Bossler, and Neumann method
S_0 and S_1	Linear temperature-dependent volume shift parameters

MMRE	Mean magnitude of relative error
$\overline{Y}$	Mean of the experimental values
λ	Mobility
$\lambda_{displaced}$	Mobility of displaced fluid
$\lambda_{displacing}$	Mobility of displacing fluid
M	Mobility ratio
V	Molar volume
x_i	Mole fraction of component i
MW	Molecular weight
NSER	Nash-Sutcliffe efficiency ratio
O/W	Oil in water emulsion
O/W/O	Oil in water in oil emulsion
n_o	Oil phase Corey's exponent
k_{ro}^0	Oil relative permeability endpoint
σ_{os}	Oil/solid interfacial tension
σ_{ow}	Oil/water interfacial tension
OOIP	Original-oil-in-place

PR-EoS	Peng-Robinson equation of state
PAP	Percentage of accuracy-precision
PV	Pore volume
PVI	Pore volume injected
P	Pressure
T_r	Reduced temperature
T_{ref}	Reference temperature
U_r	Relative expanded uncertainty
U_r	Relative expanded uncertainty
S_{orw}	Residual oil saturation
f_i	Simulated value
SG	Specific gravity
u	Standard uncertainty
u_{random}	Standard uncertainty of random error
u_{sys}	Standard uncertainty of systematic error
SAGD	Steam-assisted gravity drainage
SP	Surfactant-polymer flooding

T	Temperature
S_{1i}	Temperature dependent term for component i
TAN	Total acid number
V^{L}	Uncorrected liquid molar volume calculated by equation of state
V^{v}	Uncorrected vapor molar volume calculated by equation of state
USBM	United States Bureau of Mines
R	Universal gas constant
UASF	Urea-assisted-steam flooding
UFASF	Urea-foam-assisted-steam flooding
I_w	USBM wettability index
S_{0i}	Usual Peneloux parameter of component i
VLE	Vapor-liquid equilibrium
μ	Viscosity
$V_{O_{imbibition}}$	Volume of oil displaced by brine imbibition
$V_{O_{centrifuge}}$	Volume of oil displaced by centrifuging with brine
$V_{W_{centrifuge}}$	Volume of water displaced by centrifuging with oil
$V_{W_{imbibition}}$	Volume of water displaced by oil imbibition

S_i	Volume shift parameter of component i
W/O	Water in oil emulsion
W/O/W	Water in oil in water emulsion
n_w	Water phase Corey's exponent
k_{rw}^0	Water relative permeability endpoint
S_w	Water saturation
σ_{ws}	Water/solid interfacial tension

CHAPTER 1: INTRODUCTION AND PROBLEM STATEMENT

1.1 Introduction

Canada has the third-largest oil reserves worldwide, with more than 166 billion barrels of extra-heavy crude oil (bitumen) found in Alberta's oil sands [1]. The massive quantities of Canadian bitumen are located in Athabasca, Cold Lake, and Peace River of the province of Alberta as shown in Figure 1.1 [2]. Usually, the typical oil sands found in these places consist of 10 and 5% (mass percent) of bitumen and water, respectively, dispersed in 85% of unconsolidated loose sands, as shown in Figure 1.2. However, bitumen and water contents in the oil sands could reach 20 and 9%, respectively [3]. Albertan oil sands are water-wet due to surrounding the sand grains with a thin film of water, making it easy to detach bitumen from sand using hot aqueous phases [4]. Bitumen has an API gravity less than 10 °API and is found in shallow and cold reservoirs. Unlike conventional crude oil, bitumen does not flow freely at reservoir temperature, which is no more than 285 K (12 ℃) in most cases due to high viscosity exceeding million centipoises.

Figure 1.1. Oil sand formation distribution in Alberta province [2].

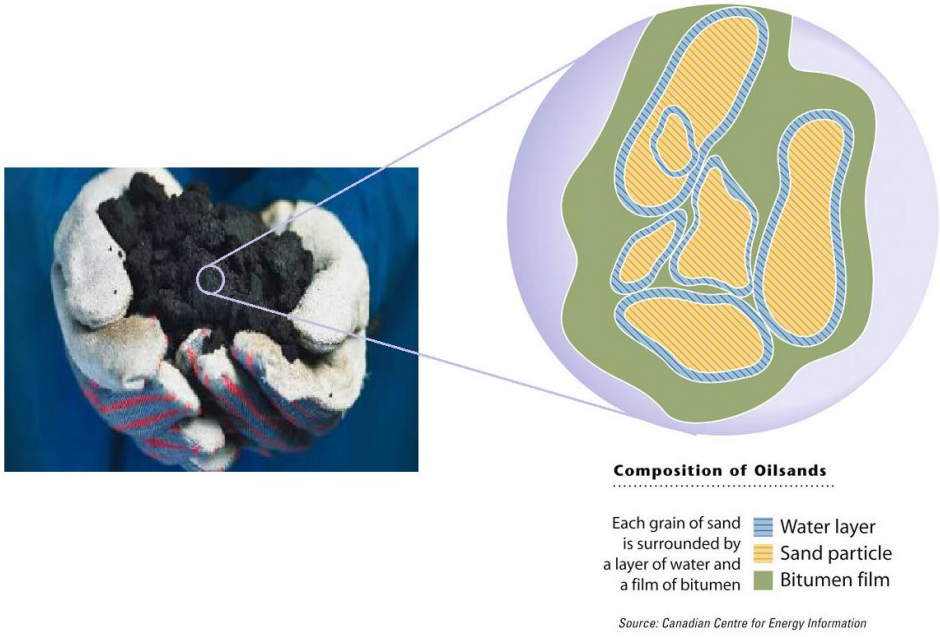

Figure 1.2. A schematic diagram shows the Albertan oil sand composition [4].

1.2 Bitumen recovery processes

There are two main methods to recover bitumen from tar sands based on reservoir depth, including surface mining and in situ recovery. Around 20% of the total recoverable bitumen is located on very shallow reservoirs (in the Athabasca region and the north of Fort McMurray) with less than 75 m depth, making it easy to produce this bitumen via the mining process [3]. The surface mining process starts by loading the oil sands in huge trucks and transferring it to crushers to prepare it for extraction. Then, the crushed oil sands are washed with hot water and sent to the extraction plant. After that, bitumen is separated from oil sand during hydro-transport and in the separation vessels. Finally, the tailing is sent into the settling basin, where water is separated and recycled again. Figure 1.3 shows steps to extract bitumen via the surface mining process[5].

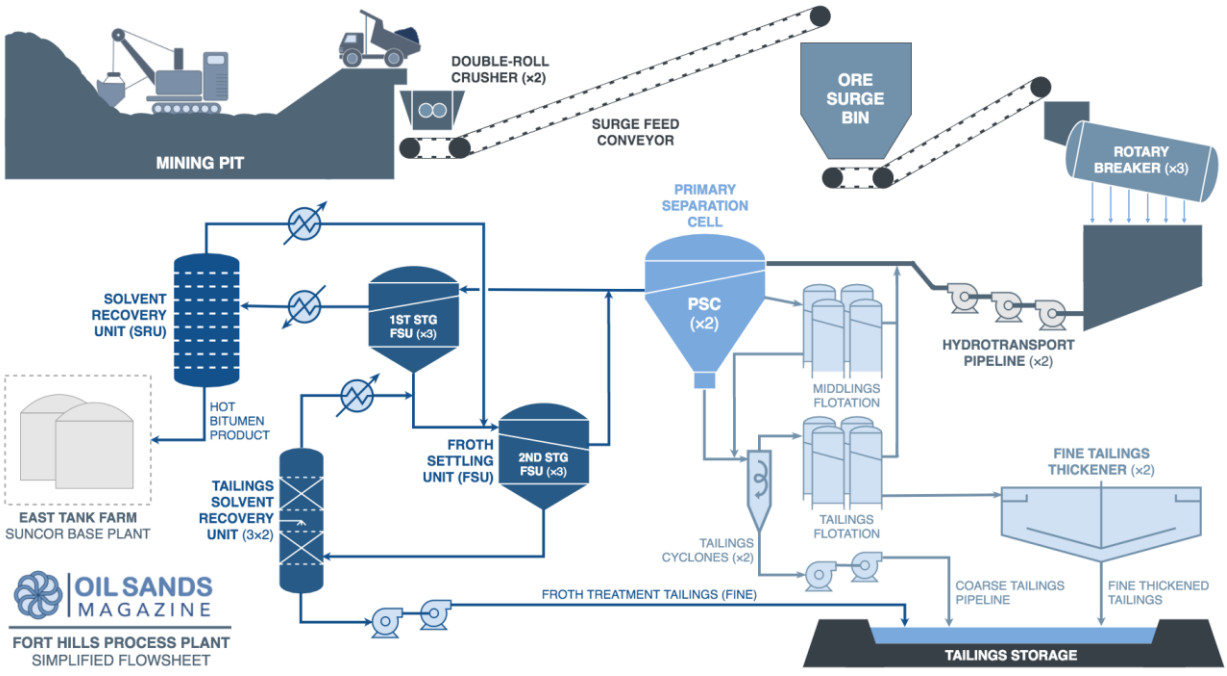

Figure 1.3. A schematic diagram shows the steps to extract bitumen via surface mining [5].

The viscosity of bitumen in deep reservoirs that are not mineable should be reduced sufficiently by heating or diluting using solvents via in situ recovery techniques [6]. At present, Steam-Assisted Gravity Drainage (SAGD) and Cyclic Steam Stimulation (CSS) processes are the main in-situ techniques used to recover bitumen from non-mineable reservoirs. The theoretical foundation and concept of the SAGD process were introduced in the late 1960s by Dr. Roger Butler (1927-2005), a prominent Imperial Oil scientist and the University of Calgary Professor [7]. Two horizontal wells are drilled in parallel inside the oil sands reservoir in this process, with one well few meters above the other. High-pressure steam is injected continuously from the upper injection well into the cold reservoir. The high latent heat of vaporization of steam is transferred into cold bitumen. It reduces the viscosity of bitumen significantly, making it easy to mobilize toward the lower production well via the gravity effect. Accumulated liquids are pumped from the production well to be sent to the surface, as shown in Figure 1.4 [8]. In cyclic steam stimulation, high-pressure steam is injected into the reservoir for some time to reduce the viscosity of the bitumen. Then, the injection well is shut-in for weeks to allow steam to distribute uniformly in the reservoir through the soaking period. Finally, the same well is returned to production to produce mobile liquids. This cycle is repeated several times until oil production becomes uneconomical. Figure 1.5 shows the stages of cyclic steam stimulation.

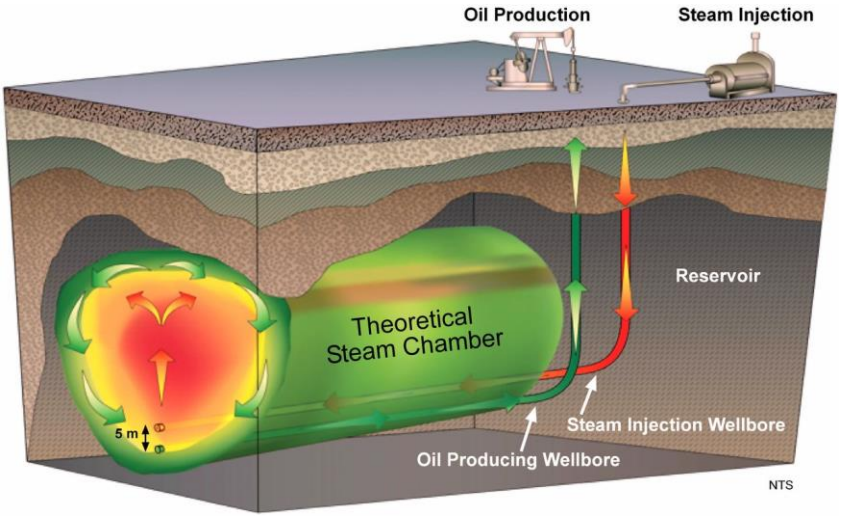

Figure 1.4. A schematic diagram shows the steam-assisted gravity drainage (SAGD) process [9].

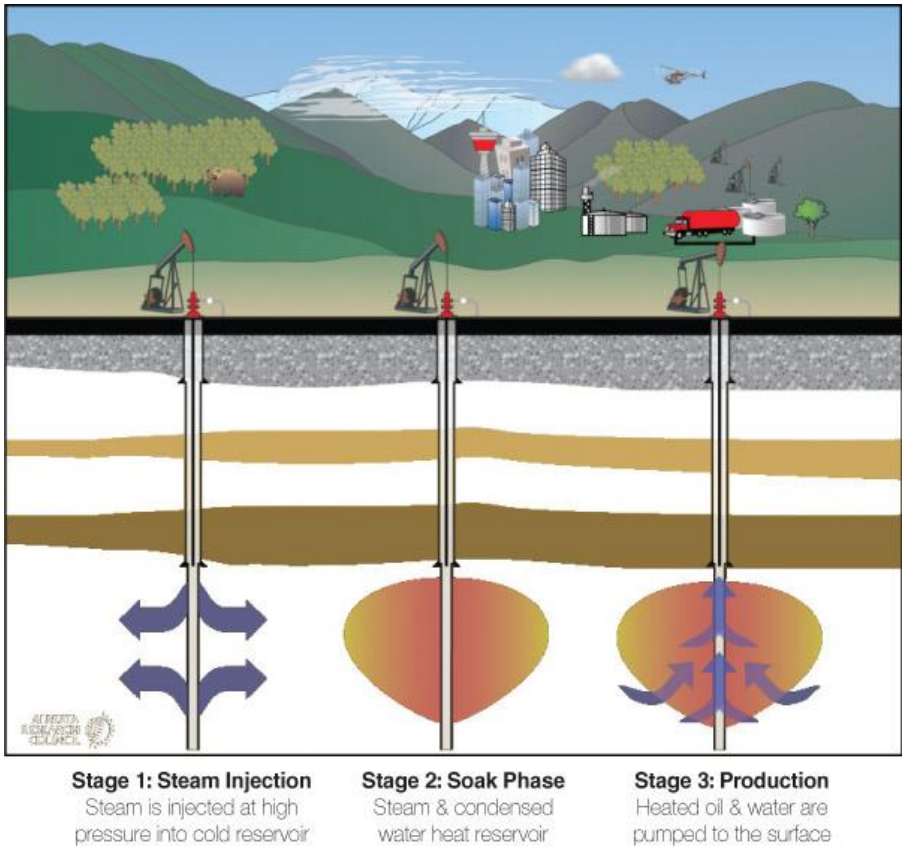

Figure 1.5. A schematic diagram shows cyclic steam stimulation (CSS) steps [10].

Both conventional in situ recovery techniques (SAGD and CSS) are associated with several disadvantages: the high cost of steam generation, carbon dioxide emission, and the treatment of large volumes of water. The addition of hydrocarbon solvents such as propane and butane have been suggested to improve the conventional in situ recovery techniques [11]. The use of solvents to improve SAGD resulted in recovery techniques called the expanding solvent steam-assisted gravity drainage (ES-SAGD) processes. The lack of resources for hydrocarbon solvents is the main drawback associated with hydrocarbon solvents. This study aims to investigate the efficiency of abundant aqueous solvents such as urea solutions to improve bitumen recovery.

1.3 An overview about ammonia and urea solvents

Ammonia is a chemical compound that consists of one atom of nitrogen bonded with three hydrogen atoms, and it takes the "NH_3" formula. It is found in a gaseous phase at ambient conditions. Ammonia was produced for the first time in the lab by Fritz Haber in 1905. Then, the process was modified for commercial production by Carl Bosch in 1910 [12]. Around 280 million tons of ammonia was produced in 2018 [13]. Stoichiometrically, one mole of nitrogen reacts with three moles of hydrogen in the presence of an iron catalyst to produce two moles of ammonia in an exothermic process as shown below:

$$N_2 + 3H_2 \underset{Iron-Catalyst}{\overset{\Delta H^o = -91.8 kJ/mol}{\rightleftharpoons}} 2NH_3 \qquad \textbf{1.1}$$

The large-scale process for the production of ammonia is started by injecting natural gas (methane), water, and air into the first stage reactor at high temperatures 973-1373 K (700-1100 ℃) to produce nitrogen (N_2), hydrogen (H_2), and carbon monoxide (CO). Then, the produced gases are passed through the second stage reactor that contains a superheated catalyst 773 K (500 ℃) to produce the synthesis mixture. This mixture is compressed into

a scrubber containing water to remove unfavourable CO_2. Then, the released nitrogen and hydrogen gases are compressed at high temperature and pressure (723 K and 30 MPa, respectively) into the mean reactor that starts converting them to ammonia in the presence of the iron catalyst. The primary function of the catalyst in the main reactor is to reduce the activation energy required to start the reaction while the high temperature and pressure accelerate the reaction process. Each cycle of this process only converts 10-18% of the potential ammonia. Therefore, the produced stream is recycled several times before leaving the system at 97% ammonia concentration [14]. Figure 1.6 shows steps followed to produce ammonia in the industry.

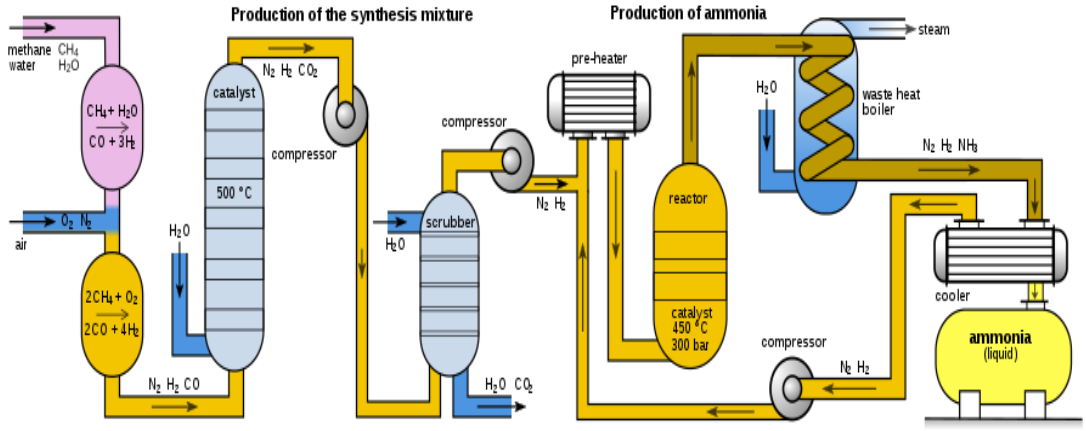

Figure 1.6. A schematic diagram shows steps followed to produce ammonia in the industry [15].

Around 80% of produced ammonia is converted into urea to produce fertilizers. Several methods were developed to convert ammonia economically into urea via two main equilibrium reactions [16]. In the first reaction, ammonium carbamate (NH_2COONH_4) is

generated by reacting gaseous carbon dioxide with liquid ammonia at high temperature and pressure in an exothermic reaction as the following:

$$2NH_{3(L)} + CO_{2(G)} \underset{11Mpa,433K}{\overset{\Delta H^{o}=-37.4KCal/mol}{\rightleftharpoons}} NH_2COONH_{4(L)} \qquad \textbf{1.2}$$

The generated ammonium carbamate is decomposed endothermically into urea and water as the following:

$$NH_2COONH_{4(L)} \underset{433K}{\overset{\Delta H^{o}=6.3KCal/mol}{\rightleftharpoons}} NH_2CONH_{2(L)} + H_2O_{(L)} \qquad \textbf{1.3}$$

The conversion of ammonia into urea is an incomplete process; so, the generated urea is separated from unchanged ammonium carbamate. Two concepts are followed through separating urea from unchanged ammonium carbamate: 1) total recycle concept, and 2) stripping concept. The total recycle concept is an old process that was introduced in the 1920s. In this concept, the overall system pressure is let down to the atmospheric pressure to force ammonium carbamate to decompose back into ammonia and CO_2. The total recycle concept has several drawbacks, such as the complexity of the flow scheme, high cost to recompress ammonia and CO_2 generated and the enormous amount of water recycled in the ammonium carbamate solution. Therefore, the stripping concept was introduced in the 1960s by Stamicarbon Company, Netherlands, to overcome challenges associated with the total recycling concept. The equilibrium condition between the formation and decomposition of ammonium carbamate depends on the product of partial pressures of ammonia and CO_2. The reduction of overall system pressure reduces the partial pressure of both ammonia and carbon dioxide, which makes it costly to recompress and recycle them again. In order to decompose unreacted ammonium carbamate without reducing the overall system pressure, the partial pressure of ammonia is suppressed via

injecting CO_2 into the stripper under the full system pressure instead of injecting it directly to the reactor. This process reduces the partial pressure of ammonia and leads to a flush out of the free ammonia and transfer it directly to a high-pressure carbamate condenser. The reconstituted ammonium carbamate solution is injected back to the main reactor. This step eliminates the cost of repressuring the generated ammonia and carbon dioxide. Figure 1.7 shows the schematic diagram for the urea conversion process.

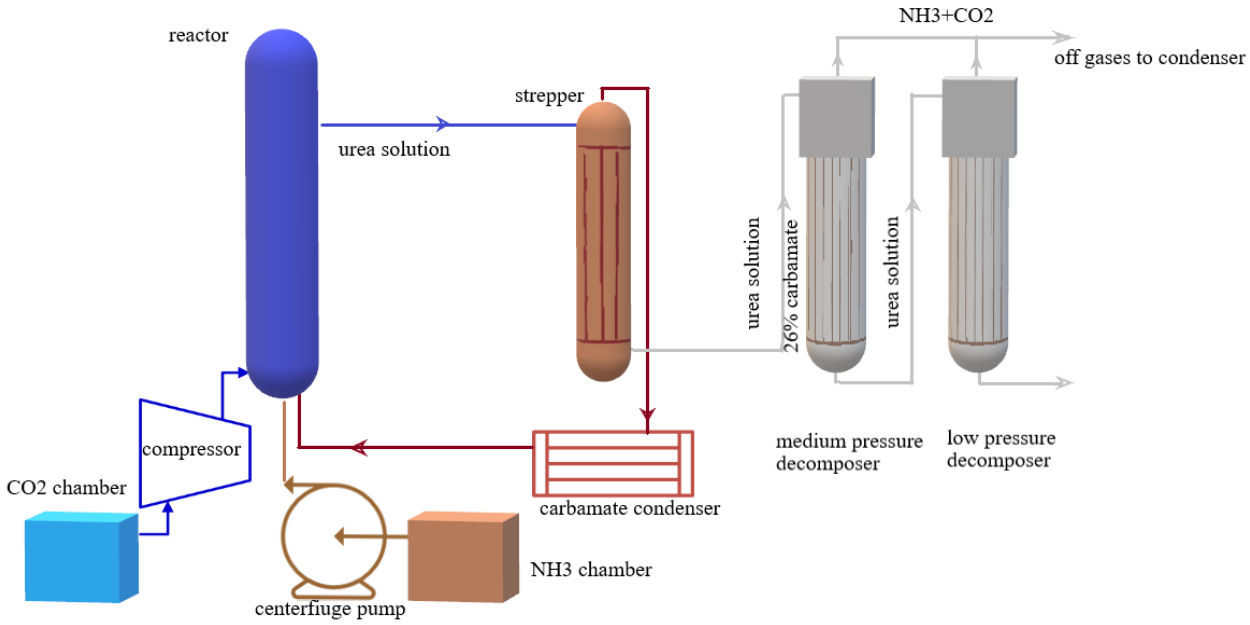

Figure 1.7. A schematic diagram of the urea conversion process from Stamicarbon, Netherlands [16].

1.4 Research problems and objectives of the current study

It is indisputable that steam has a massive latent heat enabling it to transfer a large amount of thermal energy into the reservoir through SAGD and CSS processes. However, steam is associated with several issues such as steam generation cost, significant CO_2 emission through the burning of natural gas, high cost of construction and maintenance of steam

boilers, water treatment before recycling, significant heat loss, and inapplicability in thin reservoirs. Meanwhile, the oil industry (production, transportation, and refining) is responsible for 15 to 40% of "well-to-wheels" life-cycle greenhouse gas emissions around the world [17]. The industry has implemented co-injection of gaseous and light liquid hydrocarbons with steam to improve oil recovery and decrease the amount of steam injected into the reservoir [18, 19]. The lack of hydrocarbon solvents sources and the high cost of these solvents are the main drawbacks associated with the existing in situ recovery techniques.

By using solvents, the industry aims to contribute to the Canadian government's effort in reducing the Canada's greenhouse gas emissions. The objective of this research is to investigate urea as a cost-effective additive to improve bitumen recovery. Urea, $CO(NH_2)_2$, is a synthetic component produced commercially by combining CO_2 with two amino groups to produce more than 200 million tons per year worldwide [16, 20]. It is characterized by a low cost ($300/ton), nontoxicity, and high solubility in water [21]. In the hot urea solution flooding process, latent heat for steam generation is unnecessary, and sensible heat is only used to transfer thermal energy to the reservoir during bitumen viscosity reduction. Eliminating the latent heat saves more fuel from burning and reduces greenhouse gas emissions by 42% compared to steam flooding. Moreover, eliminating steam generation saves 70.6 $M/year as a steam generator maintenance cost and $0.15/bbl as a water treatment cost before steaming [22, 23]. The high basicity of amino groups found in bitumen at reservoir conditions is responsible for the reaction of urea with naphthenic acids to generate in situ surfactants. These surfactants are capable of detaching oil efficiently and changing rock wettability toward more water-wet [24]. Furthermore, the

generated in situ surfactants form a water in oil (W/O) emulsion at the displacement front, improving the sweep efficiency of liquid urea solutions and mobility control [25]. Moreover, most Alberta's heavy oil reserves are found in thin reservoirs (less than 6 m in thickness), making 80% of the reserve not accessible with current recovery techniques [26]. Urea solution flooding utilizes the sensible heat only by reducing the viscosity of bitumen which in turn reduces the massive heat loss coming from latent heat into overburden strata and may provide a more efficient alternative to access oil sands resources in thin reservoirs that are not accessible by existing in situ recovery techniques. Furthermore, flooding with urea solution improves the quality of produced bitumen via reducing the total acid number (TAN), making it preferable for refineries. This reduction in TAN increases the price of bitumen in the oil market.

1.5 Organization of the thesis

This thesis is written in a paper-based format. Chapter 1 of this thesis is devoted to the introduction and problem statement of this study. This chapter summarizes the current bitumen recovery and the main challenges and presents a general overview of the proposed solvents that will be investigated to overcome some of these challenges. In Chapter 2, some basic concepts and definitions and previous studies are reviewed. Chapter 2 also includes the review of emulsion generation mechanism and factors that affect the emulsification process. At the end of Chapter 2, the literature on the use of ammonia and urea solutions in oil recovery processes is summarized.

In Chapter 3, the solubility and liquid density of ammonia/Athabasca bitumen mixtures were measured at wide ranges of pressures and temperatures covering SAGD process condition. The volume shift parameters of ammonia were tuned to model the experimental

density data of ammonia saturated bitumen using Peng-Robinson equation of state (PR-EoS). The binary interaction coefficient between ammonia and bitumen was also tuned to predict the solubility of ammonia in Athabasca bitumen. This data was used in Chapter 5 to build the fluid model for simulation purpose. This data was published in the Journal of Chemical and Engineering Data [27].

Chapter 4 includes hot sand pack flooding experiments conducted at high temperature 423 K (150 °C), to study the impact of urea solutions on bitumen recovery. Complementary experiments such as interfacial tension (IFT), viscosity of water in oil (W/O) emulsions, total acid number (TAN), and Fourier-transform infrared (FTIR) spectroscopy were employed to prove the generation of in situ surfactants as a result of urea solutions reaction with the naphthenic acids found in bitumen. This work has been published in ACS Omega [28].

Chapter 5 describes a fine grid numerical simulation for hot sand pack flooding experiments reported in Chapter 3. The relative permeability curves of oil and water have been obtained by history matching of the experimental oil recovery data. The simulation results have been published in the Fuel journal [29].

The viability of hot urea solutions in displacing bitumen from cold sand packs is reported in Chapter 6. The effects of injection rate, injection temperature, and urea solution concentration on oil recovery efficiency were investigated to obtain the optimum scenario. This work has been published in Journal of Industrial and Engineering Chemistry [30].

Chapter 7 presents the conclusion of this work along with some recommendations for future work in this area.

1.6 References

[1] Canada Go. Oil resources; 2019. Available from: https://www.nrcan.gc.ca/energy/energy-sources-distribution/crude-oil/oil-resources/18085. [Accessed July 22 2021].

[2] The Location of oil sands; 2019. Available from: http://history.alberta.ca/energyheritage/sands. [Accessed July 1, 2021].

[3] Oil sands geology and the properties of bitumen; 2020. Available from: https://www.oilsandsmagazine.com/technical/properties. [Accessed July 1, 2021].

[4] Spector D. What are the oil sands and why are they so valuable?; 2012. Available from: https://www.businessinsider.com/what-are-oil-sands-2012-4. [Accessed July 1, 2021].

[5] Fort Hills mine; 2018. Available from: https://www.oilsandsmagazine.com/projects/suncor-fort-hills-mine. [Accessed July 1, 2021]

[6] Speight J. Enhanced recovery methods for heavy oil and tar sands. Elsevier; 2013.

[7] Roger Butler and In Situ Development; 2019. Available from: http://www.history.alberta.ca/energyheritage/sands/underground-developments/in-situ-development/roger-butler.aspx. [Accessed July 7, 2021].

[8] Canada: Oil sands project; 2014. Available from: https://www.japex.co.jp/en/business/oilgas/hangingstone/. [Accessed Jul 1, 2021].

[9] Peacock M. Athabasca oil sands: Reservoir characterization and its impact on thermal and mining opportunities. *Geological Society, London, Petroleum Geology Conference series.* 7. Geological Society of London; 2010:1141-1150.

[10] Alvarez J, Coates R. Heavy oil recovery; cyclical solvent injection (CSI). Rogtec oil & gas news. 2009.

[11] Nasr T, Beaulieu G, Golbeck H, Heck G. Novel expanding solvent-SAGD process ES-SAGD. Journal of Canadian Petroleum Technology; 2003;42(01):13-16.

[12] Stoltzenberg D. Fritz Haber: Chemist, nobel laureate, German, jew. Chemical Heritage Foundation; 2004.

[13] Production capacity of ammonia worldwide in 2018 and 2030; 2019. Available from: https://www.statista.com/statistics/1065865/ammonia-production-capacity-globally/. [Accessed July 1, 2021].

[14] Alkusayer K. Ammonia synthesis for fertilizer production. 2015.

[15] Williams F. Flow diagram for the production of Ammonia; 2010. Available from: https://commons.wikimedia.org/wiki/File:Haber-Bosch-En.svg. [Accessed July 7, 2021].

[16] Kumar B, Das P. Manufacture of urea. 2007.

[17] Masnadi M, El-Houjeiri H, Schunack D, Li Y, Englander J, Badahdah A, et al. Global carbon intensity of crude oil production. Science 2018;361(6405):851-853.

[18] Orr B. ES-SAGD; past, present and future. *SPE Annual Technical Conference and Exhibition.* Society of Petroleum Engineers; 2009.

[19] Nasr T, Beaulieu G, Golbeck H, Heck G. Novel expanding solvent-SAGD process "ES-SAGD". *Canadian International Petroleum Conference.* Petroleum Society of Canada; 2002.

[20] Garside M. Global production capacity of carbamide 2018-2030; 2020.

[21] IndexMundi. Urea monthly price - US dollars per metric ton; 2019. Available from: https://www.indexmundi.com/commodities/?commodity=urea. [Accessed December 16 2019].

[22] Nduagu E, Sow A, Umeozor E, Millington D. Economic potentials and efficiencies of oil sands operations: processes and technologies. Canadian Energy Research Institute; 2017.

[23] Farouq Ali S, Jones J, Meldau R. Practical heavy oil recovery. University of Alberta, Alberta 1997.

[24] Guo E, Jiang Y, Gao Y, Shen D, Zhigang C, Yu P. A new approach to improve recovery efficiency of SAGD. *SPE Middle East Oil & Gas Show and Conference.* Society of Petroleum Engineers; 2017.

[25] Pei H, Zhang G, Ge J, Ma M, Zhang L, Liu Y. Improvement of sweep efficiency by alkaline flooding for heavy oil reservoirs. Journal of Dispersion Science and Technology 2013;34(11):1548-1556.

[26] Adams D. Experiences with waterflooding Lloydminster heavy-oil reservoirs. Journal of Petroleum Technology 1982;34(08):1,643-1,650.

[27] BinDahbag M, Zirrahi M, Hassanzadeh H. Solubility and liquid density of ammonia/Athabasca bitumen mixtures at temperatures up to 463 K: Measurements and modeling. Journal of Chemical & Engineering Data 2019;64(8):3592-3597.

[28] BinDahbag M, Mohammadi M, Khalifi M, Aghajamali M, Zirrahi M, Hassanzadeh H. Efficiency of urea solutions in enhanced oil recovery. ACS Omega 2020;5(11):6122-6129.

[29] BinDahbag M, Al-Gawfi A, Hassanzadeh H. Suitability of hot urea solutions for wettability alteration of bitumen reservoirs–Simulation of laboratory flooding experiments. Fuel 2020;272:117713.

[30] BinDahbag M, Zirrahi M, Hassanzadeh H. Injection of hot urea solutions as a novel process for heavy oil recovery—A proof-of-concept experimental study. Journal of Industrial and Engineering Chemistry 2021;95:244-251.

CHAPTER 2: CONCEPTS AND LITERATURE REVIEW

This chapter presents some fundamentals about the solubilities of ammonia and urea in water and hydrocarbons. It includes the concepts and methods used to measure the rock wettability alteration during the flooding process. Fundamental information about emulsion types as well as factors affecting the emulsification process are included in this chapter. Finally, a review of up-to-date literature on the oil recovery via ammonia and urea solutions is reported in this chapter.

2.1 The solubility of ammonia in water and hydrocarbons

The solubility of hydrocarbon solvents in bitumen has been reported in many previous studies [1-5]. Ammonia has a high solubility in water leading to a significant increase in the vapor pressure of the produced ammonium hydroxide (NH_4OH) [6]. The solubility of ammonia in water increases by increasing pressure, while it decreases considerably once the temperature increases. The high solubility of ammonia in water is attributed to the high polarity of ammonia molecules resulting from the difference in electronegativity between hydrogen and nitrogen atoms in the ammonia molecule. This polarity generates hydrogen bonds allowing ammonia molecules to dissolve significantly in water, a polar molecule [7]. Besides, ammonia molecules react with water and dissociate into ammonium (NH_4^+) and hydroxide (OH^-) ions, which are highly soluble in water [8].

$$NH_3(g) + H_2O(l) \rightleftharpoons NH_4^+(aq) + OH^-(aq) \qquad \textbf{2.1}$$

Several research groups studied the solubility of ammonia in pure hydrocarbons. For instance, Ishida [9] measured the solubility of liquid ammonia in several classes of hydrocarbons (paraffines, naphthenes, and olefins) at different temperatures. Results

indicated that the solubility of liquid ammonia in naphthenes is higher than its solubility in paraffines for the same number of carbon atoms at the same temperature. Also, the solubility of liquid ammonia is inversely proportional to the molecular weight of hydrocarbons. In the ammonia-aliphatic mixture, it was found that the logarithm of solubility of liquid ammonia in the aliphatic compound is proportional to the vapor pressures of these aliphatic compounds at the same temperature. In contrast, the solubility of liquid ammonia in paraffines is much smaller than its solubility in olefins.

Tremper and Prausnitz [10] measured the solubility of ammonia in n-hexadecane, bi-cyclohexyl, and 1-methyl naphthalene at low pressure and a wide range of temperatures ranging from 298 to 473 K (25 to 200 ℃). They found that the solubility of ammonia decreases with increasing temperature. At high temperatures, ammonia molecules acquire high kinetic energy that prevents the molecules from condensation into the liquid phase [10]. Additionally, ammonia has a higher solubility in aromatic solvents than aliphatic solvents [11].

Recent studies indicated that urea is decomposed gradually into ammonia and carbon dioxide (CO_2), where around 85 mass percent of urea is converted into ammonia and CO_2 once it exposes to SAGD condition (~220 ℃) [12-14]. Therefore, ammonia solubility in bitumen is important from a phase behavior standpoint. The solubility of ammonia in raw crude oil or even a mixture of hydrocarbons has not been measured in previous studies. In this study, the solubility of ammonia in Athabasca bitumen was measured.

2.2 The solubility of urea in water and hydrocarbons

The solubility of urea in water increases dramatically as a function of temperature to exceed 300 gm/100 gm water at 343 K (70 ℃) [15, 16]. The high solubility is attributed to the

polarity of water and urea molecules. A molecular dynamic simulation showed that the urea crystals follow three stages to dissolve in water [17]. Firstly, weakly bonded molecules located at the sharp edges of crystals leave the crystals early. Then, the targeted crystal takes the form of a solution annealed shape, and it keeps this shape for most of the dissolution process, and it dissolves a fixed number of urea molecules to water per unit time (it follows the fixed rate law). At the end of dissolution process, it departs the fixed rate law, and the crystal completely goes away into the solution by the end of the third stage.

Unlike ammonia, urea is insoluble in most of the aliphatic (i.e., heptane) and aromatic (i.e., benzene) hydrocarbons due to the non-polarity nature of these molecules [18]. However, urea showed some solubility in alcohols (methanol, ethanol, and isopropanol), and urea solubility was found to be decreased by increasing the length of the alcohol molecule [19].

2.3 Rock wettability alteration via ammonia and urea solutions

Wettability is defined as the tendency of one fluid (wetting fluid) to spread on the surface of solid material in the presence of another immiscible fluid (non-wetting fluid) [20]. There are four types of wettability that have been recognized for water-oil-rock systems: water-wet system, oil-wet system, fractional-wet system, and mixed-wet system [21]. More than 50% of the rock surface prefers to wet with water in the water-wet system. The water in this system fills the small pores and makes a thin film on the surface of large pores. Generally, the water forms the continuous phase in this system since it fills the small pores and exists on the surface of the large pores. In contrast, oil globules spread through large pores as a non-continuous phase.

On the contrary, water and oil phases exchange the positions in the oil-wet system where the oil fills the small pores and covers the surface of large pores with a thin oleic layer. The preferential wetting property is randomly distributed through the rock surface in the fractional-wet system due to heterogeneity in the mineral distribution [22]. There is no continuous phase that could be observed through the rock in the fractional-wet system. In the mixed-wet system, the preferential wetting property is distributed based on the size of the pores in the rock. The small pores are water-wet and filled with water, while the large pores are oil-wet and filled with oil contacted with pore walls [23].

The wettability of the reservoir rocks is measured either by the contact angle measurement or imbibition tests. There are two types of contact angles (advancing contact angle and receding contact angle) that can be measured based on the continuous phase surrounding the immersed rock surface [24]. In the advancing contact angle measurement, a pure, clean rock surface, preferentially water-wet, is immersed in a reservoir oil for some time until reaching the equilibrium condition. Then, a small brine droplet is introduced to contact the top of the rock surface, and the contact angle is measured as a function of time until reaching a horizontal equilibrium of the point of contact of the interfacial tensions given by the Young-Dupre equation [25]:

$$\sigma_{os} - \sigma_{ws} = \sigma_{ow} \cos\theta \qquad \textbf{2.2}$$

where: σ_{os} is oil-solid interfacial tension, σ_{ws} is water-solid interfacial tension, σ_{ow} is oil-water interfacial tension, and θ is the contact angle measured through the denser phase (water phase). Surfactants found in crude oil adsorb on the rock surface with time and increase the oil wetness. Oil and water phases exchange the positions in receding contact

angle measurement, and the oil droplet contacts the rock surface from the down face instead of the upper face due to the buoyancy effect. Figure 2.1 shows the advancing and receding contact angles. According to the Young-Dupre equation, if $\sigma_{os} = \sigma_{ws}$, then, the contact angle $\theta = 90^{o}$ and the rock has neutral or intermediate wettability. However, if $\sigma_{ws} < \sigma_{os}$ then, $\theta < 90^{o}$ and the rock is water-wet. On the contrary, if $\sigma_{ws} > \sigma_{os}$ then, $\theta > 90^{o}$ and the rock is oil-wet.

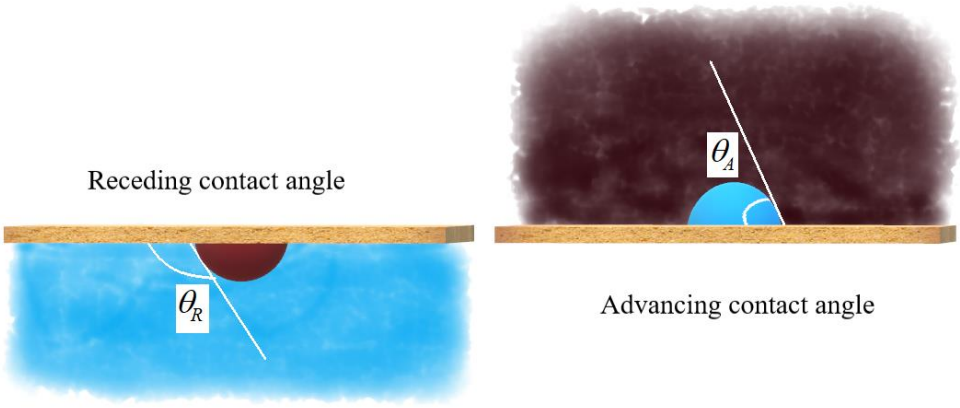

Figure 2.1. A schematic diagram shows advancing and receding contact angles.

In addition to contact angle measurement, wettability can be measured quantitatively via the Amott wettability index [26]. In this method, a real reservoir core sample is flooded with brine until reaching the residual oil saturation. Then, the core sample is immersed in a refined oil such as kerosene for 20 hours, and the volume of brine displaced by the imbibition of oil is measured. After that, a centrifuge force is used to displace other water droplets with kerosene, and the volume of these water droplets is measured. Then, the core sample is immersed again but in brine for 20 hours, and the volume of kerosene displaced

by water imbibition is measured. Finally, the core sample is centrifuged under the brine to produce extra kerosene, and the volume of this kerosene is measured. The Amott wettability indices for oil and water phases are calculated from the following equations [27].

$$WI_w = \frac{V_{O_{imbibition}}}{V_{O_{imbibition}} + V_{O_{centrefuge}}} \quad \textbf{2.3}$$

$$WI_o = \frac{V_{W_{imbibition}}}{V_{W_{imbibition}} + V_{W_{icentrifuge}}} \quad \textbf{2.4}$$

where: $V_{O_{imbibition}}$ is the volume of oil displaced by brine imbibition, $V_{O_{centrifuge}}$ is the volume of oil displaced by centrifuging with brine, $V_{W_{imbibition}}$ is the volume of water displaced by oil imbibition, and $V_{W_{centrifuge}}$ is the volume of water displaced by centrifuging with oil. For water-wet rock, WI_O equals zero and WI_W is close to one. Whereas for the oil-wet rock, WI_W equals zero and WI_O is close to one.

The United States Bureau of Mines (USBM) wettability index is another method that can be used for wettability measurement [28]. In this method, the core sample is saturated initially with water. Then, it is centrifuged in oil until reaching irreducible water saturation. The reduction in water saturation is plotted as a function of pressure resulting from centrifuge force and labeled as stage I, as shown in Figure 2.2. After that, the core sample is centrifuged in water until reaching the residual oil saturation, and the increment in water saturation is plotted as a function of pressure and is labeled as stage II on the same figure (Figure 2.2). Finally, the core sample is centrifuged again in the oil until reaching the irreducible water saturation, and the reduction in water saturation is plotted as a function

of pressure and labeled as stage III in Figure 2.2. The USBM wettability index is calculated as the following:

$$I_W = \log_{10}\left(\frac{A_1}{A_2}\right) \qquad \textbf{2.5}$$

where: A_1 and A_2 are the areas under the capillary pressure curves labeled as III and II, respectively. The USBM wettability index has positive values for water-wet rocks and negative values for oil-wet rocks, and it will be zero for neutral or intermediate wettability rocks.

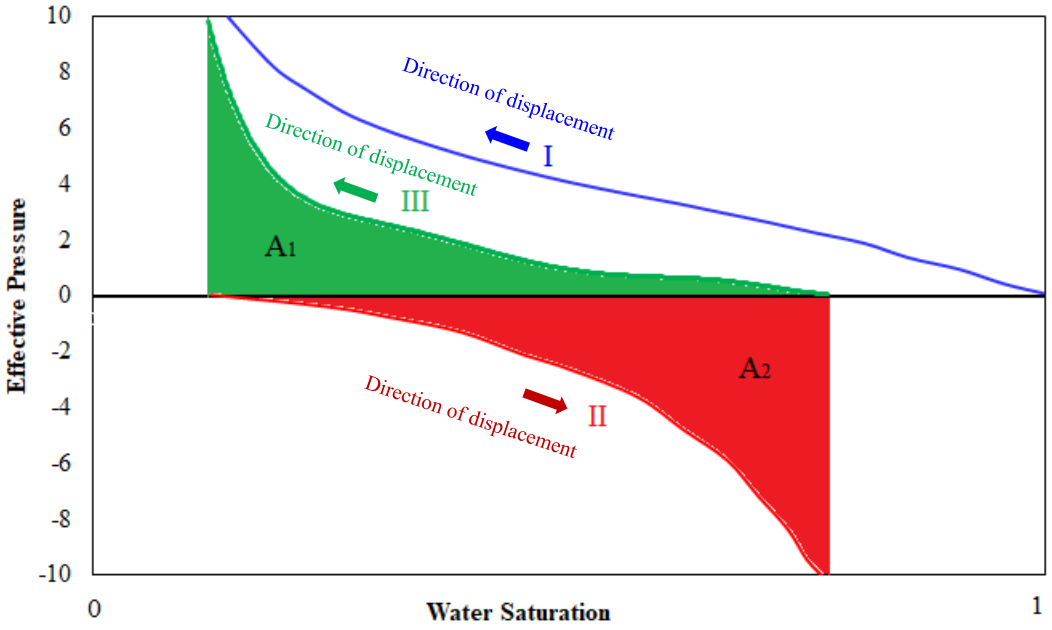

Figure 2.2. A schematic diagram shows the determination of the USBM wettability index.

Each of contact angle measurement, Amott wettability index, and USBM wettability index could be applied easily to measure the wettability alteration for consolidated rock in the presence of low viscosity crude oil (conventional crude oil) and brine. However, none of these methods are useful for measuring the wettability alteration for bitumen-brine-sand.

The high viscosity of bitumen and the nonconsolidated sands make the wettability measurement difficult, if not impossible. In order to overcome these difficulties in our work, a history matching approach was implemented to match the oil recovery data by fitting the parameters found in Brooks-Corey's correlations and getting relative permeability curves. The change in the relative permeability curves gives a reliable qualitative indication for the wettability alteration of the bitumen-brine-sand system.

A previous study found that the wettability of sandstone rocks is mostly affected by adsorbing the high molecular weight fractions found in crude oil. In contrast, the limestone rocks wettability is affected by adsorbing the nitrogen-based compounds on the surface of the grain [29, 30]. Removing asphaltenes from crude oils was found to alter rock wettability toward more water-wet [31]. A recent study showed that the alkaline materials (i.e., KOH) could react with naphthenic acids found in acidic crude oils to generate in situ surfactants. These surfactants molecules are adsorbed on the surfaces of the grains and change the rock wettability toward more water-wet and consequently increase the oil recovery efficiency [32]. As known, ammonia and urea have an intermediate basic nature due to the presence of amino functional groups in their molecular structure, which enables them to react readily with naphthenic acids found in crude oil and generate in situ surfactants [33]. Recent studies indicated that urea is decomposed gradually into ammonia and carbon dioxide (CO_2) once it exposes to SAGD condition [12, 13]. The generated ammonia dissolves quickly in the condensed water inside the reservoir to generate a basic ammonium hydroxide (NH_4OH) solution. This solution reacts with naphthenic acids found in bitumen to generate in situ surfactants capable of altering rock wettability toward more water-wet and improves oil recovery efficiency [34-36]. Furthermore, ammonia released from the

decomposition of urea increases pH of the aqueous phase leading to enhancing bitumen libration from sands. The surfaces of bitumen and sand grains acquire higher negative charges in the presence of higher pH value, leading to strong repultion force between bitumen and sand grains, which improves oil recovery efficiency [37]. Additionally, the high value of pH raises the ionization process of generated in situ surfactants at water/oil interface to reduce the interfacial tension and, hence, improve bitumen detatching from sand grains. Moreover, generating extra ammonia not only increases the pH value, but also generates higher concentration of in situ surfactants and, hence, improves liberation of bitumen from sand grains [38]. Additionally, the generated CO_2 dissolves in crude oil, making more reduction in oil viscosity and swelling the crude oil to improve the oil mobility.

2.4 Emulsion generation via ammonia and urea reaction with naphthenic acids

The emulsion is defined as a mixture of two immiscible liquids where one of them is dispersed in the forms of small droplets (dispersed or internal phase) in the other liquid (continuous or external phase) [39]. There are three common classes of emulsions that could be generated by mixing two immiscible liquids: 1) water-in-oil (W/O) emulsion, oil-in-water (O/W) emulsion, and complex or multiple emulsions such as (W/O/W or O/W/O) emulsions. Figure 2.3 shows these types of emulsions.

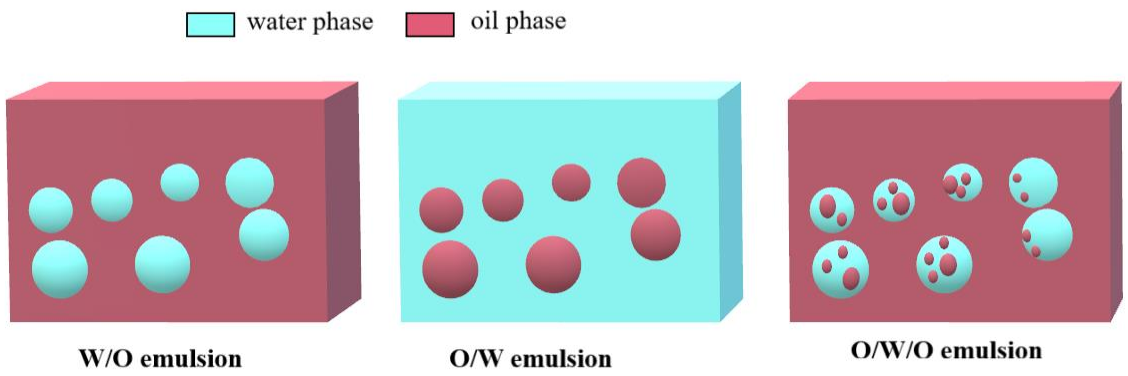

Figure 2.3. A schematic diagram shows the different types of emulsions.

Water-in-oil emulsion mainly consists of fine water droplets dispersed in a continuous phase of crude oil. This type of emulsion is common in oil fields as 95% of emulsions generated in the oil fields are W/O emulsions [40]. The W/O emulsion is characterized by high stability under reservoir conditions due to the presence of in situ surfactants, resin, and asphaltene components in crude oil [41-45]. These components form a thin film around water droplets, and this film increases the stability of W/O emulsion via increasing interfacial viscosity and decreasing the interfacial tension [46]. Water and oil exchange their positions in the oil-in-water (O/W) emulsion, where the oil droplets are dispersed in the continuous water phase. Multiple or complex (W/O/W or O/W/O) emulsions consist of very fine droplets of the continuous phase suspended in bigger droplets of the dispersed phase, which in turn are suspended in the continuous phase. Hydrophilic (water-loving) and hydrophobic (oil-loving) surfactants are generally found in the multiple emulsion systems to keep them stable after the generation process [47-50]. The water-in-oil emulsion is classified into four classes based on stability: 1) stable, 2) mesostable, 3) unstable, and 4) entrained water. The stable W/O emulsion has a high amount of water (60-80%), which makes it brown. Whereas the mesostable W/O emulsion contains less amount of water, and

it has a darker color. Unstable W/O emulsion separates rapidly into two phases due to the difference in densities of dispersed and continuous phases. The entrained water emulsion could keep 30-40% of water content for some time, but this content decreases with time to reach 10% after a few days [51].

The emulsion generation (emulsification) process requires mechanical energy to split the internal phase into fine droplets dispersed uniformly in the continuous phase. Different methods are used to apply the mechanical energy through the emulsification process, such as shaking, mixing with a magnetic stirrer, liquids injection through porous media, and ultrasound emulsion generators. Besides mechanical energy, other factors such as immiscibility between emulsion's phases and the existence of surfactants are necessary through the emulsification process. Scientists recognized four mechanisms for emulsion stability: 1) electrostatic repulsion, 2) steric repulsion, 3) the Marangoni-Gibbs effect, and 4) thin-film stabilization [46]. In the electrostatic repulsion, the molecules of ionic surfactants are adsorbed on the dispersed droplets to form charged droplets. The similar charges on the droplets repulse the droplets from each other and prevent them from contacting, as shown in Figure 2.4 (a) [52]. The steric repulsion happens when the heads of molecules of non-ionic surfactants are adsorbed on the surface of dispersed water droplets while their tails are left free in the oil phase. The surfactant molecules form a thin layer on the water droplets and prevent them from contacting each other, as shown in Figure 2.4 (b). This mechanism is responsible for stabilizing W/O emulsions generated in the oil fields [53]. In the Marangoni-Gibbs effect, the dispersed droplets elongate and come close to each other in which the continuous phase gets stuck in between them, making them separated permanently from each other [54]. Figure 2.4 (c) shows emulsion stabilization

via the Marangoni-Gibbs effect. In the thin-film stabilization mechanism, the asphaltene molecules form a rigid film surrounding water droplets and prevent them from contacting each other. This mechanism depends on the chemical structure of asphaltene molecules and the kinetics of diffusion and adsorption [55, 56].

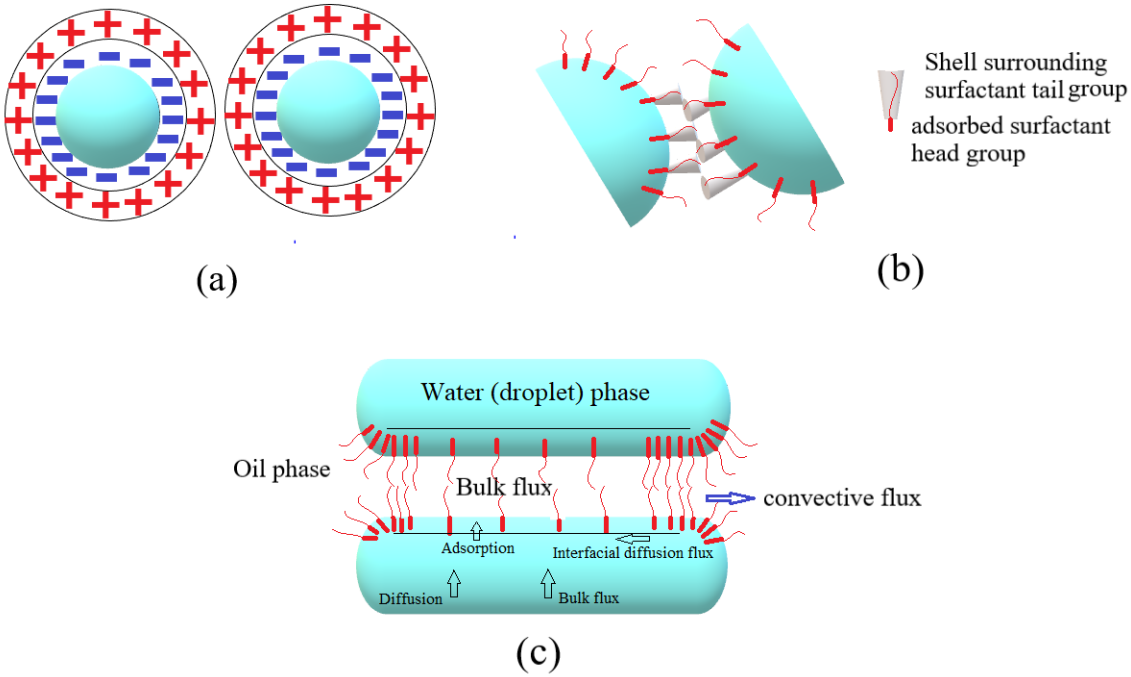

Figure 2.4. A schematic diagram shows different mechanisms for emulsion stability. a) electrostatic repulsion[57], b) steric repulsion[56], and c) Marangoni-Gibbs effect[56].

The rheological properties of emulsions are strongly affected by several parameters such as volume fraction of dispersed phase, the temperature of the system, shear stress, and shear rate. Some emulsions show Newtonian behavior (viscosity does not depend on share rate), such as diluted emulsions, whereas some emulsions show the dependence of viscosity on the shear rate (Non-Newtonian emulsions) [58, 59]. The droplet size of the dispersed phase has a dramatic effect on the viscosity of the emulsion. The smaller the size of the droplet,

the higher the viscosity of the emulsion [60]. Several factors control the droplet size of the dispersed phase, such as the type of surfactant, the procedure that followed through emulsification, the concentration of surfactant, the mixing speed, and mixing time [42].

Several studies showed the superiority of ammonia solutions in reducing the total acid number (TAN) of acidic oils such as heavy crude oils and tar sands [61-63]. Different solvent mediums such as water, ethylene glycol, and a mixture of water and methanol were used in these studies to prepare the ammonia solutions. All these solutions have proven their value in reducing naphthenic acids found in crude oil via ammonia to generate natural surfactants. The resulting in-situ surfactants are adsorbed on the surface of water droplets to generate water-in-oil emulsions [53].

2.5 Review of published works on the use of ammonia and urea solutions in oil recovery

Liu *et al.* conducted experimental studies to investigate the synergy of urea and urea-foam systems with steam in heavy oil recovery in SAGD process [64]. They compared the obtained results with conventional steam flooding as a baseline. They found that urea-foam-assisted-steam flooding (UFASF) and urea-assisted-steam flooding (UASF) are more effective than conventional steam flooding. They attributed the superiority of UFASF and UASF flooding to the capability of urea and urea-foam systems to mitigate the steam override problem and expand the SAGD chamber properly. Furthermore, urea decomposes into ammonia and carbon dioxide at SAGD condition, converting the rock wettability toward more water-wet and consequently improving oil recovery. Additionally, carbon dioxide dissolves in crude oil, causing swelling of crude oil and reducing the oil viscosity.

They extended the UFASF system in a pilot test in the Jin-1 Block at Liaohe Oilfield, China, and found promising results.

Guo *et al.* conducted 1-D flooding experiments of urea solutions to recover super-heavy crude oil [12]. Their results revealed that a 25 wt% concentration of urea solution could recover 17.7% more crude oil than conventional steam flooding at 423 K (150 ℃). Also, they found that ammonia generated by the decomposition of urea dissolves in condensed water to form a high pH ammonium hydroxide solution that generates in situ surfactants via reaction with naphthenic acids. Meanwhile, CO_2 generated dissolves in crude oil to improve the oil-water mobility ratio. Finally, Guo *et al.* extended their work on a 2-D model and compared the results of using urea, ammonia, and CO_2 as additives with the conventional steam flooding (CSF)[13]. The 2-D experimental results showed that urea-steam flooding takes advantage of ammonia-steam flooding and CO_2-steam flooding. The generated CO_2 via urea decomposition pushes the crude oil into the production well, while the generated ammonia improves the rock wettability and enhances the mobility ratio. The experimental results also showed that the ammonia-steam flooding and CO_2-steam flooding produce 10-12% extra oil recovery; whereas urea-steam flooding could recover 35% extra oil compared to the conventional steam flooding.

Yang *et al.* used a numerical simulation technique to investigate the mechanism of urea-assisted steam flooding in the cyclic steam stimulation (CSS) process [65]. They matched the production data of the CSS process in Biqian-10 block Henan oilfield, China, through 20 years of production history. Through building the simulation model, they assumed that urea decomposes into ammonia and CO_2 at reservoir conditions, and they considered the solubility of CO_2 in oil through the simulation process. However, they neglected the minor

effect of ammonia on the reduction of interfacial tension and altering the rock wettability in their reservoir simulation study. The simulation results revealed that the solubility of CO_2 in crude oil plays a primary role in oil recovery efficiency. Additionally, the reservoir pressure buildup resulting from oil swelling with CO_2 was shown to be more effective than the reduction of oil viscosity by CO_2 dissolution on the oil recovery.

Van den pol *et al.* investigated the applicability of ammonia as alkaline material in the alkaline-surfactant-polymer (ASP) flooding process [66-68]. They found that ammonia works very well with alkyl propoxy sulfate and internal olefin sulfonates surfactants. Additionally, the presence of ammonia in ASP flooding reduces the surfactant adsorption considerably on the rock surface compared to surfactant-polymer (SP) flooding alone. Comparable results of the reduction in the adsorption of surfactants were achieved by Sharma *et al.* on sandstone rocks, but not much difference was observed on carbonate rocks [69]. Southwick *et al.* found that adding a small amount of sodium chloride (NaCl), 0.5%, into the ASP solution makes ammonia better than sodium carbonate (Na_2CO_3) in the oil recovery with ASP flooding [70].

Southwick introduced a method to generate ammonia economically using the Haber-Bosch process [71]. Then, the produced ammonia is mixed with water and injected into the reservoir to recover bitumen. Methane is separated from the produced emulsion and recycled to generate ammonia again using the Haber-Bosch process. At low pressures, ammonia can be separated from the produced emulsion and then mixed with the generated ammonia for reinjection into the reservoir.

David and Mitchell introduced a method to generate in-situ surfactants leading to mobilization of viscous asphaltic or bituminous heavy crude oil [72]. The high permeability area is created firstly inside the reservoir by the fracturing process. Then, oxygen, ozone, or air is injected into a high permeability area to react with oxygen-susceptible groups or labile groups associated with bitumen to generate acidic or aldehyde groups. After that, ammonia is injected into the reservoir to react with aldehyde groups to form in-situ surfactants. Lastly, steam, steam-ammonia mixture, or steam-air mixture is injected into the treated formation to produce crude oil. This process can be applied using a single well as injection and production well or applied using two parallel wells.

Hart *et al.* claimed that heated amines or mixtures consisting of heated amine and ammonia could be injected into an underground reservoir to improve bitumen mobility toward production well by reducing the viscosity of the bitumen [73]. Steam or water, or solvents can be added into an amine or amine-ammonia mixture to improve its efficiency for bitumen recovery. The heat exchanges from hot solutions into a cold bitumen, whereas steam, will condense to form low viscosity aqueous phase, allowing hydrocarbon to move toward the production well.

Most of the early studies in the literature focused on using urea and ammonia as additives for steam during SAGD and CSS flooding processes. These solvents demonstrated superiority in the recovery efficiency of heavy crude oils compared to conventional steam flooding. To the best of my knowledge, the utilization of ammonia or urea solution to recover bitumen via the hot water flooding process has not been reported elsewhere. This point is the main key that makes this work novel and may provide a more efficient

alternative to access oil sands resources in thin reservoirs that are not accessible currently by existing in situ recovery techniques.

2.6 References

[1] Zirrahi M, Hassanzadeh H, Abedi J. Prediction of water solubility in petroleum fractions and heavy crudes using cubic-plus-association equation of state (CPA-EoS). Fuel 2015;159:894-899.

[2] Zirrahi M, Hassanzadeh H, Abedi J. Experimental and modelling studies of MacKay River bitumen and light n-alkane binaries. The Canadian Journal of Chemical Engineering. 2017;95(7):1417-14127.

[3] Haddadnia A, Azinfar B, Zirrahi M, Hassanzadeh H, Abedi J. Thermophysical properties of dimethyl ether/Athabasca bitumen system. The Canadian Journal of Chemical Engineering. 2018;96(2):597-604.

[4] Azinfar B, Haddadnia A, Zirrahi M, Hassanzadeh H, Abedi J. Effect of asphaltene on phase behavior and thermophysical properties of solvent/bitumen systems. Journal of Chemical & Engineering Data. 2017;62(1):547-557.

[5] Zirrahi M, Hassanzadeh H, Abedi J, Moshfeghian M. Prediction of solubility of CH_4, C_2H_6, CO_2, N_2 and CO in bitumen. The Canadian Journal of Chemical Engineering 2014;92(3):563-572.

[6] Wilson T. The total and partial vapor pressures of aqueous ammonia. University of Illinois 1925;146.

[7] Piela L. On the hydrogen bonding between water and ammonia molecules. Chemical Physics Letters 1972;15(2):199-202.

[8] Hales J, Drewes D. Solubility of ammonia in water at low concentrations. Atmospheric Environment. (1967) 1979;13(8):1133-1147.

[9] Ishida K. Mutual solubilities of some hydrocarbon oils and liquid ammonia. I. Solubility data. Bulletin of the Chemical Society of Japan. 1958;31(2):143-148.

[10] Tremper K, Prausnitz J. Solubility of inorganic gases in high-boiling hydrocarbon solvents. Journal of Chemical and Engineering Data. 1976;21(3):295-299.

[11] Young C, Fogg P. Ammonia, amines, phosphine, arsine, stibine, silane, germane and stannane in organic solvents. Elsevier; 2013.

[12] Guo E, Jiang Y, Gao Y, Shen D, Zhigang C, Yu P. A New approach to improve recovery efficiency of SAGD. *SPE Middle East Oil & Gas Show and Conference.* Society of Petroleum Engineers; 2017.

[13] Erpeng G, Hongyuan W, Oilfield L, Youwei J, Yongrong G, Junhui S. Experimental study of urea-SAGD process. *SPE EOR Conference at Oil and Gas West Asia.* Society of Petroleum Engineers; 2018.

[14] Schaber P, Colson J, Higgins S, Thielen D, Anspach B, Brauer J. Thermal decomposition (pyrolysis) of urea in an open reaction vessel. Thermochimica acta 2004;424(1-2):131-142.

[15] Pinck L, Kelly M. The solubility of urea in water. Journal of the American Chemical Society. 1925;47(8):2170-2172.

[16] Shnidman L, Sunier A. The solubility of urea in water. The Journal of Physical Chemistry 2002;36(4):1232-1240.

[17] Anand A, Patey G. Mechanism of urea crystal dissolution in water from molecular dynamics simulation. The Journal of Physical Chemistry B 2018;122(3):1213-1222.

[18] Weast R. Handbook of chemistry and physic 60th edition. Boca Raton, Florida: CRC Press Inc; 1979.

[19] Lee F, Lahti L. Solubility of urea in water-alcohol mixtures. Journal of Chemical and Engineering Data 1972;17(3):304-306.

[20] Ahmed T. Reservoir engineering handbook. Gulf professional publishing; 2018.

[21] Donaldson E, Alam W. Wettability. Elsevier; 2013.

[22] Brown R, Fatt I. Measurements of fractional wettability of oil fields' rocks by the nuclear magnetic relaxation method. *Fall Meeting of the Petroleum Branch of AIME*. Society of Petroleum Engineers; 1956.

[23] Salathiel R. Oil recovery by surface film drainage in mixed-wettability rocks. Journal of Petroleum Technology 1973;25(10):1,216-1,224.

[24] Peters E. Petrophysics. Department of Petroleum and Geosystems Engineering, University of Texas at Austin 2006.

[25] Tiab D, Donaldson E. Petrophysics: theory and practice of measuring reservoir rock and fluid transport properties. Gulf professional publishing; 2015.

[26] Amott E. Observations relating to the wettability of porous rock. Transactions of the AIME 1959;216(01):156-162.

[27] Peters E. Advanced petrophysics: Geology, porosity, absolute permeability, heterogeneity, and geostatistics. Greenleaf Book Group; 2012.

[28] Donaldson E, Thomas R, Lorenz P. Wettability determination and its effect on recovery efficiency. Society of Petroleum Engineers Journal 1969;9(01):13-20.

[29] Denekas M, Mattax C, Davis G. Effects of crude oil components on rock wettability. 1959.

[30] Ehrlich R, Hasiba H, Raimondi P. Alkaline waterflooding for wettability alteration-evaluating a potential field application. Journal of Petroleum Technology 1974;26(12):1,335-1,343.

[31] Johansen R, Dunning H. Relative wetting tendencies of crude oils by capillarimetric method. US Department of the Interior, Bureau of Mines; 1961.

[32] Ehrlich R. Wettability alteration during displacement of oil by water from petroleum reservoir rock. *Proceedings of the 48th National Colloid Symposium*. ACS preprints, Austin, TX, USA. 1974: 24-26.

[33] Sheng J. Investigation of alkaline–crude oil reaction. Petroleum 2015;1(1):31-39.

[34] BinDahbag M, Mohammadi M, Khalifi M, Aghajamali M, Zirrahi M, Hassanzadeh H. Efficiency of urea solutions in enhanced oil recovery. ACS Omega 2020;5(11):6122-6129.

[35] BinDahbag M, Al-Gawfi A, Hassanzadeh H. Suitability of hot urea solutions for wettability alteration of bitumen reservoirs–Simulation of laboratory flooding experiments. Fuel 2020;272:117713.

[36] BinDahbag M, AlQuraishi A, Benzagouta M. Efficiency of ionic liquids for chemical enhanced oil recovery. Journal of Petroleum Exploration and Production Technology 2015;5(4):353-361.

[37] Takamura K, Chow RS. A mechanism for initiation of bitumen displacement from oil sand. Journal of Canadian Petroleum Technology 1983;22(06): 22-30.

[38] Flury C, Afacan A, Tamiz M, Sjoblom J, Xu Z. Effect of caustic type on bitumen extraction from Canadian oil sands. Energy & fuels 2014;28(1):431-438.

[39] Tadros T. Emulsion formation, stability, and rheology. Emulsion formation and stability 2013;1:1-75.

[40] Ali M, Alqam M. The role of asphaltenes, resins and other solids in the stabilization of water in oil emulsions and its effects on oil production in Saudi oil fields. Fuel 2000;79(11):1309-1316.

[41] Fridjonsson E, Graham B, Akhfash M, May E, Johns M. Optimized droplet sizing of water-in-crude oil emulsions using nuclear magnetic resonance. Energy & fuels 2014;28(3):1756-1764.

[42] Nour A. Emulsion types, stability mechanisms and rheology: A review. International Journal of Innovative Research and Scientific Studies (IJIRSS) 2018;1(1): 14-21.

[43] Mohammadi M, Zirrahi M, Hassanzadeh H. Adsorption kinetics of asphaltenes at the heptol–water interface. Energy & Fuels 2020;34(3):3144-3152.

[44] Mohammadi M, Zirrahi M, Hassanzadeh H. An analytical model for estimation of the self-diffusion coefficient and adsorption kinetics of surfactants using dynamic interfacial tension measurements. The Journal of Physical Chemistry B 2020;124(15):3206-3213.

[45] Mohammadi M, Haddadnia A, Zirrahi M, Hassanzadeh H. Interfacial tension of n-pentane/bitumen and n-heptane/bitumen mixtures at T= 298.15–413.15 K and P= 3.45 MPa. Journal of Chemical & Engineering Data 2020;65(4):1787-1794.

[46] Sullivan A, Kilpatrick P. The effects of inorganic solid particles on water and crude oil emulsion stability. Industrial & Engineering Chemistry Research 2002;41(14):3389-3404.

[47] Yaqoob A, Talegaonkar S, Iqbal Z, Jalees F, Krishan R. Multiple emulsions: an overview. Current drug delivery. 2006;3(4):429-443.

[48] Muschiolik G. Multiple emulsions for food use. Current Opinion in Colloid & Interface Science 2007; 12(4-5):213-220.

[49] Pal R. Rheology of simple and multiple emulsions. Current Opinion in Colloid & Interface Science 2011; 16(1):41-60.

[50] Jiao J, Burgess D. Rheology and stability of water-in-oil-in-water multiple emulsions containing Span 83 and Tween 80. Aaps Pharmsci 2003;5(1):62-73.

[51] Fingas M, Fieldhouse B. Formation of water-in-oil emulsions and application to oil spill modelling. Journal of hazardous materials 2004;107(1-2):37-50.

[52] Molnes S. Physical properties of gelatin based solid emulsions: Effects on drug release in the GI tract. Norwegian University of Science and Technology. 2013.

[53] Zhang Y. The fabrication and application of semi-crystalline and thermoset-thermoplastic composite colloidal particles with well-defined microstructures. Johannes Gutenberg-Universität Mainz; 2013.

[54] Mosayebi A, Abedini R. Using demulsifiers for phase breaking of water/oil emulsion. Petroleum & Coal 2013;55(1): 26-30.

[55] Ekott E, Akpabio E. A review of water-in-crude oil emulsion stability, destabilization and interfacial rheology. Journal of Engineering and Applied Science. 2010;5(6):447-452.

[56] Spiecker P. The impact of asphaltene chemistry and solvation on emulsion and interfacial film formation. 2001.

[57] Liu Y, Sellmyer D, Shindo D. Handbook of advanced magnetic materials. Springer Science & Business Media; 2008.

[58] Barnes H. Rheology of emulsions-A review. Colloids and Surfaces A: Physicochemical and Engineering Aspects. 1994;91:89-95.

[59] Derkach S. Rheology of emulsions. Advances in Colloid and Interface Science 2009;151(1-2):1-23.

[60] Pal R. Effect of droplet size on the rheology of emulsions. AIChE Journal 1996;42(11):3181-3190.

[61] Lu R, Xu X, Yang J, Gao J. Reduction of total acid number of crude oil and distillate. Energy Sources, Part A 2007;29(1):47-57.

[62] Wang Y, Chu Z, Qiu B, Liu C, Zhang Y. Removal of naphthenic acids from a vacuum fraction oil with an ammonia solution of ethylene glycol. Fuel. 2006;85(17-18):2489-2493.

[63] Wu C, De Visscher A, Gates I. On naphthenic acids removal from crude oil and oil sands process-affected water. Fuel. 2019;253:1229-1246.

[64] Liu P, Li W, Shen D. Experimental study and pilot test of urea-and urea-and-foam-assisted steam flooding in heavy oil reservoirs. Journal of Petroleum Science and Engineering 2015;135:291-298.

[65] Yang C, Lin Y, Zhang Z, Deng R, Wu X, Niu B, et al. A Study on the mechanism of urea-assisted steam flooding in heavy oil reservoirs. Journal of Petroleum Science and Technology 2015;5(2):36-44.

[66] Van P, Esther R, Carl H, Van H , Diederik W, Jeffrey G, Ahmad A, Arif A, Sitimazura A . Alkali surfactant polymer flooding using ammonia for offshore use.

International Petroleum Technology Conference. Society of Petroleum Engineering; 2014.

[67] Southwick J, Van E, Van C, Van D, Boersma D, Svec Y, et al. Ammonia as alkali for ASP floods–comparison to sodium carbonate. *IOR 2015-18th European Symposium on Improved Oil Recovery*. European Association of Geoscientists & Engineers; 2015.

[68] Southwick J, Van E, Van C, Van D, Boersma D, Svec Y, et al. Ammonia as alkali for alkaline/surfactant/polymer floods. Spe Journal 2016;21(01):10-21.

[69] Sharma H, Lu J, Weerasooriya U, Pope G, Mohanty K. Adsorption in chemical floods with ammonia as the alkali. *SPE Improved Oil Recovery Conference*. Society of Petroleum Engineers; 2016.

[70] Southwick J, Brewer M, Pieterse S, Van D. Ammonia as alkali for high acid number oils. *SPE EOR Conference at Oil and Gas West Asia*. Society of Petroleum Engineers; 2018.

[71] Southwick J. Process for oil recovery. Google Patents; 2017.

[72] Redford D, Mitchell D. Method for recovering viscous asphaltic or bituminous petroleum. Google Patents; 1976.

[73] Hart P, Stefan B, Srivastava P, Debord J. Method for enhancing heavy hydrocarbon recovery. Google Patents; 2009.

CHAPTER 3: SOLUBILITY AND LIQUID DENSITY OF AMMONIA /ATHABASCA BITUMEN MIXTURES AT TEMPERATURES UP TO 463 K – MEASUREMENTS AND MODELING [*]

3.1 Abstract

We report experimental data of ammonia solubility in Athabasca bitumen measured at different temperatures and pressures ranging from 348 to 463 K (75 to 190 °C) and 1 to 4 MPa, respectively. Liquid phase density of ammonia saturated bitumen was measured for the samples that have been taken during solubility measurements. The experimental data for ammonia solubility in bitumen was modeled using the Peng-Robinson equation of state (PR-EoS). The volume shift parameters of ammonia were tuned to represent the experimental density data of ammonia saturated bitumen with an average absolute relative deviation percent (AARD%) of 0.218%. Also, tuning the binary interaction coefficient between ammonia and bitumen allowed the prediction of solubility data with an AARD of 8.537%. The data and the tuned model find applications in reservoir modeling of solvent-aided thermal recovery of bitumen and heavy oil.

3.2 Introduction

The energy demand around the world is growing while conventional reservoirs are being depleted. Heavy oil and bitumen are important resources with higher than 2,100 billion barrels reserve of bitumen in place around the world [1]. Steam-assisted gravity drainage

[*] BinDahbag, M., Zirrahi, M. and Hassanzadeh, H., 2019. Solubility and liquid density of ammonia/Athabasca bitumen mixtures at temperatures up to 463 K: Measurements and modeling. Journal of Chemical & Engineering Data, 64(8), pp.3592-3597.

(SAGD) and cyclic steam stimulation (CSS) are the most common in situ bitumen recovery methods. However, these techniques are associated with challenges such as high energy consumption, the necessity of treatment of large volume of water, the high viscosity of the product, and the low value of the produced bitumen. To overcome these challenges, solvents have been suggested to be co-injected with steam during the SAGD process [2-4]. Several studies investigated co-injection of non-condensable gases with steam using physical models [5-10]. Solubilities of different gaseous and liquid solvents in several types of bitumen and heavy oils were investigated at wide ranges of temperatures and pressures. Jacobs *et al.* studied the effect of solubility of carbon dioxide (CO_2), nitrogen (N_2) and methane (CH_4) on the viscosity of Athabasca bitumen at different temperatures ranging from 293 to 473 K (20 to 200 ℃) and pressures (up to 13.8 MPa) [11]. They found that CO_2 outperforms other gases with respect to reduction in bitumen viscosity because it has the highest solubility compared to other gases at the same pressure and temperature.

Zirrahi *et al.*[12] and Haddadnia *et al*.[13-15] measured solubility and thermophysical properties of CO_2, N_2, dimethyl ether (DME) and light n-alkanes in Athabasca bitumen at a wide range of temperatures up to 513 K (240 ℃) and pressures up to 6 MPa. Haddadnia *et al*.[15] found that behavior of nitrogen solubility in bitumen is different from other gases and increases by increasing temperature [15].

Azinfar *et al.* fractionated Athabasca bitumen to four fractions and investigated phase behavior and thermophysical properties of light n-alkanes (methane, ethane, propane, and n-butane)/bitumen fractions at pressures up to 4 MPa and temperatures up to 473 K (200 ℃) [16-18]. They also measured the solubility of the aforementioned solvents in Cold Lake bitumen. Utilizing the experimental data of n-alkanes solubility in bitumen fractions, they

developed a generalized Peng-Robinson equation of state (PR-EoS) model for the prediction of n-alkanes solubility in bitumen. They verified the proposed model against the experimental solubility data of n-alkanes in Cold Lake bitumen.

Zirrahi *et al.* studied the solubility of water in Athabasca bitumen through a wide range of temperatures up to 493 K (220 ℃) [19]. The effect of water dissolution on the physical properties of bitumen, such as density and viscosity, were investigated. Peng-Robinson equation of state (PR-EoS) with linear mole fraction mixing rules was utilized to model the experimental results of water solubility, density, and viscosity of water-saturated bitumen.

The solubility of ammonia (NH_3) in a wide variety of pure hydrocarbon solvents was investigated extensively. Solubility of ammonia in non-aromatic compounds (i.e. C_6H_{12}, C_6H_{14}, C_7H_{14}, C_8H_{18}, $C_{10}H_{18}$, $C_{12}H_{22}$, $C_{12}H_{26}$, and $C_{16}H_{34}$), aromatic compounds (i.e. C_6H_6, C_7H_8, and $C_{11}H_{10}$), and alcohols (i.e. CH_4O, C_2H_6O, C_3H_8O, $C_4H_{10}O$, $C_5H_{12}O$, $C_6H_{12}O$, $C_8H_{18}O$, C_2H_7NO, $C_4H_{10}O_3$, and $C_3H_8O_3$) have been reported in the literature[20]. The obtained results indicated that ammonia is more soluble in alcohols than in aromatic and non-aromatic compounds. The results also showed that Raoult's law overestimates ammonia solubility in aromatic and non-aromatic solvents [20].

To the best of our knowledge, there is no experimental data of ammonia solubility in bitumen or heavy oils in the open literature. Ammonia has great potentials to be used as a solvent in solvent-aided thermal recovery processes of bitumen, such as expanding solvent steam-assisted gravity drainage (ES-SAGD) process. Ammonia reacts easily with naphthenic acids found in bitumen to generate in-situ surfactants and reduce the total acid number (TAN) of bitumen [21, 22]. In this study, solubility and density of ammonia in Athabasca bitumen mixtures were measured at wide ranges of temperatures and pressures

applicable to the thermal recovery of bitumen. Then, the obtained experimental results were modeled using the Peng-Robinson equation of state (PR-EoS) that can be used to generate input data for reservoir simulation of ammonia-aided thermal recovery processes.

3.3 Experimental work section

3.3.1 Experimental setup for solubility measurement

The solubility of ammonia in Athabasca bitumen was measured using apparatuses shown in Figure 3.1. This experimental setup consists of a mixing cell that uses a magnetic mixer to mix ammonia and bitumen. The purpose of the mixing process is to reduce the time required to reach the equilibrium condition between gas and liquid phases. After reaching the equilibrium condition, the ammonia/bitumen mixture was passed through an inline Anton Paar densitometer to measure the density of the liquid phase at desired temperature and pressure. The density of ammonia/bitumen mixtures was measured with the Anton Paar densitometer with an accuracy of 0.00001 g/cm^3, which is capable of measuring density in the range of 0-3 g/cm^3. This densitometer is capable of dealing with pressure up to 70 MPa and temperature up to 460 K (187 ℃). The mixing cell and densitometer were placed inside a temperature-controlled oven to ensure accuracy during density measurements at the desired temperature. An ISCO D500 pump was used to inject ammonia and maintain the system at a constant desired pressure. The accuracy of the injection rate is ±0.001 cm^{3,} whereas the maximum flow rate and maximum pressure that can be achieved are 200 cm^3/min and 41 MPa, respectively. Two receiving cells were used for sample collection. The first one was used to receive all ammonia saturated bitumen that fills the dead volume of lines and densitometer until the density of mixture became constant; then, the flow of mixture was directed to the second receiving cell to take a fresh

sample. The reliability of this setup for measuring gas solubility of bitumen-containing systems was checked using bitumen-ethane system at two temperatures, 373 and 423 K (100 and 150 °C), and different pressures ranging from 1.22 to 4.27 MPa. Our results were compared with data collected from literature by Fu et al.,[23] where only about 2% deviation was observed.

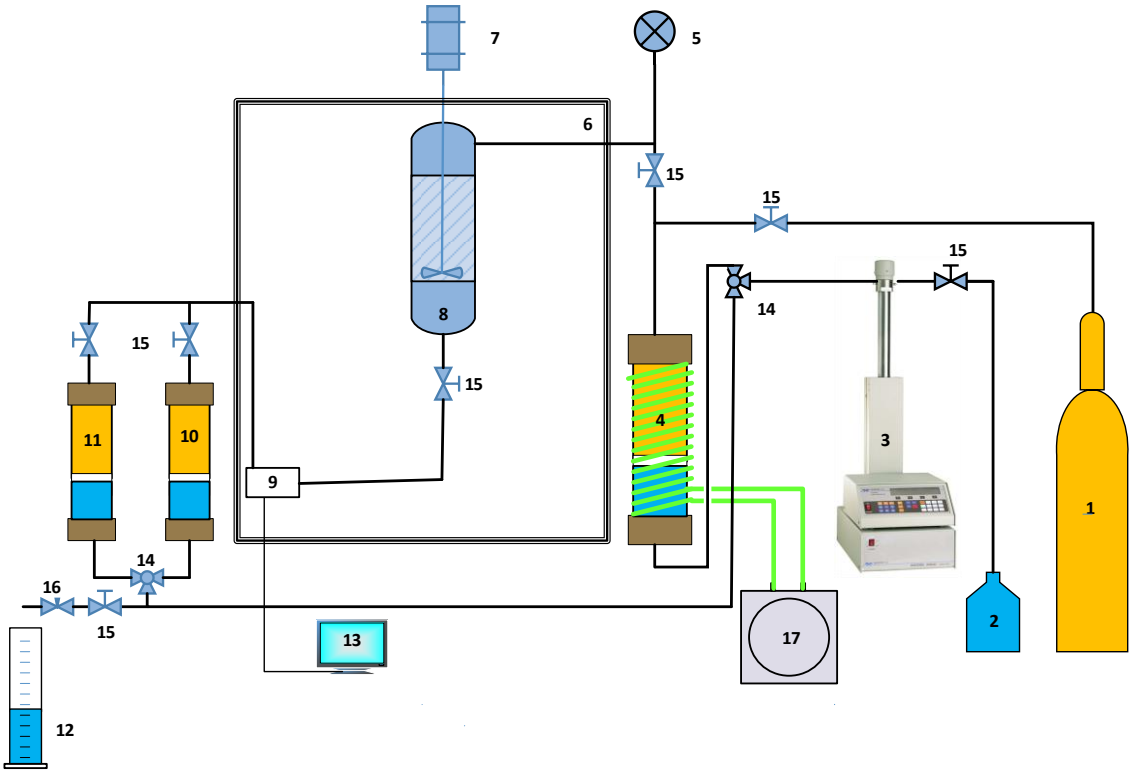

Figure 3.1. Experimental setup used to measure ammonia solubility in bitumen at different temperatures and pressures. 1) Ammonia cylinder, 2) distillated water, 3) ISCO pump, 4) Ammonia accumulator, 5) pressure transducer, 6) oven, 7) electrical motor, 8) mixing cell, 9) Anton Parr densitometer, 10) receiving cell, 11) fresh sample cell, 12) graduated tube, 13) monitor for densitometer, 14) 3 ways valve, 15) 2 ways valve, 16) needle valve, 17) cooler.

3.3.2 Materials

The bitumen sample used in this study is from Athabasca oil sands, Alberta, Canada, with a specific gravity of 1.004. Bitumen molecular weight of 513 g/mole was measured using the freezing point depression technique. A simulated distillation test (ASTM 7169) of the bitumen has been reported by Zirrahi et al. [19], as shown in Figure 3.2 (a). The carbon number distribution is also shown in Figure 3.2 (b) [24]. High purity anhydrous ammonia, 99.99%, was provided from Praxair Inc., USA. The provided ammonia was used directly in the experiments without any further purification. The critical properties, boiling point temperature, and acentric factor of ammonia were taken from the chemical properties handbook [25]. Table 3.1 shows the IUPAC systematic names, CAS registry number, supplier, and purity of the chemicals.

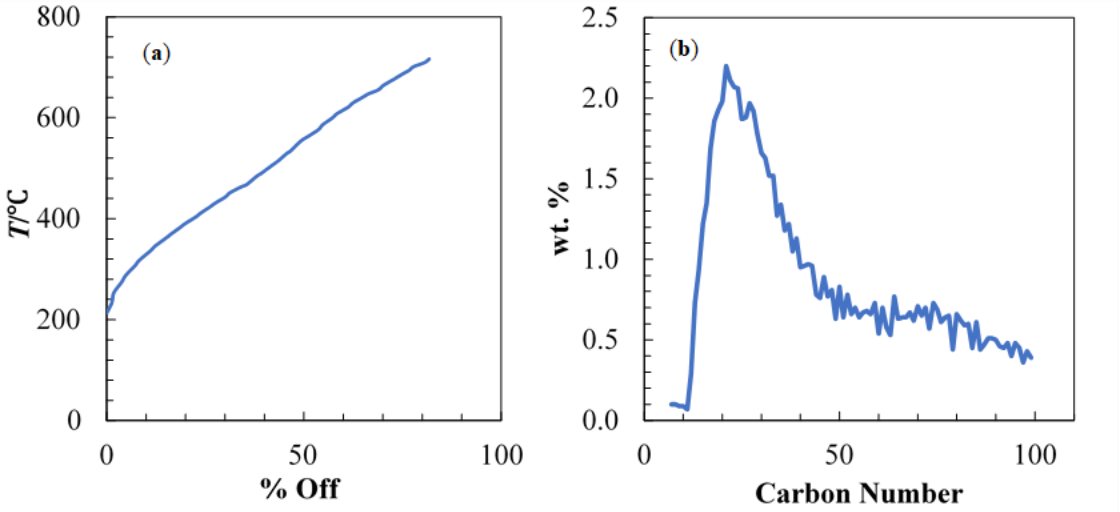

Figure 3.2. (a) Simulated distillation (ASTM 7169) results of bitumen,[19] and (b) carbon number distribution [24].

Table 3.1. The IUPAC systematic names, CAS registry number, supplier, and purity of the chemicals.

IUPAC systematic name	CAS Registry Number	Supplier	Purity[a]
Ammonia (nitrogen trihydride)	7664 - 41 - 7	Praxair	99.995%

[a] The provided ammonia was used directly in the experiments without any further purification. The boiling point and carbon number distribution of the bitumen used in experiments are shown in Figures 3.2(a) and 3.2(b).

3.3.3 Experimental procedure

First, the system is vacuumed to remove air in the mixing cell and lines. Next, ammonia is introduced into the mixing cell in the gaseous phase at 0.3 MPa pressure. Then, a pre-determined volume of bitumen is charged into the system using the receiving cell. After that, mixing is started while pressure and temperature are set at the desired values using the ISCO pump and Blue M oven, respectively. The mixing process is continued at constant pressure and temperature until an equilibrium condition between gas and liquid phases is reached and no ammonia can be further dissolved in bitumen. The mixer is stopped once reaching equilibrium condition, and the pressure of the system is increased 0.06 MPa above the desired pressure to ensure there is no gas ex-solution from the liquid phase while taking a sample. About 10 cm^3 of the liquid phase is taken firstly in the receiving cell to ensure a fresh sample can be collected. Then, a considerable amount of mixture is taken in the fresh sample cell (cell No. 11) at a very low flow rate, less than 2 cm^3/min. The sample is flashed at atmospheric pressure, and the flashed bitumen is heated for some time to ensure there is no ammonia left dissolved in bitumen after the flashing process. Evolved gas is measured using a Chandler Engineering Gasometer with an accuracy of 0.2%. Both temperature and

gas volume in the gasometer are recorded to calculate the mole numbers of ammonia dissolved in bitumen.

3.4 Thermodynamic model

The experimental data of ammonia solubility in Athabasca bitumen was modeled using Peng-Robinson equation of state (PR-EoS) [26] via PVT package (WINPROP) accessible in computer modeling group (CMG) software [27]. Peng-Robinson equation of state (PR-EoS) is expressed as the following:

$$P = \frac{RT}{V-b} - \frac{a\alpha(T)}{V(V+b)+b(V-b)} \quad \textbf{3.1}$$

where P is the absolute pressure in MPa, T is the absolute temperature in K, V is the molar volume in cm^3, and R is the universal gas constant 8.3144 MPa-cm^3/mole-K. The constants a and b are a function of critical properties of components as given:

$$a = \frac{\Omega_a R^2 T_c^2}{P_c} \quad \textbf{3.2}$$

$$b = \frac{\Omega_b R T_c}{P_c} \quad \textbf{3.3}$$

where $\Omega_a = 0.45724,\ \Omega_b = 0.07780$, T_c is the critical temperature in K, P_c is the critical pressure in MPa. The parameter $\alpha(T)$ is calculated as:

$$\alpha(T) = \left[1 + k\left(1 - T_r^{0.5}\right)\right]^2 \quad \textbf{3.4}$$

where T_r is the reduced temperature (T/T_c). The coefficient k is a function of the acentric factor (ω) and is expressed in two forms. The first form was proposed for light hydrocarbons (when $\omega < 0.49$) as:

$$k = 0.37464 + 1.54226\omega - 0.26992\omega^2 \quad \textbf{3.5}$$

In 1978, Peng and Robinson [28] introduced a cubic equation to calculate the coefficient k for heavier components (when $\omega > 0.49$) as the following [28]:

$$k = 0.3796 + 1.485\omega - 0.1644\omega^2 + 0.01667\omega^3 \quad \textbf{3.6}$$

A more recent form for calculating $\alpha(T)$ has been reported elsewhere [29].

Specific gravity (*SG*) and molecular weight (*MW*) of Athabasca bitumen were taken from Zirrahi *et al.* [19], and they were used to calculate the normal boiling point temperature (T_b) of bitumen using Goossen's correlation [30]. The specific gravity and boiling point temperature were used to calculate the critical temperature and acentric factor of the Athabasca bitumen using the Lee-Kesler correlation [31]. The critical pressure of Athabasca bitumn was tuned to match the experimental density data for bitumen at room temperature. The physical and critical properties of Athabasca bitumen and ammonia are given in Table 3.2.

The classical van der Waals mixing rules are used to calculate *a* and *b* parameters of the Peng-Robinson equation of state (PR-EoS) as:

$$a = \sum_i \sum_j x_i x_j \sqrt{a_i a_j}\,(1 - k_{ij}) \quad \textbf{3.7}$$

$$b = \sum_i x_i b_i \quad \textbf{3.8}$$

Where k_{ij} is the binary interaction coefficient between ammonia and Athabasca bitumen, and it was introduced to account for the molecular interactions between these dissimilar molecules.

Table 3.2. Physical and critical properties of Athabasca bitumen and ammonia

Property	Bitumen	Ammonia
Specific gravity (SG)	1.0004 (water =1)	0.6 (air =1)
MW (g/mol)	513	17.031
T_b (K)	822.03	239.72
T_c (K)	980.98	405.65
P_c (MPa)	1.137	11.278
ω	1.208	0.252

To improve the prediction of liquid phase density with equation of state, the volume shift parameter (S) was introduced into the Peng-Robinson equation of state (PR-EoS). This parameter modifies the liquid and vapor molar volumes as [32]:

$$V_{corr}^{L} = V^{L} - \sum_{i} x_i S_i \quad \textbf{3.9}$$

$$V_{corr}^{v} = V^{v} - \sum_{i} y_i S_i \quad \textbf{3.10}$$

where V^L and V^v are uncorrected liquid and vapor molar volumes calculated by equation of state in cm^3/mol, respectively. V_{corr}^{L} and V_{corr}^{v} are corrected liquid and vapor molar volumes in cm^3/mol, respectively. S_i is the volume shift parameter for the component *i*. In this study, the volume shift parameter was considered to be a linear function of temperature as [33]:

$$S_i = S_{0i} + S_{1i}(T - T_{ref}) \quad \textbf{3.11}$$

where S_{0i} is usual Peneloux parameter of component *i,* S_{1i} is the temperature dependent term for component *i*, T is the temperature in K, and T_{ref} is the reference temperature 288.15 K (15 °C). Usual Peneloux parameter of component *i* (S_{0i}) is calculated as:

$$S_{0i} = MW_i / \rho_i - V_i^{L} \quad \textbf{3.12}$$

where MW_i is the molecular weight of component i in gm/mol, ρ_i is the density of component i at 288.15 K and atmospheric pressure in gm/cm^3, and V_i^L is the molar volume of component i calculated by EoS (at 288.15 K and atmospheric pressure) in cm^3/mol.

3.5 Results

3.5.1 Experimental data

The solubility of ammonia in Athabasca bitumen was measured at six temperatures 348, 373, 398, 423, 448, and 463 K (75, 100, 125, 150, 175, and 190 ℃, respectively) and four pressures ranging from 1 to 4 MPa except for 348 K (75 ℃) where the saturation pressure of ammonia is less than 4 MPa. Figure 3.3 shows the saturation pressure of ammonia and the experimental conditions of this study at which solubility measurements were conducted. In this work, the solubilities of ammonia were measured at pressures below the saturation pressures to ensure vapor-liquid equilibrium (VLE) conditions.

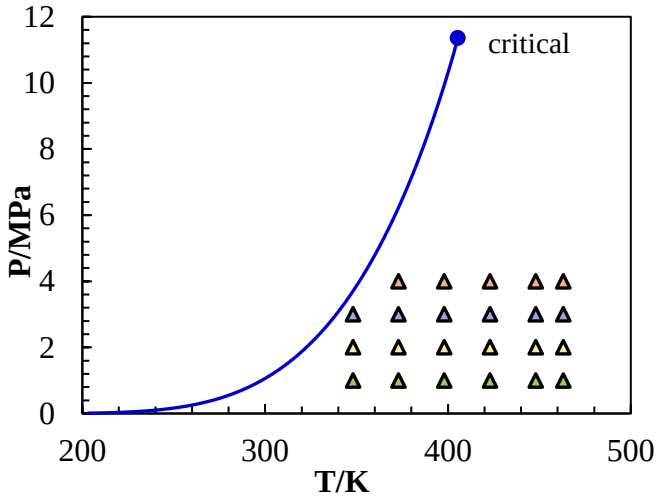

Figure 3.3. Saturation pressure of ammonia and the experimental conditions.

All data measured at 398 K (125 ℃) were repeated to check the repeatability of the experimental results. The experiments that were repeated at 1 and 4 MPa revealed excellent repeatability with less than 1% error in ammonia solubility whereas, those repeated at 2

and 3 MPa revealed a 3% error in ammonia solubility. The solubility of ammonia in bitumen and the density of ammonia saturated bitumen at different temperatures and pressures are summarized in Table 3.3.

Table 3.3. Experimental density, and solubility data of ammonia saturated-bitumen measured in this work. [a]

Pressure (MPa)	Temperature (K)	Density (kg/m^3)	NH_3 Solubility (mole fraction)
1.00	348.0	963.71	0.267
1.00	373.0	950.25	0.196
1.00	398.0	937.25	0.168
1.00	423.0	923.90	0.125
1.00	448.0	910.47	0.090
1.00	463.0	902.06	0.080
2.00	348.0	948.75	0.474
2.00	373.0	941.89	0.348
2.00	398.0	932.96	0.307
2.00	423.0	918.23	0.245
2.00	448.0	906.57	0.200
2.00	463.0	899.47	0.193
3.00	348.0	934.32	0.593
3.00	373.0	932.76	0.466
3.00	398.0	922.75	0.407
3.00	423.0	912.07	0.338
3.00	448.0	901.37	0.284
3.00	463.0	894.00	0.265
4.00	373.0	926.40	0.504
4.00	398.0	917.66	0.456
4.00	423.0	908.08	0.381
4.00	448.0	898.55	0.338
4.00	463.0	891.35	0.303

[a] The standard uncertainties (u) of pressures, temperatures, and ammonia solubilities are $u(P)$ = 0.008 MPa, $u(T)$ = 0.1 K, and $u(x)$ = 0.057, respectively. The relative expanded uncertainty (U_r) of density is $U_r(\rho)$ = 0.011. Uncertainty of density was calculated as follows. Combined uncertainty (u_c) was calculated by combining standard uncertainty of random error (u_{random}) due to the precision limitations of the instrument with a standard uncertainty of systematic error (u_{sys}) as $u_c = \sqrt{(u_{random})^2 + (u_{sys})^2}$. Then, the expanded uncertainty (U) was re-scaled by multiplying u_c with a coverage factor of 2, which corresponds to 95% confidence level as $U = 2u_c$. Expanded uncertainty was converted to the relative expanded uncertainty by dividing it by the average measurements of density and multiplying it by 100 as $U_r = U / \rho_{avg} \times 100$.

3.5.2 Modeling of the experimental data

Linear temperature-dependent volume shift parameters for the Athabasca bitumen (S_{0b} and S_{1b}) were tuned to match the experimental density data of pure bitumen at different temperatures ranging from 315 to 447 K (42 to 174 ℃) and two pressures, 1.12 and 3.5 MPa. The average absolute relative deviation percent (AARD%) between the calculated and experimental density data of pure bitumen was found as 0.146%. The tuned volume shift parameters of the Athabasca bitumen are given in Table 3.4. Figure 3.4 shows the calculated density versus the experimental density data of pure bitumen. Interaction coefficient between ammonia and Athabasca bitumen (k_{ij}) was tuned in the next step to match the experimental solubility data of ammonia in bitumen at different temperatures and pressures ranging from 348 to 463 K (75 to 190 ℃) and from 1 to 4 MPa, respectively. The AARD% between calculated and experimental solubility data is 8.537%. Figure 3.5 shows the solubility of ammonia in Athabasca bitumen versus pressure at different temperatures. The binary interaction coefficient between ammonia and Athabasca bitumen is given in Table 3.4.

Table 3.4. Volume shift parameters of Athabasca bitumen and ammonia and the interaction coefficient between ammonia and bitumen.

Component	Volume shift (S_0)	Volume shift coefficient (S_1) (1/°C)
Athabasca bitumen	0.066273	-0.000335
Ammonia	0.880000	-0.001341
Interaction coefficient between ammonia and Athabasca bitumen $\left(k_{ij} = 0.010584\right)$		

After determination of the interaction coefficient between ammonia and bitumen, linear temperature dependent volume shift parameters for ammonia (S_{0a} and S_{1a}) were also

tuned to match the experimental density data of ammonia saturated bitumen at different temperatures and pressures ranging from 348 to 463 K (75 to 190 °C) and from 1 to 4 MPa, respectively. The AARD% between the calculated and experimental density data is 0.218%. Figure 3.6 compares the calculated density with the experimental density data of ammonia saturated bitumen at different temperatures and pressures. The tuned volume shift parameters of ammonia are given in Table 3.4.

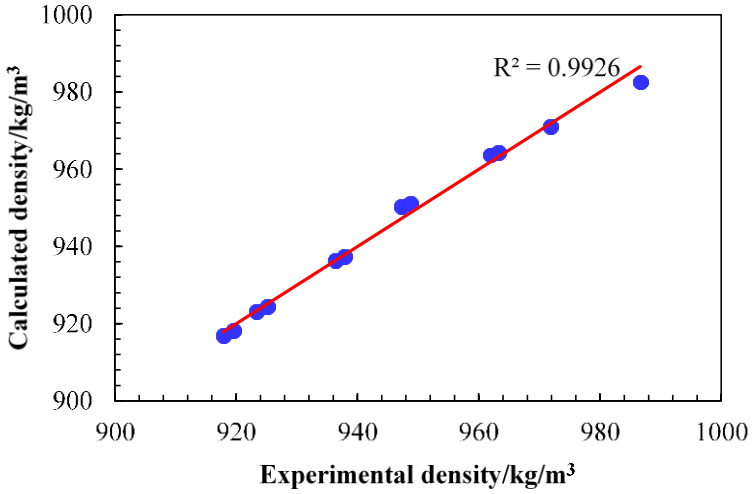

Figure 3.4. The calculated density versus the experimental density data of pure bitumen at different temperatures ranging from 315 to 447 K (42 to 174 °C) and two pressures, 1.12 and 3.5 MPa.

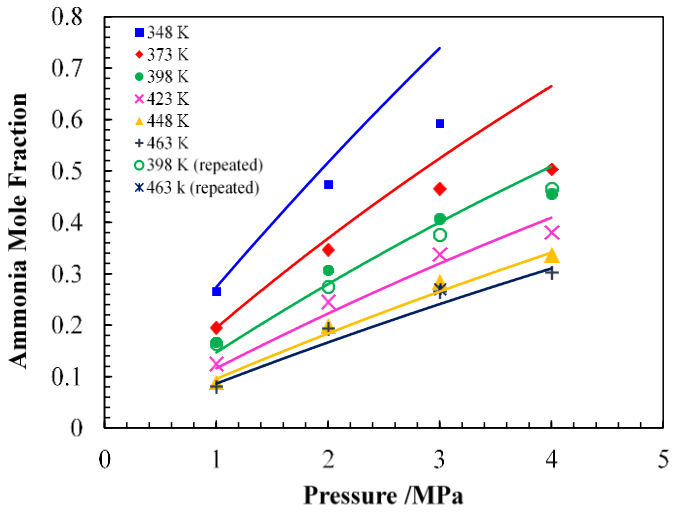

Figure 3.5. Experimental solubility data of ammonia/bitumen mixtures versus pressure at different temperatures of 348 K (■), 373 K (◆), 398 K (●), 423 K (x), 448 K (▲) and 463 K (+) compared with the predicted solubility obtained using equation of state.

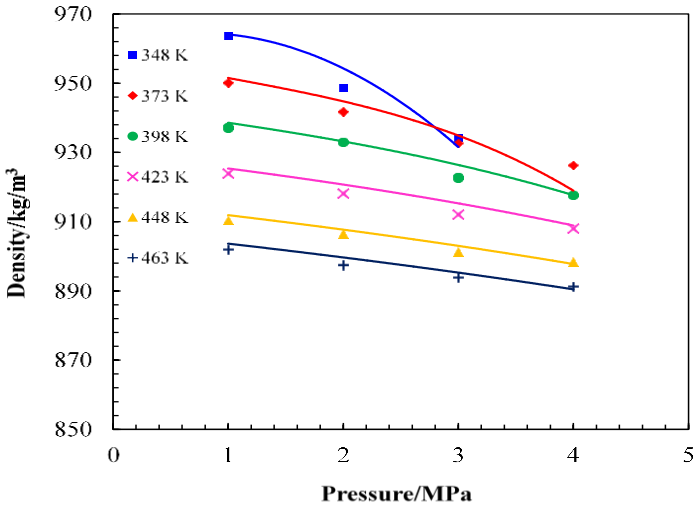

Figure 3.6. Experimental density data of ammonia saturated bitumen versus pressure at different temperatures of 348 K (■), 373 K (◆), 398 K (●), 423 K (x), 448 K (▲) and 463 K (+) compared with the predicted density obtained using the equation of state (lines).

3.6 Summary and conclusion

A new set of experimental data of ammonia solubility in Athabasca bitumen as well as density of bitumen-rich phase at different temperatures and pressures ranging from 348 to 463 K (75 to 190 °C**)** and 1 to 4 MPa, respectively, have been reported. The experimental data find applications in reservoir simulation of solvent-aided thermal recovery of bitumen and heavy oil. The experimental solubility and density data were modeled using the PR-EoS and classical Van der Waals mixing rules. Tuning of the linear temperature-dependent volume shift parameters for the Athabasca bitumen allowed matching the experimental density data of pure bitumen with an AARD of 0.146%. In addition, the interaction coefficient between ammonia and Athabasca bitumen was tuned to match the experimental ammonia solubility data with an AARD% of 8.537%. Linear temperature-dependent volume shift parameters for ammonia were tuned to represent the experimental density data of ammonia saturated bitumen with an AARD% of 0.218%. The results reveal that the PR-EoS gives an acceptable prediction of ammonia solubility in bitumen. The results showed that the density of ammonia-saturated bitumen at pressure and temperature ranges of solvent-aided thermal recovery of bitumen and heavy oil are in good agreement with the experimental data. The tuned model finds applications in reservoir modeling of solvent-aided thermal recovery of bitumen and heavy oil.

3.7 References

[1] Deo M, Wang C, Hanson F. Solubility of carbon dioxide in tar sand bitumen: experimental determination and modeling. Industrial & Engineering Chemistry Research 1991;30(3):532-536.

[2] Zirrahi M, Hassanzadeh H, Abedi J. Experimental measurements and correlation of K-value, viscosity, and density data for mixtures of light to heavy solvents and Athabasca bitumen with applications of ES-SAGD process. *SPE Canada Heavy Oil Technical Conference.* Society of Petroleum Engineers; 2016.

[3] Zirrahi M, Hassanzadeh H, Abedi J, Moshfeghian M. Prediction of solubility of CH_4, C_2H_6, CO_2, N_2 and CO in bitumen. The Canadian Journal of Chemical Engineering 2014;92(3):563-572.

[4] Yamchi H, Zirrahi M, Hassanzadeh H, Abedi J, Fadaei H. Effect of additives on liquid–liquid equilibrium properties of butane/bitumen systems with applications to solvent aided bitumen recovery processes. Chemical Engineering Research and Design 2018;137:452-460.

[5] Gümrah F, Baĝcı S. Steam—CO_2 drive experiments using horizontal and vertical wells. Journal of Petroleum Science and Engineering 1997;18(1-2):113-129.

[6] Stone T, Ivory J. An Examination of steam-CO processes. Journal of Canadian Petroleum Technology 1987;26(03): 54-61.

[7] Stone T, Malcolm J. Simulation of a large steam-CO co-injection experiment. Journal of Canadian Petroleum Technology 1985;24(06): 51-59.

[8] Redford D. The use of solvents and gases with steam in the recovery of bitumen from oil sands. Journal of Canadian Petroleum Technology 1982;21(01): 45-53.

[9] Meldau R, Shipley R, Coats K. Cyclic gas/steam stimulation of heavy-oil wells. Journal of Petroleum Technology 1981;33(10):1,990-1,998.

[10] Hornbrook M, Dehghani K, Qadeer S, Ostermann R, Ogbe D. Effects of CO_2 addition to· steam on recovery of West Sak crude oil. *SPE California Regional Meeting.* Society of Petroleum Engineers; 1989.

[11] Jacobs F, Donnelly J, Stanislav J. Viscosity of gas-saturated bitumen. Journal of Canadian Petroleum Technology 1980;19(04): 46-50.

[12] Zirrahi M, Hassanzadeh H, Abedi J. Experimental and modelling studies of MacKay River bitumen and light n-alkane binaries. The Canadian Journal of Chemical Engineering 2017;95(7):1417-1427.

[13] Haddadnia A, Azinfar B, Zirrahi M, Hassanzadeh H, Abedi J. Thermophysical properties of dimethyl ether/Athabasca bitumen system. The Canadian Journal of Chemical Engineering 2018;96(2):597-604.

[14] Haddadnia A, Sadeghi Yamchi H, Zirrahi M, Hassanzadeh H, Abedi J. New Solubility and viscosity measurements for methane–, ethane–, propane–, and butane–Athabasca bitumen systems at high temperatures up to 260° C. Journal of Chemical & Engineering Data 2018;63(9):3566-3571.

[15] Haddadnia A, Zirrahi M, Hassanzadeh H, Abedi J. Solubility and thermo-physical properties measurement of CO_2-and N_2-Athabasca bitumen systems. Journal of Petroleum Science and Engineering 2017;154:277-283.

[16] Azinfar B, Haddadnia A, Zirrahi M, Hassanzadeh H, Abedi J. A thermodynamic model to predict propane solubility in bitumen and heavy oil based on experimental

fractionation and characterization. Journal of Petroleum Science and Engineering 2018;168:156-177.

[17] Azinfar B, Haddadnia A, Zirrahi M, Hassanzadeh H, Abedi J. Generalized approach to predict K-values of hydrocarbon solvent/bitumen mixtures. *SPE Canada Heavy Oil Technical Conference.* Society of Petroleum Engineers; 2018.

[18] Azinfar B, Haddadnia A, Zirrahi M, Hassanzadeh H, Abedi J. Phase behaviour of butane/bitumen fractions: Experimental and modeling studies. Fuel 2018;220:47-59.

[19] Zirrahi M, Hassanzadeh H, Abedi J. Experimental and modeling studies of MacKay River bitumen and water. Journal of Petroleum Science and Engineering 2017;151:305-310.

[20] Fogg P. Ammonia solubilities. School of Chemistry, Polytechnic of North London, Holloway, London, U.K.; 1984.

[21] Shohaimi N, Bakar W, Jaafar J, Shukri N. Treatment of acidic petroleum crude oil utilizing catalytic neutralization technique of magnesium oxide catalyst. Modern Chemistry & Applications 2013; 1(3) 1000103.

[22] Dias H, Gonçalves G, Freitas J, Gomes A, De Castro E, Vaz B, et al. Catalytic decarboxylation of naphthenic acids in crude oils. Fuel 2015;158:113-121.

[23] Fu C, Puttangunla R, Vilcsak G. Vapour-liquid equilibrium properties for gas-Cold Lake bitumen. *Annual Technical Meeting.* Petroleum Society of Canada; 1986.

[24] Azinfar B, Zirrahi M, Hassanzadeh H, Abedi J. Characterization of heavy crude oils and residues using combined gel permeation chromatography and simulated distillation. Fuel 2018;233:885-893.

[25] Yaws CL. Chemical properties handbook. McGraw-Hill; 1999.

[26] Peng D, Robinson D. A new two-constant equation of state. Industrial & Engineering Chemistry Fundamentals 1976;15(1):59-64.

[27] Winprop. Winprop User's Manual. Calgary, Alberta, Canada 2004.

[28] Robinson D, Peng D. The characterization of the heptanes and heavier fractions for the GPA Peng-Robinson programs. Gas processors association; 1978.

[29] Heidaryan E. Comments on "Understanding cubic equations of state: A search for the hidden clues of their success". AIChE Journal 2019;65(1):460-461.

[30] Goossens A. Prediction of molecular weight of petroleum fractions. Industrial & engineering chemistry research 1996;35(3):985-988.

[31] Kesler M. Improve prediction to enthalpy of fractions. Hydrocarbon Processing 1976;55:153-158.

[32] Péneloux A, Rauzy E, Fréze R. A consistent correction for Redlich-Kwong-Soave volumes. Fluid phase equilibria 1982;8(1):7-23.

[33] Pedersen K, Milter J, Sørensen H. Cubic equations of state applied to HT/HP and highly aromatic fluids. *SPE Annual Technical Conference and Exhibition.* Society of Petroleum Engineers; 2002.

CHAPTER 4: EFFICIENCY OF UREA SOLUTIONS IN ENHANCED OIL RECOVERY*

4.1 Abstract

We examine the applicability of urea solutions as a novel and cost-effective chemical for enhanced oil recovery processes. Two sand pack flooding experiments were conducted using 5 and 10 wt.% urea solutions. Another flooding experiment was also carried out using the same sand pack with fresh water and used as a reference. Supporting experiments such as interfacial tension (IFT), viscosity of water in oil (W/O) emulsions, total acid number (TAN), and Fourier-transform infrared (FTIR) spectroscopy were conducted to confirm the generation of in situ surfactants by reacting urea solutions with the naphthenic acids in bitumen and evaluate their impact on the oil recovery. The analyses of FTIR, IFT, TAN and viscosity measurements support the generation of in situ surfactants that leads to the formation of stable water in oil emulsions and hence more stable displacement front resulting in higher oil recovery.

Keywords: Urea solution; thermal recovery; solvent-aided recovery; naphthenic acids; enhanced oil recovery; in situ surfactants.

4.2 Introduction

Global reserves of bitumen and extra heavy crude oils are three times higher than the conventional crude oils with 10 trillion barrels of bitumen around the world [1]. Steam-assisted gravity drainage (SAGD) and cyclic steam stimulation (CSS) are the most

* BinDahbag, M., Mohammadi, M., Khalifi, M., Aghajamali, M., Zirrahi, M. and Hassanzadeh, H., 2020. Efficiency of urea solutions in enhanced oil recovery. ACS omega, 5(11), pp.6122-6129.

common techniques that have been utilized to recover the bitumen [2]. These recovery techniques are associated with high energy consumption for steam generation, excessive water treatment, and greenhouse gas emissions. To overcome these challenges, co-injection of solvents with steam has been suggested [3, 4]. Hydrocarbons such as pentane and hexane are examples of the solvents that have been proposed to reduce the required steam in expanding solvent steam-assisted gravity drainage (ES-SAGD) process [5]. Recovery processes such as CSS and SAGD mobilize viscous bitumen through viscosity reduction by heating, while in solvent-aided methods, both heat and dilution effects are utilized to mobilize the bitumen [6]. To the best of our knowledge, only a few studies have examined factors other than viscosity reduction to improve the recovery of bitumen using ES-SAGD processes [6, 7]. Urea is a potential candidate that can synergize the reduction in bitumen viscosity and sweep efficiency improvement [8]. Several chemicals such as surfactants, alkaline, and ionic liquids have been proposed in the literature to decrease the interfacial tension and change the rock wettability toward more water-wet, thereby improving the sweep efficiency of crude oil [9-17].

Urea solution has a basic nature due to the presence of amino functional groups in the urea molecular structure, enabling it to react with naphthenic acids found in bitumen and generate in situ surfactants [18]. Urea melts at 406 K (133 ℃) and starts to decompose to ammonia and isocyanic acid (HCNO) at 425 K (152 ℃), which is much lower than the usual SAGD temperature [19, 20]. However, at the steam chamber condition of SAGD, above 473 K (200 ℃), the urea solution partially decomposes into ammonia and carbon dioxide [6]. As a result of the decomposition at high temperatures, urea combines the advantages of ammonia and carbon dioxide. Ammonia also dissolves strongly in water

condensing from steam to generate a basic solution of ammonium hydroxide (NH_4OH) which in turn reacts with naphthenic acids found in bitumen to generate in situ surfactants [6, 21]. By virtue of in situ surfactant, water in oil (W/O) emulsion is generated and thus, the sweep efficiency of the process is improved through the reduction of viscous fingering as a result of a more stable displacement front. Water in oil (W/O) emulsions formed through an alkaline environment are usually more viscous than fresh water in the SAGD process, leading to the suppression of viscous fingers formed through the flooding process [22]. Moreover, flooding the reservoir with alkaline solutions changes the rock wettability toward more water-wet due to the presence of polar compounds in alkaline solutions, which are adsorbed to rock surface containing different charges [23]. In addition to the generation of in situ surfactants, ammonia effectively reduces the viscosity and the total acid number (TAN) of acidic crude oil, making it more valuable and desired for refining [21, 24, 25]. According to ASTM D664, the total acid number is the milligram of potassium hydroxide (KOH) that should be added into the solution to neutralize the acidic compounds found in 1 gram of the crude oil [26]. Carbon dioxide is another important product resulting from the decomposition of the urea solution at the SAGD steam chamber conditions. Carbon dioxide easily dissolves in bitumen and improves oil mobility due to the viscosity reduction, oil swelling, and lowering the interfacial tension with formation brine [7, 27, 28]. Furthermore, carbon dioxide is a non-condensable gas at the conditions of the steam chamber that can reduce heat loss to the overburden formation leading to the recovery improvement [6, 29].

This study aims to investigate the capability of urea solution to improve the sweep efficiency of bitumen via altering the rock wettability toward water-wet and/or reduction

of IFT. Sand pack flooding experiments were conducted to investigate the efficiency of urea solutions in the recovery of bitumen. The overall goal of this work is to investigate the generation of in situ surfactants through the reaction of naphthenic acids found in bitumen with urea solutions and improving our understanding of the underlying mechanisms.

4.3 Materials

Athabasca bitumen with a specific gravity of 1.004 (°API = 9.44), a viscosity of 29 cP at 423 K (150 ℃) and 3.45 MPa, and molecular weight of 513 g/mol was used as an oleic phase through the flooding experiments. The molecular weight of bitumen was measured using the freezing point depression technique. Simulated distillation test (ASTM 7169) and the carbon number distribution of the Athabasca bitumen have been reported in the literature [30, 31]. High purity urea (99.9%) provided by Amresco VWR Chemicals was dissolved in deionized water to prepare urea solutions. A sand pack was prepared and packed with fine glass beads of 120 mesh size to generate the porous medium for the flooding experiments.

4.4 Experimental work

4.4.1 Sand pack flooding setup

Flooding experiments were conducted using a 1-D sand pack flooding experimental rig shown in Figure 4.1. The experimental rig consists of an axial vertical core holder packed with glass beads to prepare the sand pack. A hydraulic hand pump is used to apply vertical pressure on the sand pack to imitate the overburden pressure. A vacuum pump is utilized to vacuum the sand pack and ensure there is no air trapped in the sand during the flooding tests. A back-pressure regulator designed and made by a machine shop at the University

of Calgary is installed to keep the pore pressure at the desired value. A Quizix pump (QX6000) is used to inject water, bitumen, and urea solutions through imbibition and drainage processes. The accuracy of the injection rate of Quizix pumps is ±0.001 $cm^{3,}$ whereas the maximum flow rate and maximum pressure that can be achieved are 50 cm^3/min and 41 MPa (6000 psi), respectively. To protect the pump from corrosion, the urea solutions are injected indirectly into the sand pack from an external stainless-steel transfer cylinder. A pressure transducer from Sensotec Company with a range from 0 to 100 psi (~ 0.7 MPa) is used to measure the pressure drop along the sand pack during the bitumen recovery process. Pressure drop data is recorded and logged using SOLO 9696 data acquisition. The core holder, back-pressure regulator, and bitumen accumulator were placed inside a temperature-controlled oven from VWR Company to control the temperature. A heat exchanger is used for heating the urea solution before being injected into the sand pack to ensure the solution enters the sand pack at the desired temperature. All fluids produced from the sand pack are collected in graduated flasks to obtain the recovery data as a function with time.

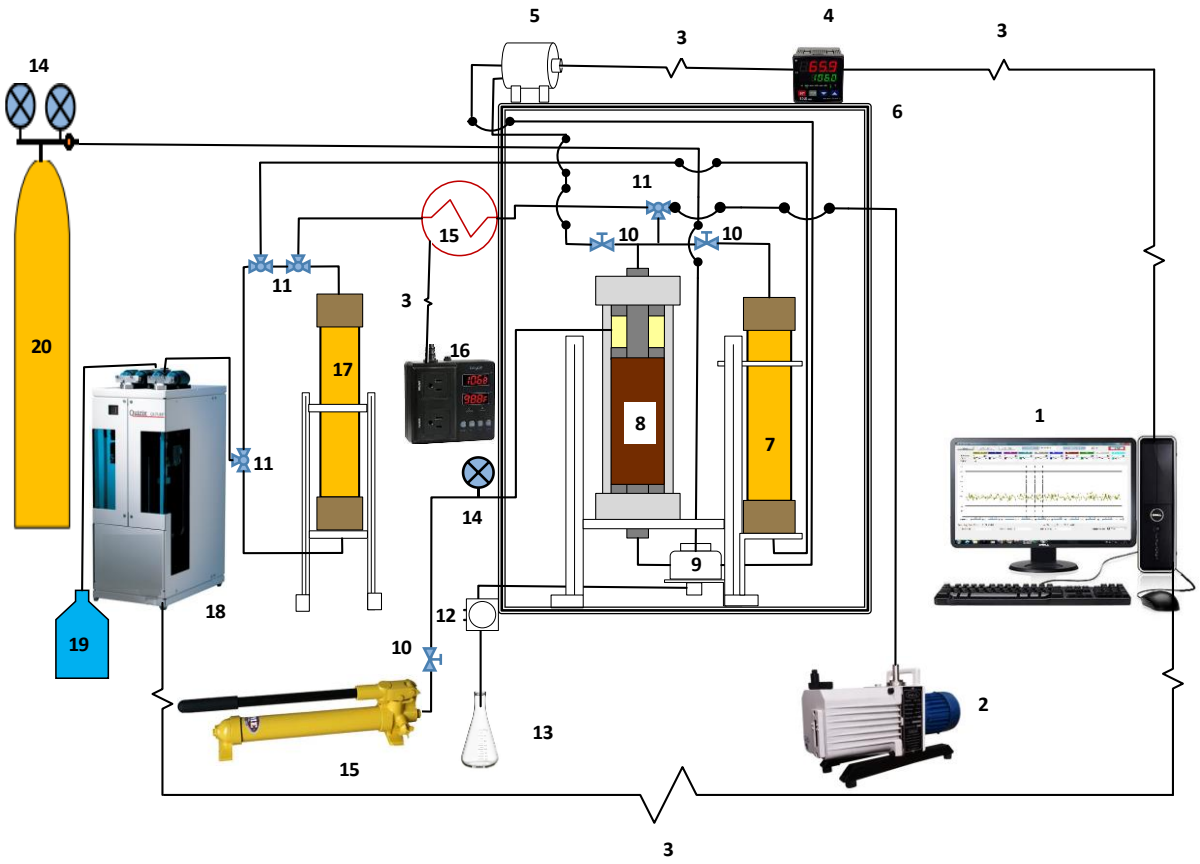

Figure 4.1. A schematic diagram shows the sand pack flooding setup used for the flooding experiments. 1) computer, 2) vacuum pump, 3) USB cable, 4) data acquisition unit, 5) pressure transducer, 6) oven, 7) bitumen accumulator, 8) axial sand pack core holder, 9) back pressure regulator, 10) 2-ways valve, 11) 3-ways valve, 12) water cooler, 13) graduated flask, 14) pressure gauge, 15) heat exchanger, 16) heat controller, 17) urea solution accumulator, 18) Quizix pump, 19) distilled water container, 20) nitrogen cylinder.

4.4.2 Flooding experiments procedure

The axial core holder is packed with glass beads using the hammering technique to achieve porosity and permeability as close as to the reservoir condition. Porosity and absolute permeability measured in these experiments are shown in table 4.1. Then, the sand pack is confined vertically with 1000 psig (~ 7 MPa) overburden pressure and flooded with

carbon dioxide (CO_2) for 30 minutes at 50 psig (~ 0.345 MPa) inlet pressure while the outlet is open to the atmosphere to displace air from the sand pack. After that, the sand pack is vacuumed for 1 hour to remove CO_2 as much as possible prior to water imbibition. The sand pack is then fully saturated with distilled water and pressurized to 500 psig (3.45 MPa) using the Quizix pump. Porosity and pore volume of the sand pack are reported based on the amount of water imbibed into the sand pack. Absolute permeability of the sand pack is calculated using Darcy's law after measuring the pressure drop through the sand pack at different water flow rates ranging from 1 to 16 cm^3/min. The sand pack is brought to 423 K (150 ℃) for three hours to ensure a thermal equilibrium at the desired temperature and then flooded with hot bitumen to establish the initial oil saturation (S_{oi}). The flooding with hot bitumen is continued for more than one pore volume (PV) of the sand pack to ensure no further water is produced. The displaced water is cooled and collected using graduated flasks to measure the irreducible water saturation (S_{wirr}) of the sand pack after eliminating the dead volume of tubes. Finally, the urea solution is injected from the top side of the sand pack at a flow rate of 1 cm^3/min and 500 psig (3.45 MPa) pore pressure to recover bitumen from the bottom side. In all flooding experiments, pressure drops of 0.003 to 0.007 MPa are observed. The flooding process is continued until the effluent fluid is only water. The produced emulsion is collected as discrete samples with volumes ranging from 50 to 100 cm^3 based on the abundance of bitumen in the produced emulsion. The produced bitumen volume is then used to calculate the residual oil saturation left in the sand pack.

4.5 Results and discussion

4.5.1 Sand pack flooding experiments

Three flooding experiments, including water flooding, 5 wt.% urea solution flooding, and 10 wt.% urea solution flooding, were conducted. The properties of the sand packs used in these experiments (length, bulk volume, pore volume, porosity, absolute permeability, and irreducible water saturation) are reported in Table 4.1. In the first experiment, the water flooding was started at initial oil saturation (S_{oi}) of 0.873. More than 5.2 pore volumes (PV), 1430 cm^3, of fresh water was injected continuously into the sand pack at a flow rate of 1 cm^3/min until an effluent water cut of 99% is reached. The results shown in Figure 4.2 demonstrate that ~73% of the original-oil-in-place (OOIP) was produced at the end of the hot water flooding process. In addition, the result shows an early water breakthrough at 6% of the PV of water injection.

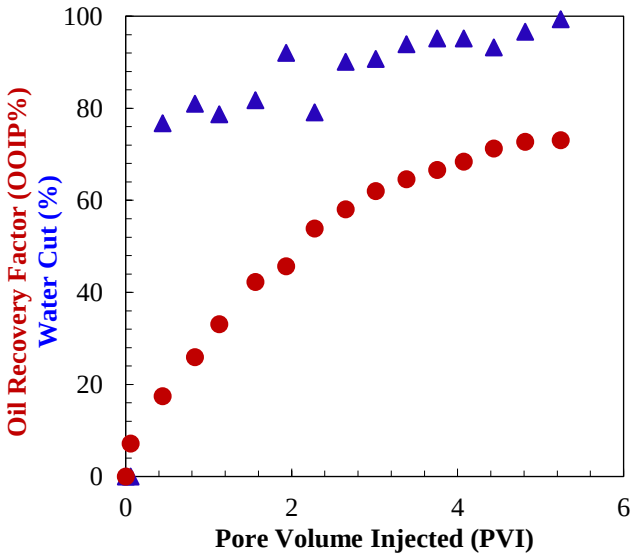

Figure 4.2. Oil recovery (●), and water cut (▲) of the first scenario (hot water flooding at T = 150 ºC).

In the second experiment, the sand pack with an initial oil saturation of 0.911 was flooded with 4.37 PV (1174 cm^3) of 5 wt.% urea solution until a water cut of 93% was achieved. The results reported in Figure 4.3 show that the breakthrough occurred at 12.2% of the pore volume injection compared to 6% in the first experiment, which indicates a noticeable delay in the breakthrough time. Around 72% of the OOIP was produced at the end of the flooding experiment.

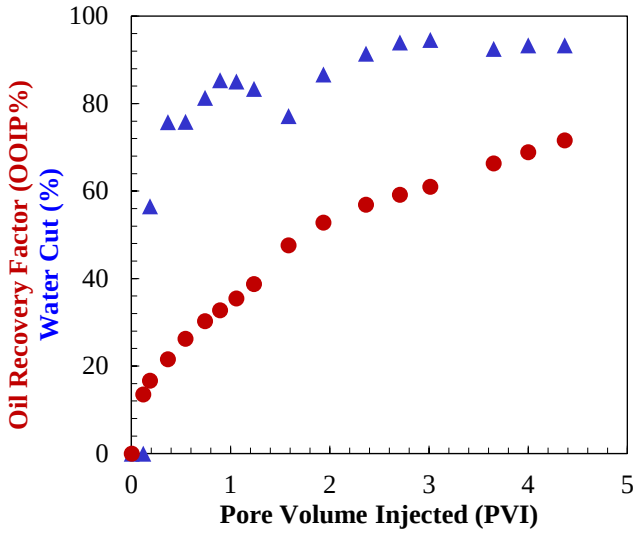

Figure 4.3. Oil recovery (●), and water cut (■) of the second scenario (5 wt. % urea solution at T = 150 ºC).

In the third experiment, 3.93 PV (1044 cm^3) of 10 wt.% urea solution was injected into the sand pack at an initial oil saturation of 0.863. The results shown in Figure 4.4 demonstrate breakthrough time at 12.8% PV of injection, which is comparable with the 5 wt.% urea solution injection. About 76% of the original-oil-in-place (OOIP) was produced at the end of the displacement with a water cut of 91% for the 10 wt.% urea solution flooding process.

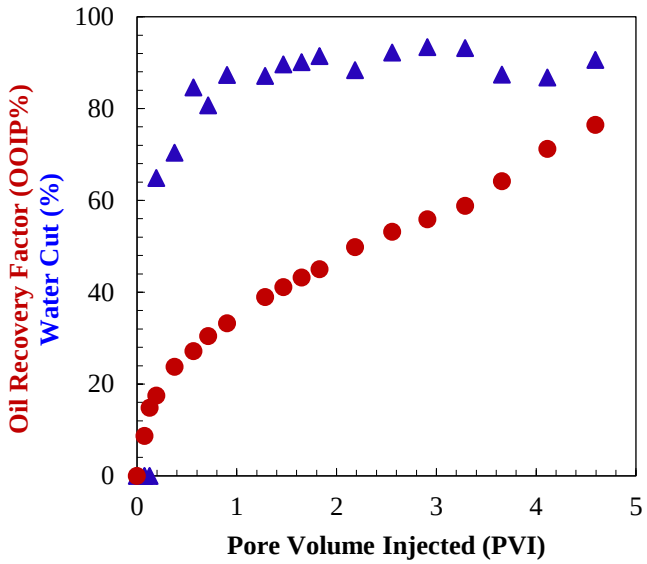

Figure 4.4. Oil recovery (●), and water cut (▲) of the third scenario (10 wt.% urea solution at T = 150 ºC).

Table 4.1. The sand pack petrophysical properties.

Injected solution	Length, cm	Bulk volume, cm^3	Pore volume, cm^3	Porosity, %	Absolute permeability, D	Irreducible water saturation after oil flooding
Water flooding	26.0	736.4	273.2	37.1	14.1	0.127
5 wt.% urea solution	26.2	742.1	268.9	36.2	11.4	0.089
10 wt.% urea solution	26.0	736.4	265.4	36.0	12.3	0.137

4.5.2 Comparison of the flooding experiments

Figure 4.5 presents the oil recovery factor at one and two pore volumes of injection for all the sand pack flooding experiments. The results show that both 5 and 10 wt.% urea solutions outperform water flood at 1 PV of injection, while 5 wt.% urea solution is more efficient than water flood and 10% urea solution at 2 PV of injection. The results clearly indicate that the recovery of bitumen has improved when the urea solution is injected. One reason behind the additional oil recovery can be due to the generation of in situ surfactants

and subsequent emulsification. The emulsification caused by the presence of surfactants leads to the formation of a high viscous zone leading to a more stable displacement front (less severe viscous fingering) and thus improves the oil recovery. In addition, in situ surfactants generated as a result of the interaction of urea solutions with naphthenic acids found in bitumen at high temperature the dispersion of water droplets inside the oil phase. In the following section, we have measured the interfacial tension (IFT) of the urea solutions with bitumen, the viscosity of W/O emulsions, the total acid number (TAN), and Fourier-Transform Infrared (FTIR) to further support this observation.

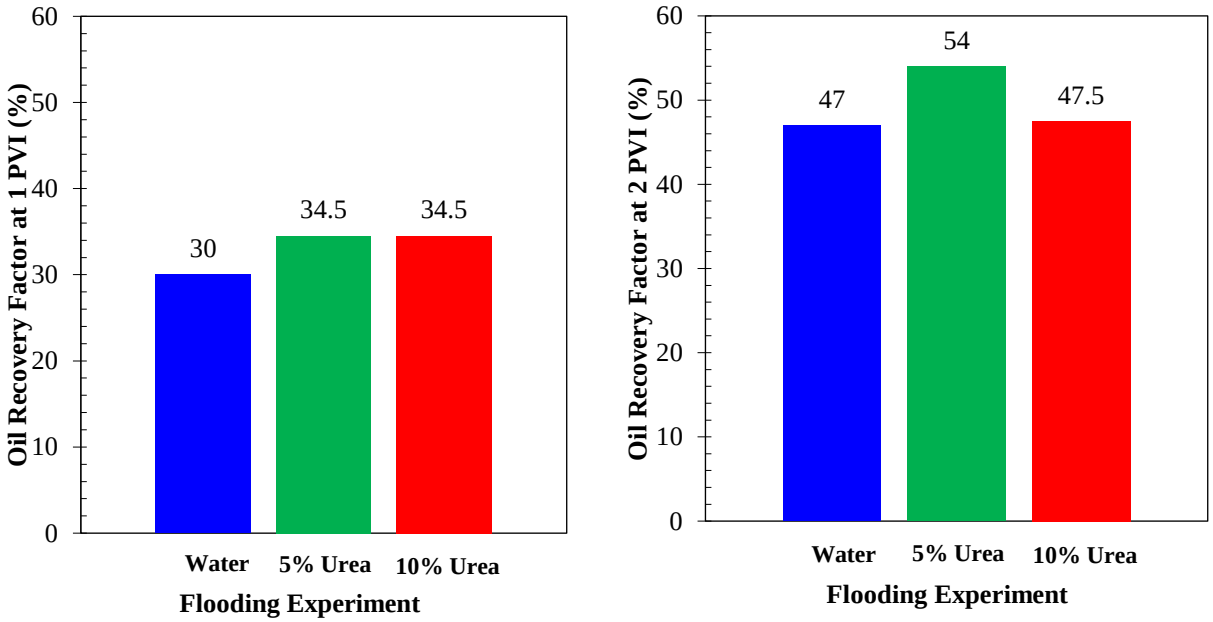

Figure 4.5 . Oil recovery factor of all three flooding experiments at one (left) and two (right) pore volumes injected.

4.5.3 Measurements of interfacial tension (IFT)

Two concentrations of urea solutions (10 and 15 wt.%) were prepared to measure the interfacial tension (IFT) with bitumen at 373 K (100 ℃) and 500 psig (3.45 MPa) using a

pendant drop tensiometer as shown in Figure 4.6 [32]. The tensiometer has a high-pressure, high-temperature isolated cell with a volume of 600 cm^3. A Quizix pump was utilized to inject a small droplet of bitumen from a standard needle into the isolated cell which was prefilled with urea solution. Two thermocouple probes were used to monitor and control the temperature inside and outside of the isolated cell using a temperature controller. A cell containing water and pressurized by nitrogen was connected to the system to keep the pressure of the system constant at 500 psig (3.45 MPa). The light, digital camera, and software from Rame-hart Instrument Company were used to record video frames and process them to obtain interfacial tension using Young–Laplace equation [33]. Densities of water and bitumen are nearly equal at 423 K (150 ℃), which makes the IFT measurements using the pendant drop tensiometer very difficult, if not impossible. For that reason, IFT measurements for bitumen/water and bitumen/urea solutions using the pendant drop tensiometer were not feasible. However, for the purpose of this study, a qualitative trend of the IFT would allow interpretation of our experimental observations of the bitumen recovery factor. To increase the density difference between bitumen and urea solutions, the IFT measurements have been conducted at high concentrations of urea (10 and 15 wt.%) and 373 K (100 ℃). The IFT measurements were started as soon as the oil drop was formed at the tip of the needle, and the IFT data were recorded at the rate of 1 frame/second for 2000 seconds. To ensure the reproducibility of the results, each experiment was repeated twice, and the final value was reported as an average of the last 100 second experimental data. The IFT of bitumen and water measured by the pendant drop method at 363 K (90 ℃) has been reported to be 34 mN/m [34]. The results shown in Figure 4.7 reveal that the interfacial tension of the urea solution and bitumen decreases by increasing

the urea concentration. This observation supports the fact that urea promotes water and oil emulsification due to the generation of in situ surfactants,[34-36], leading to the additional recovery of bitumen [34-36].

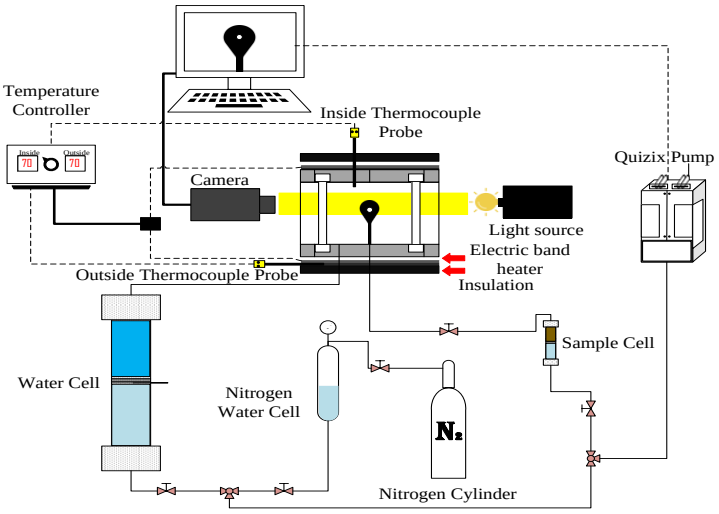

Figure 4.6. A schematic diagram of the high-temperature, high-pressure IFT apparatus.[32]

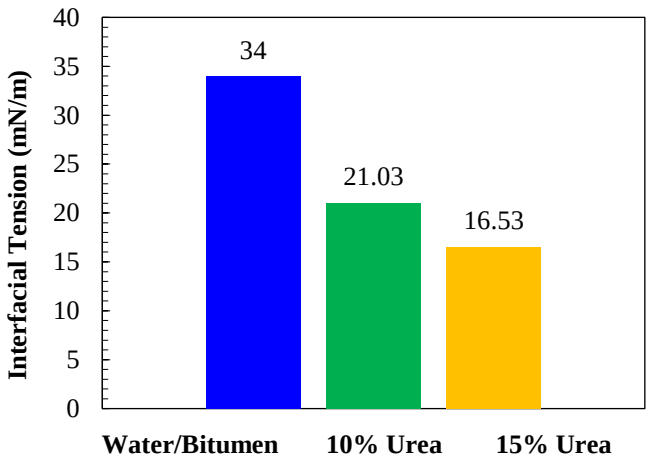

Figure 4.7. Equilibrium interfacial tension between bitumen and different concentrations of urea solutions at 373 K (100 ℃) and 500 psig (3.45 MPa). The IFT of water/bitumen system is reported elsewhere [34].

4.5.4 Measurements of viscosity of W/O emulsions

Two W/O emulsions were prepared by stirring 15 g of bitumen with 30 g of 5 and 10 wt.% urea solutions for two days at 423 K (150 ℃) and 400 rpm. Then, the mixtures were left for two weeks to allow the separation of the two stable phases, including W/O emulsion on the top and O/W emulsion at the bottom. Small samples of each W/O emulsion were charged into the pressure cell of an MCR 302 Anton Paar rheometer to measure the viscosity of emulsions at 423 K (150 ℃) and 500 psig (3.45 MPa). The results shown in Figure 4.8 reveal that the W/O emulsion treated with 10 wt.% urea solutions has a higher viscosity compared to 5 wt.% urea solution in the typical shear rate of 20-100 s^{-1}. The high viscosity of the W/O emulsion treated with 10 wt.% urea solution is attributed to the small droplet size of water inside oil through generation W/O emulsion [37]. The measured higher viscosity of the 10 wt.% urea solution is consistent with the lower interfacial measurements for the same solution. Certainly, viscosities of these emulsions are higher than the viscosity of oil in water (O/W) emulsions produced through the water flooding, which are less than 1 cP at the operating condition of our experiments. The high viscosity of W/O emulsions generated through urea solution flooding leads to the suppression of viscous fingering and delays the water breakthrough to 0.12 PV compared to 0.06 for the case of water flooding.

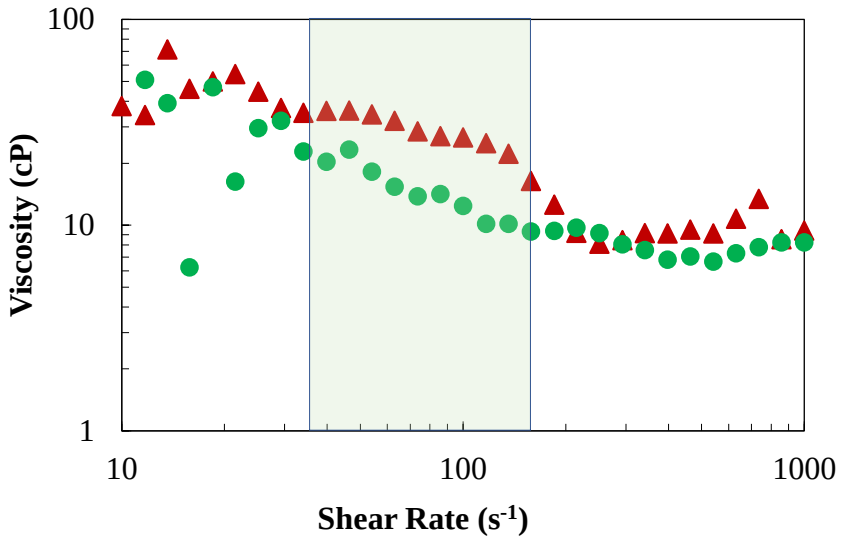

Figure 4.8. The viscosity of W/O emulsions as a function with shear rate at 423 K (150 °C) and 500 psi (3.45 MPa). (●) 5 wt.% urea solution, (▲) 10 wt.% urea solution. The shaded area shows the typical shear rate.

4.5.5 Measurements of total acid number (TAN)

The total acid number of the untreated bitumen was measured to be 3.768 mg/g. To measure the total acid number of the urea-treated bitumen, three samples of the bitumen produced from each experiment (5 and 10 % urea solution flooding) were collected separately at different times. The total acid number (TAN) of each sample was measured three times using a Metrohm 848 Titrino Plus instrument, and the results are reported in Table 4.2. First, 1.5 g of each sample was diluted in 10 cm^3 of toluene to break the W/O emulsion formed through the flooding process. Then, the solution was washed four times with 40 cm^3 of deionized water and centrifuged for two minutes at 4000 rpm to remove acidic water droplets and urea contaminations from the treated bitumen. The arithmetic average of the TAN values as a function of the pore volume injected (collection time) is reported in Table 4.2. The results shown in Figure 4.9 reveal a significant reduction in the

total acid number of the urea-treated bitumen. The TAN values for the produced bitumen through the urea solution flooding decrease sharply for the first two pore volumes of injected, followed by gradual increases over time. The results shown in Figure 4.9 confirm the reaction of urea solution by the naphthenic acids as evidenced in TAN reduction and formation of stable water in oil emulsion in sand pack flooding experiments. The sharp decrease in the total acid number is due to the sufficient contact and the reaction between the urea solution and the naphthenic acids in bitumen. The small gradual increase in TAN may be attributed to the poor contact between the injected urea solution and bitumen at the later stage of the displacement process that prevents the reaction with the naphthenic acids.

Table 4.2. Total acid number (TAN) of treated bitumen at different collection times.

Solution	**Collection time, hrs**	**TAN Measurements (mg/g)**			**Average (mg/g)**
Untreated bitumen	-	3.77			3.77
5 wt.% urea solution	7	1.46	1.62	1.46	1.51
5 wt.% urea solution	13	1.86	2.10	1.95	1.97
5 wt.% urea solution	18	2.29	2.08	2.18	2.18
10 wt.% urea solution	6	2.54	2.45	2.50	2.50
10wt.% urea solution	10	1.91	1.76	1.59	1.75
10 wt.% urea solution	19	1.97	2.06	1.82	1.95

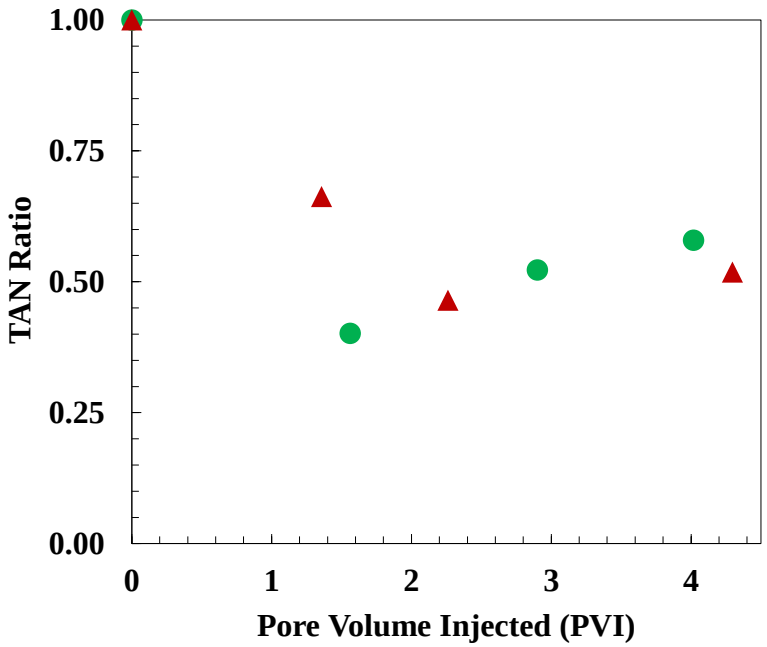

Figure 4.9. Total acid number (TAN) of bitumen treated with 5% and 10% wt. urea solutions at different collection times. (●) 5 wt.% urea solution, (▲) 10 wt.% urea solution.

4.5.6 Fourier-transform infrared spectroscopy (FTIR)

The FTIR spectroscopy provides information on the chemical structure and composition of bitumen. Representative FTIR spectra of bitumen samples obtained after the water flooding experiment and reactions with 5 and 10 wt.% urea solutions are presented in Figure 4.10. The FTIR spectra of all samples indicate expected features, as evident in the FTIR spectrum of bitumen derived from Athabasca oilsands [38] . Figure 4.10 shows intense absorptions at 2850−2950 and 1370−1465 cm^{-1} corresponding to C−H stretching (ν(C−H)) and bending (δ(C−H)) vibrations, respectively. The peaks at 1601 and 3052 cm^{-1} represent, respectively, the aromatic C=C and C−H stretching vibrations, which indicate the presence of aromatic rings in bitumen samples. Also, the absorptions at 1650−1710 and

3175−3550 cm^{-1} corresponds to C=O and overlapping O−H/N−H stretching vibrations, respectively; this verifies the presence of carboxyl or amide groups in bitumen samples. As seen in Figure 4.10, the carbonyl peak in the water flooding sample is around 1700 cm^{-1}. Interestingly, after the reaction of bitumen with 5 or 10 wt.% urea solutions at 423 K (150 ℃), the carbonyl peak shifts to around 1670 cm^{-1} and becomes more evident in the FTIR spectra of 5 and 10 wt.% urea-treated samples. This is an indication of the formation of the amide functional group and consequently verifies the formation of amide surfactants through the reaction of carboxylic acids found in bitumen with urea in 5 and 10 wt.% urea solutions.

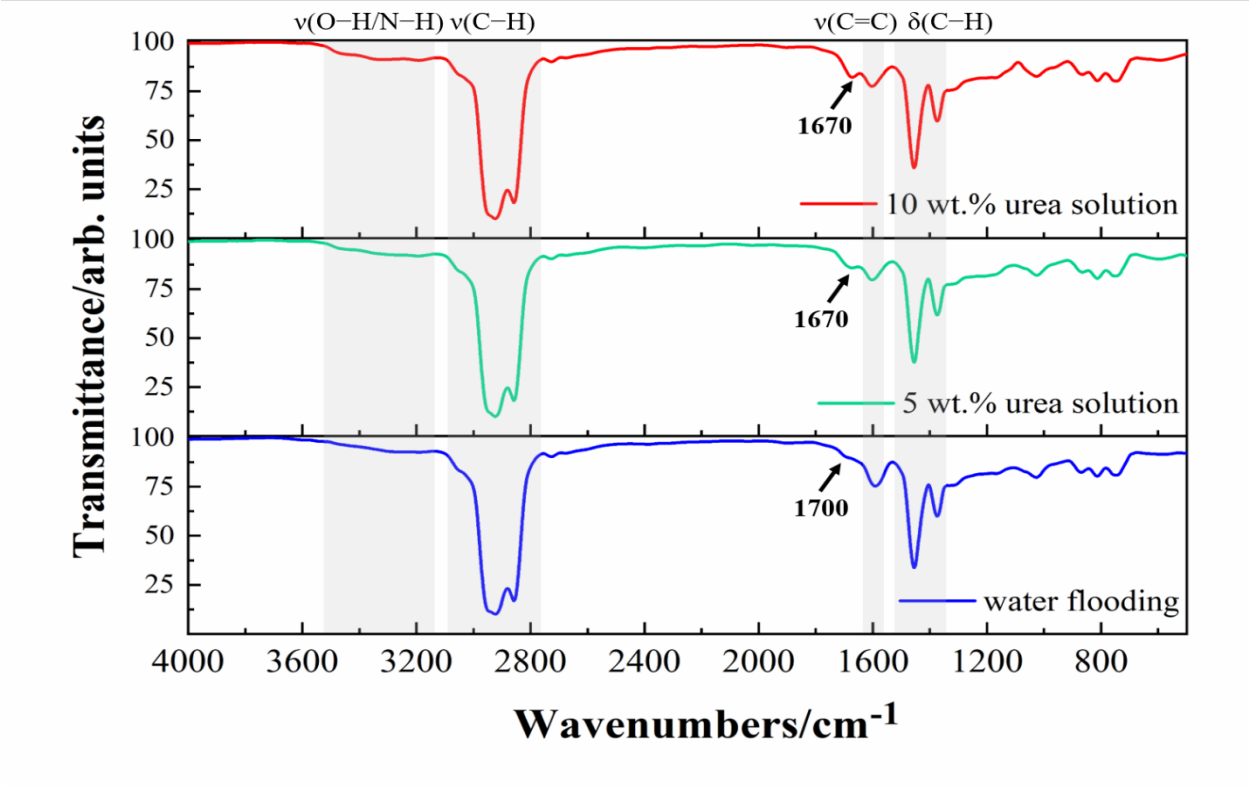

Figure 4.10. Fourier transform infrared spectra of bitumen samples obtained after the water flooding experiment and reactions with 5 and 10 wt.% urea solutions.

4.6 Conclusion

Three sand pack flooding experiments were conducted to investigate the efficiency of urea solutions as a novel solvent for solvent-aided thermal recovery processes. Our results indicated that urea solutions accelerate the oil recovery due to generating W/O emulsion, highlighting the synergy between the reduction in viscosity of bitumen and the generation of in situ surfactant through the flooding process. The results indicated that emulsification at the displacement front leads to the formation of an emulsion that has a significantly higher viscosity than the aqueous urea solution leading to a more stable displacement front through the suppression of the viscous fingering and consequently higher oil recovery. Interfacial tension measurements revealed a noticeable reduction in the interfacial tension of the bitumen/water in the presence of urea in the aqueous phase solution. In addition, measurements verified a significant reduction in the total acid number (TAN) of the treated bitumen. To reveal the source of the IFT and TAN reductions, FTIR measurements were conducted. The analysis of the FTIR measurements indicated that the reaction of carboxylic acids found in bitumen with the aqueous urea solutions led to the formation of amide functional group, and thus the formation of amide surfactants, which confirms IFT and TAN reductions. Comparisons of the flooding experiments revealed that there is an optimum concentration of urea solution that leads to more efficient displacement of oil by urea solutions, which may be due to the effect of urea solutions on the wettability of the sand. Future studies should focus on the wettability alteration of sands due to the generation of in-situ surfactants resulted from the reaction of urea solutions with naphthenic acids.

4.7 References

[1] Farouq Ali S, Jones J, Meldau R. Practical heavy oil recovery. University of Alberta, Alberta 1997.

[2] Yang P, Li H, Yang D. Determination of saturation pressures and swelling factors of solvent (s)–heavy oil systems under reservoir conditions. Industrial & Engineering Chemistry Research 2014;53(5):1965-1972.

[3] Zirrahi M, Hassanzadeh H, Abedi J. Experimental measurements and correlation of K-value, viscosity, and density data for mixtures of light to heavy solvents and Athabasca bitumen with applications of ES-SAGD process. *SPE Canada Heavy Oil Technical Conference.* Society of Petroleum Engineers; 2016.

[4] Sherratt J, Sharifi Haddad A, Rafati R. Hot solvent-assisted gravity drainage in naturally fractured heavy oil reservoirs: A new model and approach to determine optimal solvent injection temperature. Industrial & Engineering Chemistry Research 2018;57(8):3043-3058.

[5] Orr B. ES-SAGD; past, present and future. *SPE Annual Technical Conference and Exhibition.* Society of Petroleum Engineers; 2009.

[6] Guo E, Jiang Y, Gao Y, Shen D, Zhigang C, Yu P. A new approach to improve recovery efficiency of SAGD. *SPE Middle East Oil & Gas Show and Conference.* Society of Petroleum Engineers; 2017.

[7] Erpeng G, Hongyuan W, Oilfield L, Youwei J, Yongrong G, Junhui S. Experimental study of urea-SAGD process. *SPE EOR Conference at Oil and Gas West Asia.* Society of Petroleum Engineers; 2018.

[8] Li K. Performace of urea-based in-situ CO_2 EOR: Influences of different porous media. University of Oklahoma, USA 2018.

[9] BinDahbag M, Al Quraishi A, Benzagouta M, Kinawy M, Al Nashef I, Al Mushaegeh E. Experimental study of use of ionic liquids in enhanced oil recovery. Journal of Petroleum & Environmental Biotechnology 2014;4(165): 1000165.

[10] BinDahbag M, AlQuraishi A, Benzagouta M. Efficiency of ionic liquids for chemical enhanced oil recovery. Journal of Petroleum Exploration and Production Technology 2015;5(4):353-361.

[11] Javanmard H, Seyyedi M, Nielsen S. On oil recovery mechanisms and potential of DME–brine injection in the North Sea chalk oil reservoirs. Industrial & Engineering Chemistry Research 2018;57(46):15898-15908.

[12] BinDahbag M, Hossain M, AlQuraishi A. Efficiency of ionic liquids as an enhanced oil recovery chemical: simulation approach. Energy & Fuels 2016;30(11):9260-9265.

[13] BinDahbag M, Hossain M. Simulation of ionic liquid flooding for chemical enhance oil recovery using CMG STARS software. *SPE Kingdom of Saudi Arabia Annual Technical Symposium and Exhibition.* Society of Petroleum Engineers; 2016.

[14] Rezk M, Allam N. Impact of nanotechnology on enhanced oil recovery: A mini-review. Industrial & Engineering Chemistry Research 2019;58(36):16287-16295.

[15] BinDahbag M, Hassanzadeh H, AlQuraishi A, Benzagouta M. Suitability of ionic solutions as a chemical substance for chemical enhanced oil recovery–A simulation study. Fuel 2019;242:368-373.

[16] Kumar S, Panigrahi P, Saw R, Mandal A. Interfacial interaction of cationic surfactants and its effect on wettability alteration of oil-wet carbonate rock. Energy & Fuels 2016;30(4):2846-2857.

[17] Pillai P, Kumar A, Mandal A. Mechanistic studies of enhanced oil recovery by imidazolium-based ionic liquids as novel surfactants. Journal of industrial and engineering chemistry 2018;63:262-274.

[18] Sheng J. Investigation of alkaline–crude oil reaction. Petroleum 2015;1(1):31-39.

[19] Yim S, Kim S, Baik J, Nam I, Mok Y, Lee J, et al. Decomposition of urea into NH_3 for the SCR process. Industrial & engineering chemistry research 2004;43(16):4856-4863.

[20] Johar J. An experimental investigation of the urea-water decomposition and selective catalytic reduction (SCR) of nitric oxides with urea using V_2O_5-WO_3-TiO_2 catalyst. Texas A&M University; 2005.

[21] Lu R, Xu X, Yang J, Gao J. Reduction of total acid number of crude oil and distillate. Energy Sources, Part A 2007;29(1):47-57.

[22] Pei H, Zhang G, Ge J, Ma M, Zhang L, Liu Y. Improvement of sweep efficiency by alkaline flooding for heavy oil reservoirs. Journal of Dispersion Science and Technology 2013;34(11):1548-1556.

[23] Ehrlich R, Hasiba H, Raimondi P. Alkaline waterflooding for wettability alteration-evaluating a potential field application. Journal of Petroleum Technology 1974;26(12):1,335-1,343.

[24] Sharma H, Weerasooriya U, Pope G, Mohanty K. Ammonia-based ASP processes for gypsum-containing reservoirs. *SPE Annual Technical Conference and Exhibition.* Society of Petroleum Engineers; 2014.

[25] BinDahbag M, Zirrahi M, Hassanzadeh H. Solubility and liquid density of ammonia/Athabasca bitumen mixtures at temperatures up to 463 K: Measurements and modeling. Journal of Chemical & Engineering Data 2019;64(8):3592-3597.

[26] ASTM committee on petroleum products. Standard test method for acid number of petroleum products by potentiometric titration. ASTM international; 2011.

[27] Verma M. Fundamentals of carbon dioxide-enhanced oil recovery (CO_2-EOR): A supporting document of the assessment methodology for hydrocarbon recovery using CO_2-EOR associated with carbon sequestration. US Department of the Interior, US Geological Survey Washington, DC; 2015.

[28] Wang S, Yuan Q, Kadhum M, Chen C, Yuan N, Shiau B, et al. In situ carbon dioxide generation for improved recovery: Part II. concentrated urea solutions. *SPE Improved Oil Recovery Conference.* Society of Petroleum Engineers; 2018.

[29] Liu Y, Xi C, Liu S, Liu C. Impact of non-condensable gas on SAGD performance. *SPE Heavy Oil Conference Canada.* Society of Petroleum Engineers; 2012.

[30] Zirrahi M, Hassanzadeh H, Abedi J. Experimental and modeling studies of MacKay River bitumen and water. Journal of Petroleum Science and Engineering 2017;151:305-310.

[31] Azinfar B, Zirrahi M, Hassanzadeh H, Abedi J. Characterization of heavy crude oils and residues using combined gel permeation chromatography and simulated distillation. Fuel 2018;233:885-893.

[32] Mohammadi M, Haddadnia A, Zirrahi M, Hassanzadeh H. Interfacial tension of n-pentane/bitumen and n-heptane/bitumen mixtures at T= 298.15–413.15 K and P= 3.45 MPa. Journal of Chemical & Engineering Data 2020, 65 (4): 1787-1795.

[33] Barnes G, Gentle I. Interfacial science-an introduction Oxford University Press. New York, USA 2005.

[34] Chaverot P, Cagna A, Glita S, Rondelez F. Interfacial tension of bitumen− water interfaces. Part 1: Influence of endogenous surfactants at acidic pH. Energy & Fuels 2007;22(2):790-798.

[35] Kumar N, Mandal A. Surfactant stabilized oil-in-water nanoemulsion: stability, interfacial tension, and rheology study for enhanced oil recovery application. Energy & Fuels 2018;32(6):6452-6466.

[36] Pal N, Saxena N, Laxmi K, Mandal A. Interfacial behaviour, wettability alteration and emulsification characteristics of a novel surfactant: Implications for enhanced oil recovery. Chemical Engineering Science 2018;187:200-212.

[37] Pal R. Effect of droplet size on the rheology of emulsions. AIChE Journal 1996;42(11):3181-3190.

[38] Yoon S, Bhatt S, Lee W, Lee H, Jeong S, Baeg J, et al. Separation and characterization of bitumen from Athabasca oil sand. Korean Journal of Chemical Engineering 2009;26(1):64-71.

CHAPTER 5: SUITABILITY OF HOT UREA SOLUTIONS FOR WETTABILITY ALTERATION OF BITUMEN RESERVOIRS – SIMULATION OF LABORATORY FLOODING EXPERIMENTS *

5.1 Abstract

We report a highly fine grid numerical simulation of sand pack flooding experiments conducted using 5 and 10 wt % hot urea solutions for wettability alteration of bitumen reservoirs. Another hot water flooding experiment was also simulated as a baseline for comparison with hot urea solutions. The relative permeability curves have been obtained through history matching of the experimental oil recovery. The results indicated that urea solutions have proved to be efficient in wettability alteration toward more water-wet and attenuation of viscous fingering leading to delayed water breakthrough as was confirmed by the shape of the relative permeability curves. Wettability alteration led to incremental oil recovery compared to the hot water flooding. It was shown that wettability alteration and the in-situ generation of water in oil (W/O) emulsions previously observed in experiments can be captured using the relative permeability curves. These results find application in the design and optimization of thermal bitumen recovery processes.

Keywords: Urea solution; Bitumen; Relative Permeability; Wettability alteration; Simulation; History matching

*BinDahbag, M., Al-Gawfi, A., Hassanzadeh, H., Suitability of hot urea solutions for wettability alteration of bitumen reservoirs - Simulation of laboratory flooding experiments, Fuel. Volume 272, 117713, July 2020.

5.2 Introduction

The wettability of reservoir rock plays an important role in enhanced oil recovery. Wettability is defined as the ability of a phase to spread or adhere to the surface of the grains in the presence of another phase [1]. Different wettability alteration agents such as surfactants, alkaline materials, ionic liquids, low/high salinity water, partly deionized (smart) water, and nanofluids have been investigated on different types of reservoir rocks containing light crude oils [2]. Surfactants alter rock wettability toward more water-wet via two main mechanisms: ion-pair formation and surfactant molecules adsorption on rock surface [3]. Charged functional groups found in surfactant molecules are paired with the opposite charge components of crude oil adsorbed on the rock surface to form ion-pairs groups capable of altering the rock wettability toward more water-wet. A recent study has indicated that the conjunction of the charged head groups of surfactant molecules with the adsorbed oppositely charged oil components over ion-pair formation is more effective in the rock wettability alteration compared to the adsorption of surfactant molecules directly as a monolayer on the rock surface [4]. Previous studies have shown that chemicals (i.e., alkaline) might be added through the water flooding period to change the rock wettability toward more water-wet and thereby to improve oil recovery for high acidity crude oils [5-9]. Alkaline solutions react with naphthenic acids found in crude oil to generate in situ surfactants to change rock wettability toward water-wet [10, 11]. Ionic liquids are also found to have the ability to improve the rock wettability toward water-wet since their charged molecules adsorb on the opposite charge rock surface [12-20]. Only a few studies have investigated the wettability alteration of heavy oil/bitumen reservoirs through the thermal recovery process. A previous study has shown that surfactants improve the ultimate

recovery of heavy crude oil from weakly water-wet limestone through the imbibition process due to altering the rock wettability toward more water-wet [21]. However, the stability of surfactants does not tolerate the harsh condition of the reservoir through the flooding process [21]. A series of recent studies have indicated that nanoparticles (i.e., alumina, silica, and zirconium nanoparticles) dispersed in base fluids improve the wettability of sandstone and carbonate rocks toward more water-wet [22-25]. Another study suggests that silica nanoparticles adsorb and aggregate at the interface of silica-oil droplets to decrease the interfacial tension and thereby reduce contact angle from 100 to 0º [26].

To the best of our knowledge, no previous study has investigated the suitability of urea solutions as an additive to alter rock wettability through thermal recovery processes. Urea solutions are potential candidates for enhancing the wettability of heavy oil/bitumen reservoirs since oxygen compounds form a considerable part (around 1 wt %) of the composition of these heavy hydrocarbons [27]. Urea solutions react with naphthenic acids found in bitumen at high temperatures to generate in situ surfactants, thereby improving the sweep efficiency of thermal processes [28-30].

This study aims to investigate the role of urea solutions in altering the rock wettability toward more water-wet and consequently enhancing bitumen recovery efficiency. To achieve that, relative permeability curves of three sand pack flooding experiments were generated and compared to explore the alteration of the rock wettability. Due to the high viscosity of bitumen, Johnson, Bossler, and Neumann (JBN) method was replaced with the history matching technique through the generation of relative permeability curves from history matching of highly fine grid numerical simulations. The key contribution of this

work is the experimental verification of wettability alteration toward more water-wet and the generation of relative permeability curves for the hot urea solution flooding of bitumen and heavy oil reservoirs.

5.3 Material and methods

5.3.1 Experimental section

Three sand pack flooding experiments were carried out with a 1-D vertical sand pack model at a constant temperature of 423 K (150 ℃) and pore pressure and confining pressure 500 psig (3.45 MPa) and 1000 psig (6.895 MPa), respectively. A cylindrical core holder with 6 and 26 cm in diameter and length, respectively, was packed with glass beads (120 mesh size) using the hammering technique to create the porous medium. The sand pack was saturated with fresh water and then flooded with warm Athabasca bitumen until an irreducible water saturation (S_{wirr}) is reached and no more water was produced. Two urea solutions of 5 and 10 wt % were prepared by dissolving urea in deionized water and were used separately in two flooding experiments to recover bitumen from the saturated sand pack. One more flooding experiment was conducted with hot water as the displacing phase and was used as the baseline for comparison with the two aqueous hot urea solution flooding experiments. More details related to the experimental procedure and analysis of the experimental data have been reported elsewhere [31]. Table 5.1 presents the petrophysical properties reported through the flooding experiments [31].

Table 5.1. The petrophysical properties of sand pack for all scenarios [31].

Implemented scenario	Length, cm	Bulk volume, cm^3	Pore volume, cm^3	Porosity, fraction	Absolute permeability, mD
Water flooding	26.05	736.42	273.18	0.371	14060
5 wt % urea solution	26.25	742.08	268.86	0.362	11380
10 wt % urea solution	26.05	736.42	265.36	0.360	12320

5.3.2 Simulation section

Numerical simulations of the flooding experiments were conducted using a commercial thermal reservoir simulator, CMG-STARS [32], to obtain the relative permeability curves through a history matching of the experimental oil production data. The relative permeability curves for oil and water phases can be represented using Brooks-Corey's correlations as follows:

$$k_{ro} = k_{ro}^{0}\left(\frac{1-S_w-S_{orw}}{1-S_{wirr}-S_{orw}}\right)^{n_o}, \quad \textbf{5.1}$$

$$k_{rw} = k_{rw}^{0}\left(\frac{S_w-S_{wcrit}}{1-S_{wcrit}-S_{oirw}}\right)^{n_w}, \quad \textbf{5.2}$$

where S_w is the water saturation, n_w is the water phase Corey's exponent, k_{rw}^{0} is the water relative permeability endpoint at the irreducible oil saturation (S_{oirw}), S_{wcrit} is the critical water saturation, S_{orw} is the residual oil saturation, S_{wirr} is the irreducible water saturation, k_{ro}^{0} is the oil relative permeability endpoint at the irreducible water saturation (S_{wirr}), and n_o is the oil phase Corey's exponent. Figure 5.1 shows the schematic water-oil relative permeability curves [33].

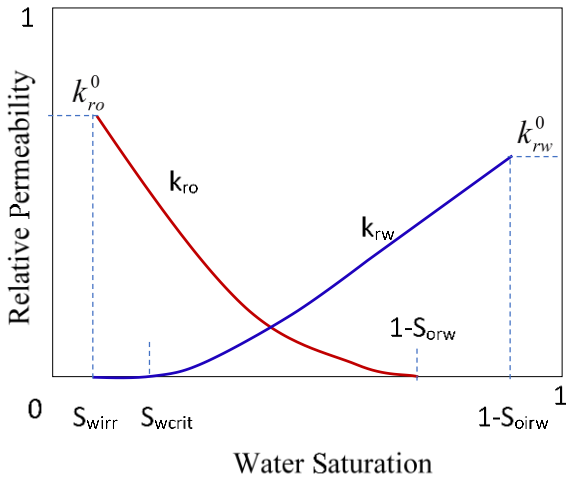

Figure 5.1. Schematic water-oil relative permeability curves [33].

Oil relative permeability endpoint (k_{ro}^0), the initial oil saturation (S_{oi}), and irreducible water saturation (S_{wirr}) were obtained from the flooding experiments and used as input data in the rock-fluid section, as shown in Table 5.2. CMOST [34], a history matching/optimization tool from CMG, was utilized to obtain the water relative permeability endpoint (k_{rw}^0) at residual oil saturation (S_{orw}), critical water saturation (S_{wcrit}), irreducible oil saturation (S_{oirw}), and the Corey exponents for oil and water through the history matching of the cumulative oil recovery.

The flooding experiments models were simulated using a cylindrical shape geometry with 100 grid blocks (Δx = 2.6 mm) in the axial direction, 50 grid blocks (Δr = 0.6 mm) in the radial direction, and 50 grids ($\Delta\theta$ = 7.2°) in the angular direction. Figure 5.2 shows a schematic diagram of the dimensions, grid blocks, injector, and producer of the sand pack. The inlet and outlet grids representing the injection and production faces were assigned very high permeability (10^6 mD) to ensure uniform fluid distribution at the inlet and outlet for the sand pack. The porosity and permeability of the sand pack were assigned to all other

grid blocks. The input petrophysical properties of sand pack for all scenarios are shown in Table 5.1. Thermophysical properties of the bitumen and urea solutions used in this work have been reported elsewhere [13, 35, 36].

Table 5.2. Oil relative permeability endpoints and fluids saturations from flooding experiments.

Implemented scenario	k_{ro}^{0}	S_{oi}	S_{wirr}
Water flooding	0.362	0.873	0.127
5 wt % urea solution	0.492	0.911	0.089
10 wt % urea solution	0.390	0.863	0.137

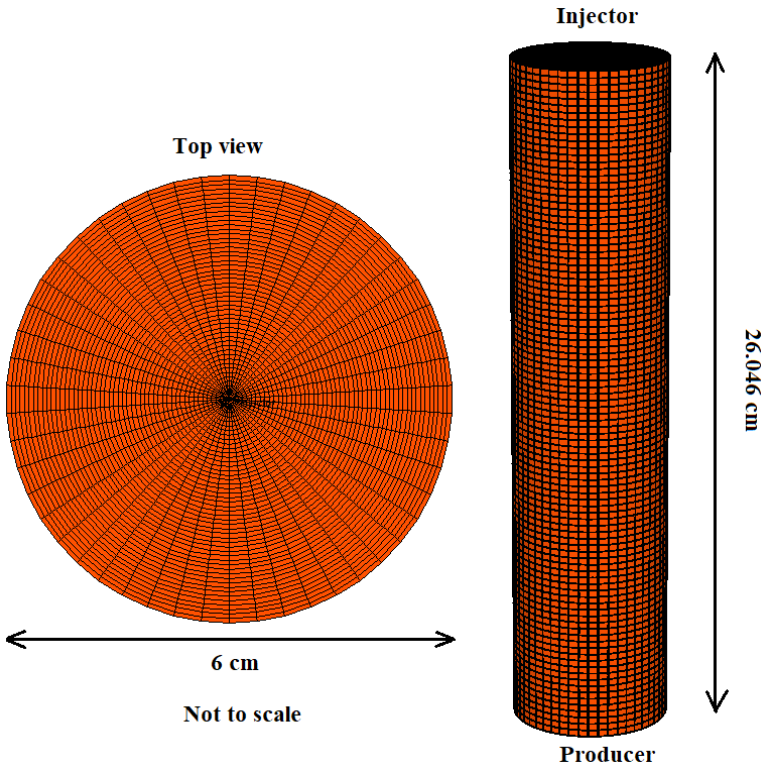

Figure 5.2. A schematic diagram shows the dimensions, grid blocks, injector, and producer of the sand pack.

5.4 Simulation results

5.4.1 Simulation of hot water flooding experiment

Simulation of hot water flooding experiment is conducted by injection of 5.25 pore volumes (PV) of hot water into the sand pack at an initial oil saturation (S_{oi}) of 0.873. The simulation run is continued to 1432 min with a 1 cm^3/min injection flowrate similar to the experimental conditions until a water cut of 99% is achieved. The pore pressure and temperature of the system are set at constant values of 500 psig (~3450 kPa) and 423 K (150 ℃), respectively. CMG CMOST tool is utilized to match the cumulative oil recovery with a global history matching error (GHME) of 2%. Both water cut and the injection well bottom-hole pressure data have been extracted from the simulation output and compared with their corresponding experimental data for validation. The simulated water cut and bottom-hole pressure have shown a reasonable match with the experimental data, which confirms the reliability of simulation results. Figure 5.3 shows the cumulative oil recovery, water cut, and well bottom-hole pressure for experimental and simulation results of the water flooding scenario. The relevant statistical parameters are shown in Table 5.3. The water saturation increased from the value of 0.127, which represents the irreducible water saturation (S_{wirr}), to 0.765 at the end of water flooding process. Table 5.4 and Figure 5.4 present the converged parameters of the simulation run, and the final results of the relative permeability curves generated using the history matching technique, respectively. As shown in Figure 5.4, the oil relative permeability curve shows an endpoint of 0.362 at an irreducible water saturation of 0.127 and crosses the water relative permeability curve at a water saturation of 0.75. The results obtained from history matching of the experimental

data suggest the following Brooks-Corey relative permeability relations for the oil- and water-phases.

$$k_{ro} = 0.362\left(\frac{1-S_w-0.235}{1-0.127-0.235}\right)^{0.422} = 0.362\left(\frac{0.765-S_w}{0.638}\right)^{0.422}, \qquad \textbf{5.3}$$

$$k_{rw} = 0.029\left(\frac{S_w-0.133}{1-0.133-0.051}\right)^{0.466} = 0.029\left(\frac{S_w-0.133}{0.816}\right)^{0.466}. \qquad \textbf{5.4}$$

The oil and water relative permeability parameters are summarized in Table 5.4.

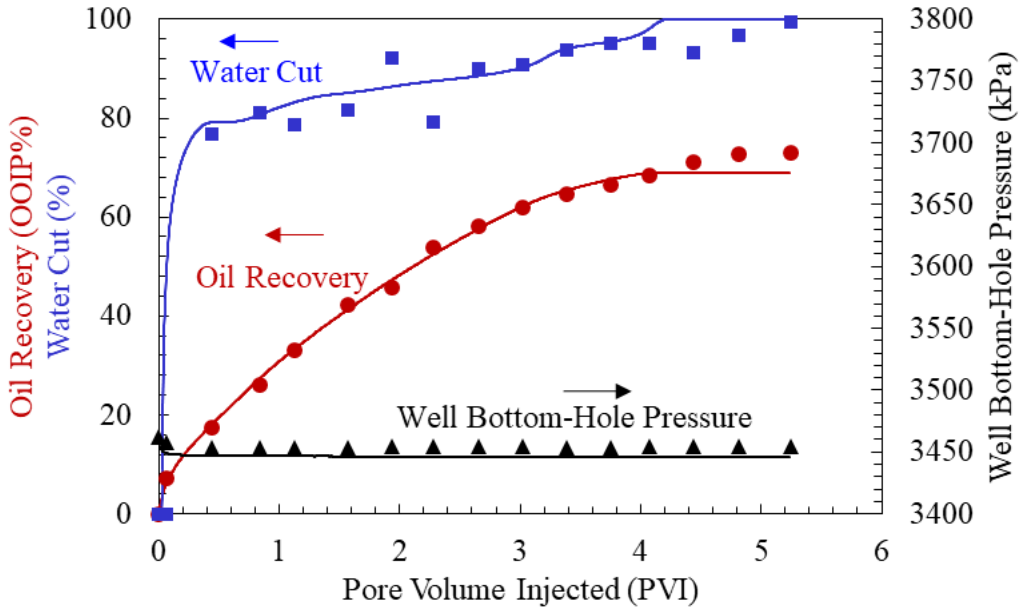

Figure 5.3. Experimental (markers) and simulated (curves) results for the oil recovery (●), water cut (■), and well bottom-hole pressure (▲) for water flooding experiment.

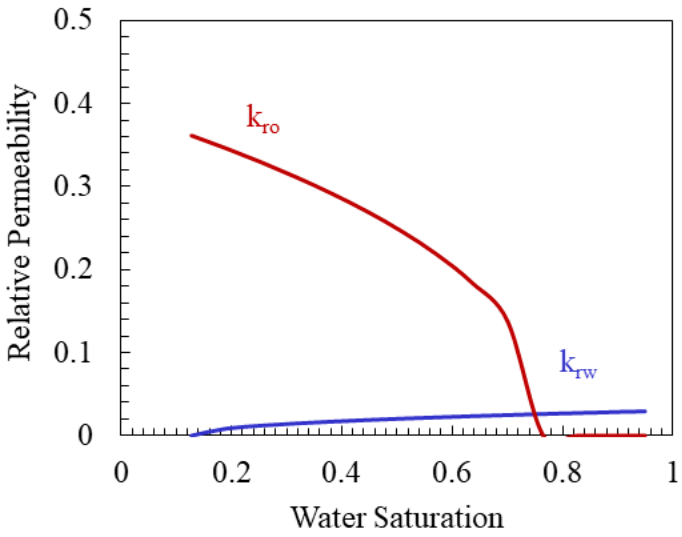

Figure 5.4. Relative permeability curves for oil and water obtained from reservoir simulation of water flooding experiment.

In the following section, the simulation of 5 wt % urea solution flooding experiment is described, and the corresponding oil and water relative permeability curves are presented.

5.4.2 Simulation of 5 wt % urea solution flooding experiment

Simulation of the second flooding experiment is conducted by injection of 4.37 PV of the 5 wt % urea doped solution into the sand pack at the initial oil saturation of 0.911. The flooding process is continued for 1174 min until water cut 93% is reached. Like the first scenario, the same injection flow rate, pressure, and temperature are used for consistency. An excellent match between the oil recovery from experimental data and simulations results is obtained with a global history matching error (GHME) of 2.2%; and, at the same time, water cut, and well bottom-hole pressure have been matched with the experimental data as shown in Figure 5.5. The relevant statistical parameters are shown in Table 5.3. A final value of 0.741 for water saturation has been achieved by the end of flooding with the

5 wt % urea solution. The converged relative permeability curves are shown in Figure 5.6. The results obtained from history matching of the experimental data suggest the following Brooks-Corey relative permeability relations for the oil- and water-phase.

$$k_{ro} = 0.493\left(\frac{1-S_w-0.259}{1-0.089-0.259}\right)^{0.342} = 0.493\left(\frac{0.741-S_w}{0.652}\right)^{0.342}, \qquad \textbf{5.5}$$

$$k_{rw} = 0.028\left(\frac{S_w-0.129}{1-0.129-0.055}\right)^{0.483} = 0.028\left(\frac{S_w-0.129}{0.816}\right)^{0.483}. \qquad \textbf{5.6}$$

The oil and water relative permeability parameters are summarized in Table 5.4.

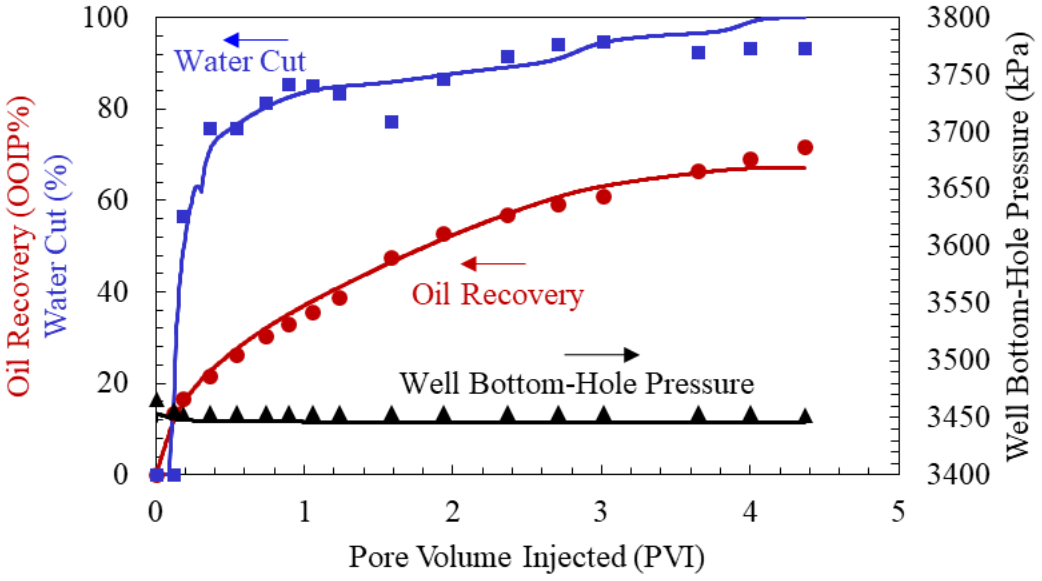

Figure 5.5. Experimental (markers) and simulated (curves) results for the oil recovery (●), water cut (■), and well bottom-hole pressure (▲) for the flooding with a 5 wt % urea solution experiment.

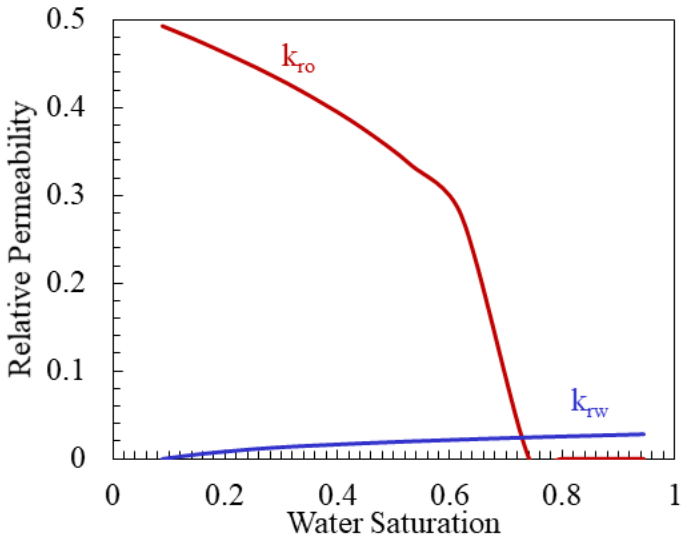

Figure 5.6. Relative permeability curves for oil and water obtained from reservoir simulation of 5 wt % urea solution experiment.

In the next section, a simulation of 10 wt % urea solution flooding experiment is described, and the corresponding oil and water relative permeability curves are presented.

5.4.3 Simulation of 10 wt % urea solution flooding experiment

The fluid model of this scenario is built similar to the one used in 5 wt % urea solution, except for the composition of urea is changed to 10 wt %. The sand pack with an initial oil saturation of 0.863 is flooded for 1219 min with 4.6 PV of 10 wt % urea solution. The flooding process is stopped at a water cut of 91%. The experimental conditions of injection flow rate of 1 cm^3/min, pore pressure of 3445 kPa, temperature of 423 K (150 ℃), and oil production data are used in numerical simulation. An excellent match with a global history matching error (GHME) of 2.3% has been obtained for the cumulative oil recovery. The water cut and well bottom-hole pressure curves are matched with the experimental results. Figure 5.7 presents the experimental and simulated results of the cumulative oil recovery, water cut, and well bottom-hole pressure. The relevant statistical parameters are shown in

Table 5.3. The results show a deviation in the cumulative oil recovery between simulation results and experiment at the end of urea solution flooding. The additional oil recovery for the experiment may be attributed to the gravity segregation that happened where the experiment was stopped and resumed later. The maximum water saturation achieved at the end of injection with 10 wt % urea solution is 0.796. The converged parameters for the simulation run and relative permeability curves are presented in Table 5.4 and Figure 5.8, respectively. The results obtained from the history matching of the experimental data suggest the following Corey relative permeability relations for the oil- and water-phase.

$$k_{ro} = 0.390\left(\frac{1 - S_w - 0.204}{1 - 0.137 - 0.204}\right)^{0.439} = 0.390\left(\frac{0.796 - S_w}{0.659}\right)^{0.439}, \quad \textbf{5.7}$$

$$k_{rw} = 0.020\left(\frac{S_w - 0.190}{1 - 0.190 - 0.133}\right)^{0.4935} = 0.020\left(\frac{S_w - 0.190}{0.677}\right)^{0.4935}. \quad \textbf{5.8}$$

The oil and water relative permeability parameters are summarized in Table 5.3. The findings of experimental and simulation runs of the three flooding scenarios are discussed in the following section.

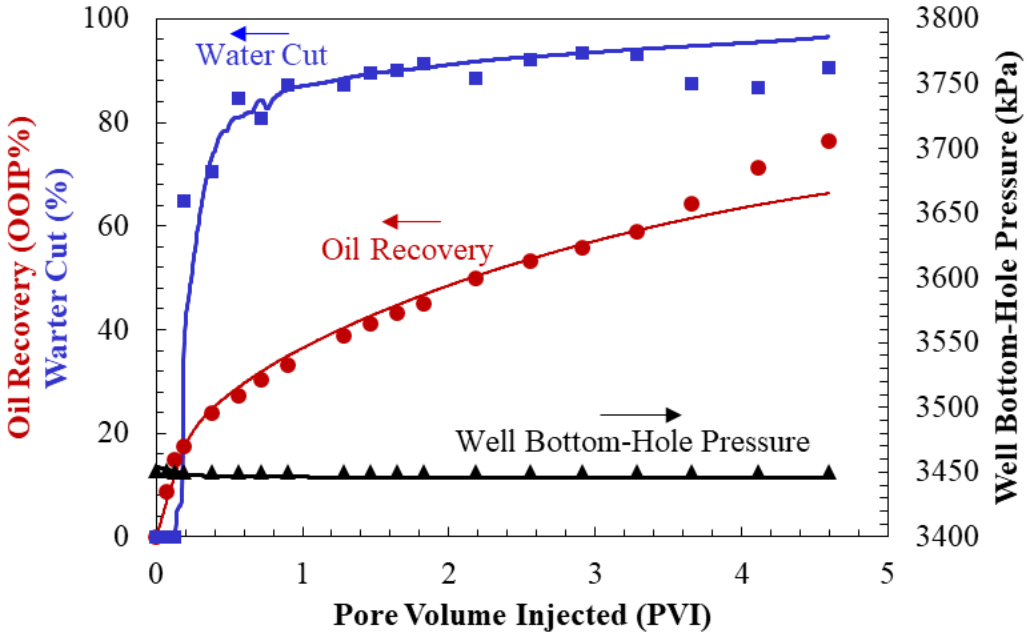

Figure 5.7. Experimental (markers) and simulated (curves) results for the oil recovery (●), water cut (■), and well bottom-hole pressure (▲) for the flooding with a 10 wt % urea solution experiment.

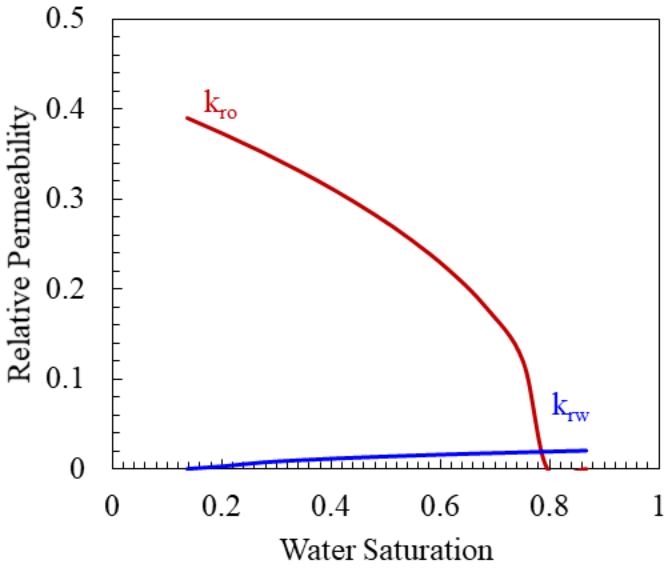

Figure 5.8. Relative permeability curves for oil and water obtained from reservoir simulation of 10 wt % urea solution experiment.

Table 5.3. Statistical parameters of the results shown in Figures 5.3, 5.5, and 5.7.

Statistical parameter	Figure 5.3 (water flooding)			Figure 5.5 (5 wt % urea solution)			Figure 5.7 (10 wt % urea solution)		
	Oil recovery	Water cut	Well bottom-hole pressure	Oil recovery	Water cut	Well bottom-hole pressure	Oil recovery	Water cut	Well bottom-hole pressure
MMRE	0.03654	0.03215	0.00004	0.04711	0.04009	0.00004	0.05775	0.05071	0.00003
NSER	0.00728	0.08792	0.08236	0.01100	0.04540	0.08234	0.02974	0.06806	0.01710
PAP	97.3658	93.3806	94.1766	96.5795	95.7175	94.1780	95.4071	93.9985	98.7907

The statistical parameters were calculated as follows [37]:

The mean magnitude of relative error $(MMRE) = \frac{1}{n}\sum_{i=1}^{n}\left|\frac{Y_i - f_i}{Y_i}\right|$ **5.9**

The Nash-Sutcliffe efficiency ratio $NSER = \frac{\sum_{i=1}^{n}(Y_i - f_i)^2}{\sum_{i=1}^{n}(Y_i - \overline{Y})^2}$ **5.10**

The percentage of accuracy-precision

$$PAP = 100\left(1 - \frac{\sqrt{2}}{2}\sqrt{\left(\frac{1}{n}\sum_{i=1}^{n}\left|\frac{Y_i - f_i}{Y_i}\right|\right)^2 + \left(\frac{\sum_{i=1}^{n}(Y_i - f_i)^2}{\sum_{i=1}^{n}(Y_i - \overline{Y})^2}\right)^2}\right) \quad \textbf{5.11}$$

where: Y_i is the experimental value, f_i is the simulated value, and $\overline{Y}$ is the mean of the experimental values.

Table 5.4. Converged parameters for generation relative permeability curves via CMG-CMOST

Relative permeability parameters	Water flooding	5 wt % urea	10 wt % urea
Corey correlation exponent for k_{ro}	0.422	0.342	0.439
Corey correlation exponent for k_{rw}	0.466	0.483	0.494
Oil relative permeability endpoint (k_{ro}^{0}) at (S_{wirr})	0.362	0.493	0.390
Water relative permeability endpoint (k_{rw}^{0}) at (S_{oirw})	0.029	0.028	0.020
Irreducible water saturation (S_{wirr})	0.127	0.089	0.137
Critical water saturation (S_{wcrit})	0.133	0.129	0.190
Residual oil saturation (S_{orw})	0.235	0.259	0.204
Irreducible oil saturation (S_{oirw})	0.051	0.055	0.133

5.5 Discussion

The comparison of water cut results presented in the previous section revealed an early breakthrough in all three scenarios due to the high mobility ratio resulting from the low viscosity of displacing aqueous phase compared to the high viscosity of the bitumen. However, both experiments and simulation results indicated that urea solutions delay the breakthrough of the injected fluid considerably. The experimental results show that breakthrough for both of 5 and 10 wt % urea solutions scenarios occurs after injection of about 0.12 pore volume (PV) of the urea solutions compared to 0.06 PV in case of water flooding scenario. However, while the simulation results follow the same trend, the breakthrough of the injected fluid in simulations occurred earlier at 0.02, 0.09, and 0.12 PV for water flooding, 5 and 10 wt % urea solutions, respectively. This finding is attributed to the generation of viscous water-in-oil (W/O) emulsion that helps to attenuate the viscous fingering and delay the breakthrough. While the in situ generated water-in-oil (W/O)

emulsion has not been simulated explicitly, the effect of urea solutions on weakening the effect of viscous fingering has been partly captured through the relative permeability curves. Oil saturation maps generated by simulation shown in Figure 5.9 confirm this finding where the displacement is more stable for 5 and 10 wt % urea solutions, whereas water flooding suffers from more severe viscous fingering. This observation is consistent with previous studies that have shown W/O emulsions improve the recovery of heavy oils in high permeability reservoirs [37].

The urea solution has the potential to change the rock wettability toward more water-wet since it reacts with naphthenic acids found in bitumen to generate in situ surfactants responsible for adhering to the polar compounds on rock surface [11]. It is expected that some of the effects of urea solution on the rock wettability can be captured in the oil and water relative permeability curves. The relative permeability curves generated from the history matching revealed that 5 wt % urea solution has the highest values of the oil relative permeability, whereas the water flooding scenario has the lowest, as shown in Figure 5.10. This finding suggests that it is easier to displace the oil once it is flooded with 5 wt % urea solution. The oil relative permeability curves for all three scenarios show Corey exponent values less than one, which confirms that channeling resulting from viscous fingering is responsible for the early breakthrough. The convex oil relative permeability curves are consistent with the previous studies reported in the literature [38]. The water relative permeability curves for the three flooding experiments are nearly identical with minor differences.

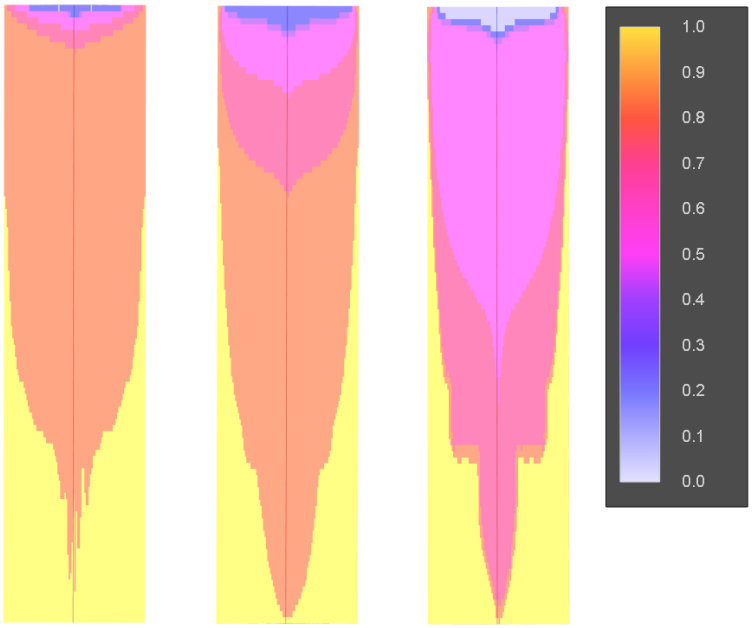

Figure 5.9. Distribution of oil saturation at breakthrough times for the three flooding scenarios: a) after 8 min (0.02 PVI) injection with water flooding, b) after 26 min (0.09 PVI) injection with 5 wt % urea solution, c) 34 min (0.12 PVI) injection with 10 wt % urea solution.

Another observation is that 5 wt % urea solution is found to be the optimum concentration among the tested scenarios since it recovers more oil through the first 3 PV of injection. On the contrary, while 10 wt % urea solution gives the same oil recovery as in 5 wt % urea solution at the early stages (less than one PVI of injection), its performance deteriorates over time and falls below the water flooding performance after the first two PV of injection as shown in Figure 5.11. This finding is attributed to the formation of more viscous and finer emulsions in the case of flooding with 10 wt % urea solution, which has been previously observed in flooding experiments conducted with 10 wt % urea solution [31].

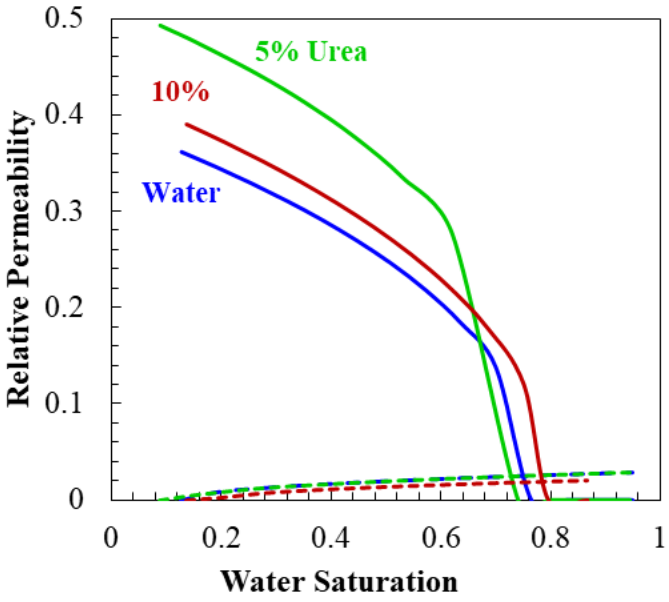

Figure 5.10. Relative permeability curves for three flooding experiments, (▬) oil relative permeability of water flooding experiment, (▪▪▪) water relative permeability of water flooding experiment, (▬) oil relative permeability of 5 wt % urea solution experiment, (▪▪▪)water relative permeability of 5 wt % urea solution experiment, (▬) oil relative permeability of 10 wt % urea solution experiment, (▪▪▪) water relative permeability of 10 wt % urea solution experiment.

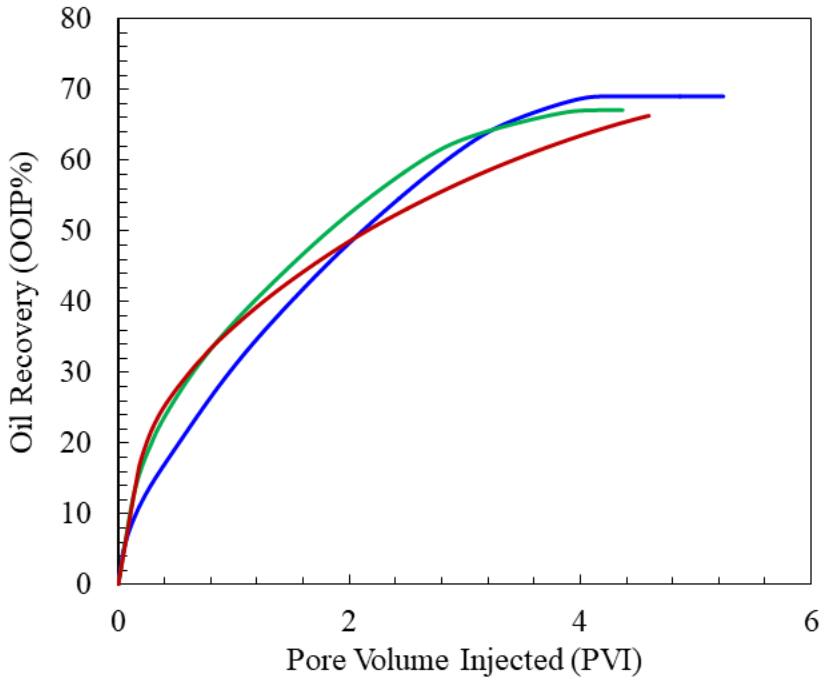

Figure 5.11. Simulated oil recovery of three scenarios, water flooding experiment (▬), 5 wt % urea solution experiment (▬), 10 wt % urea solution experiment (▬).

Figures 5.12a and 5.12b show the oil saturation maps of the three scenarios at 1 and 2 PV of injection, respectively. It is worth noting that the breakthrough of the injected fluid in simulations occurred at 0.02, 0.09, and 0.12 PV for water flooding, 5 and 10 wt % urea solutions, respectively, as shown in Figure 5.9. Figure 5.12b clearly shows that 5 wt % urea solution sweeps the sand pack more efficiently. The flooding with 5 wt % urea solution sweeps the sand pack more stably compared to 10 wt % urea solution with higher macroscopic displacement efficiency, as shown in Figure 5.12 (a). However, for the case of 10 wt % urea solution, a significant volume of oil has been left at the end of two pore volumes of injection due to poor macroscopic displacement efficiency as shown in Figure 5.12 (b). This observation is in accordance with the higher irreducible oil saturation for 10 wt % urea solution compared to the other cases (S_{oirw} = 0.133 compared to 0.05). The higher

irreducible oil saturation indicates more oil left behind. The higher irreducible oil saturation might be due to the formation of more viscous and finer emulsions in the case of 10 wt % urea solution, which has been observed in experiments [31].

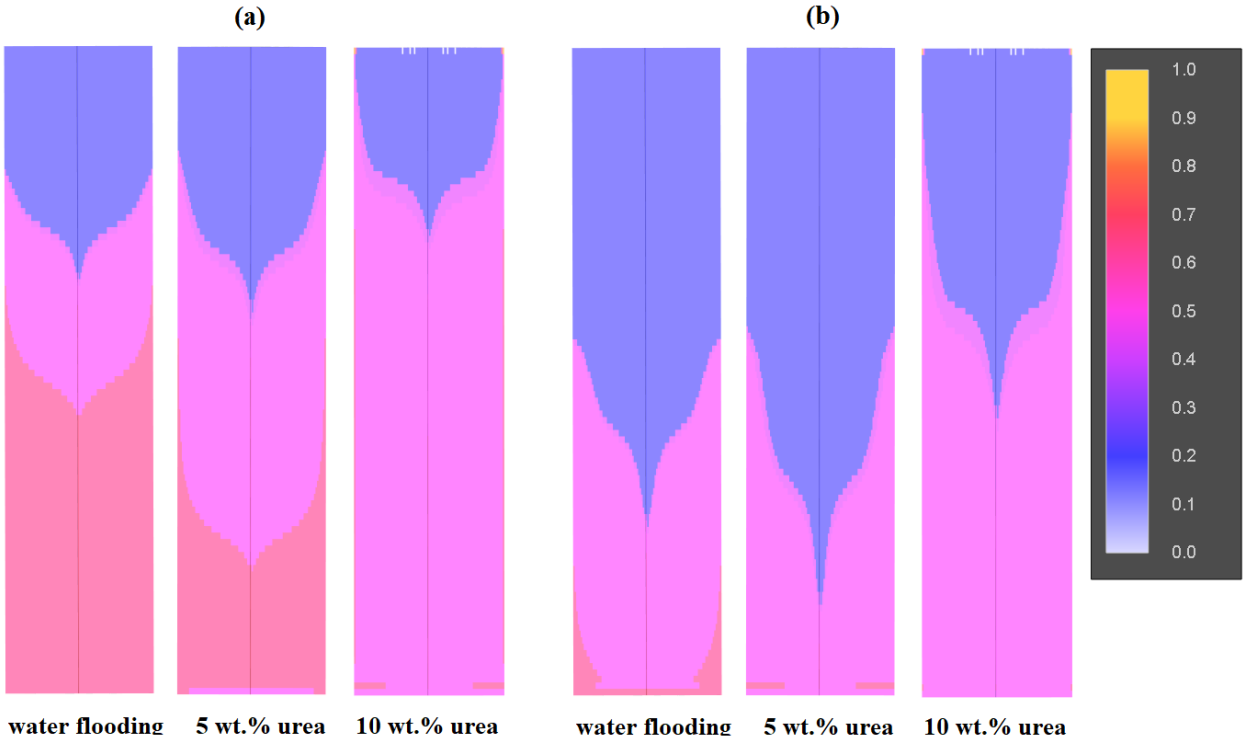

Figure 5.12. Oil saturation maps for three scenarios at: a) 1 PV of injection, b) 2 PV of injection.

5.6 Conclusion

Two sand pack flooding experiments were conducted to investigate the efficiency of urea solutions (5 and 10 wt %) for wettability alteration of bitumen reservoirs. Another experiment was carried out using fresh water and used as a baseline for comparison with urea solutions scenarios. A commercial reservoir simulator (CMG-STARS) was used to predict the oil and water relative permeability curves of the flooding experiments using

history matching of the cumulative oil recovery with the experimental results. The following main conclusions can be drawn from this study:

- Both urea solutions have proved efficient in changing the rock wettability toward more water-wet as was shown by increasing the oil relative permeability values. However, 5 wt % urea solution was shown to be more efficient at lower pore volume of the injected solution.
- Urea solutions have shown to be more effective than hot water flooding and recovered ~36% of the OOIP compared to 31% through the first pore volume of injection.
- The oil relative permeability curves decline in convex shape for all scenarios, which confirms the channeling and viscous fingering phenomena. It was shown that 5 and 10 wt % urea solutions delayed the water breakthrough leading to higher oil recovery.
- It was demonstrated that wettability alteration as well as in situ generation of water in oil (W/O) emulsions previously observed in experiments can be partly captured using relative permeability curves.
- A 10 wt % urea solution leaves a high oil saturation behind, as evident in higher irreducible oil saturation. This finding explains the lower oil recovery of 10 wt % urea solution flooding.

5.7 References

[1] Crain E. Crain's petrophysical handbook. Spectrum 2000 Mindware Limited; 2002.

[2] Cao N, Mohammed M, Babadagli T. Wettability alteration of heavy-oil-bitumen-containing carbonates by use of solvents, high-pH solutions, and nano/ionic liquids. SPE Reservoir Evaluation & Engineering 2017;20(02):363-371.

[3] Salehi M, Johnson S, Liang J. Mechanistic study of wettability alteration using surfactants with applications in naturally fractured reservoirs. Langmuir 2008;24(24):14099-14107.

[4] Salehi M, Johnson S, Liang J. Enhanced wettability alteration by surfactants with multiple hydrophilic moieties. Journal of Surfactants and Detergents 2010;13(3):243-246.

[5] Wagner O, Leach R. Improving oil displacement efficiency by wettability adjustment. Transactions of the AIME 1959;216(01):65-72.

[6] Leach R, Wagner O, Wood H, Harpke C. A laboratory and field study of wettability adjustment in water flooding. Journal of Petroleum Technology 1962;14(02):206-212.

[7] Mungan N. Certain wettability effects in laboratory waterfloods. Journal of Petroleum Technology 1966;18(02):247-252.

[8] Emery L, Mungan N, Nicholson R. Caustic slug injection in the Singleton field. Journal of Petroleum Technology 1970;22(12):1,569-1,576.

[9] Zirahi A, Sadeghi H, Haddadnia A, Zirrahi M, Hassanzadeh H, Abedi J. Ethyl acetate as a bio-based solvent to reduce energy intensity and CO_2 emissions of in situ bitumen recovery. AIChE Journal 2020;66(2):e16828.

[10] Ehrlich R. Wettability alteration during displacement of oil by water from petroleum reservoir rock. *Proceedings of the 48th National Colloid Symposium ACS preprints*, Austin, TX, USA. 1974.

[11] Ehrlich R, Hasiba H, Raimondi P. Alkaline waterflooding for wettability alteration-evaluating a potential field application. Journal of Petroleum Technology 1974;26(12):1,335-1,343.

[12] BinDahbag M, Al Quraishi A, Benzagouta M, Kinawy M, Al Nashef I, Al Mushaegeh E. Experimental study of use of ionic liquids in enhanced oil recovery. Journal of Petroleum & Environmental Biotechnology 2014;4(165): 1000165.

[13] BinDahbag M, Zirrahi M, Hassanzadeh H. Solubility and liquid density of ammonia/Athabasca bitumen mixtures at temperatures up to 463 K: Measurements and modeling. Journal of Chemical & Engineering Data 2019;64(8):3592-3597.

[14] BinDahbag M, Hossain M. Simulation of ionic liquid flooding for chemical enhance oil recovery using CMG STARS software. *SPE Kingdom of Saudi Arabia Annual Technical Symposium and Exhibition.* Society of Petroleum Engineers; 2016.

[15] BinDahbag M, AlQuraishi A, Benzagouta M. Efficiency of ionic liquids for chemical enhanced oil recovery. Journal of Petroleum Exploration and Production Technology 2015;5(4):353-361.

[16] BinDahbag M, Hossain M, AlQuraishi A. Efficiency of ionic liquids as an enhanced oil recovery chemical: simulation approach. Energy & Fuels 2016;30(11):9260-9265.

[17] Painter P, Williams P, Mannebach E. Recovery of bitumen from oil or tar sands using ionic liquids. Energy & Fuels 2009;24(2):1094-1098.

[18] Painter P, Williams P, Lupinsky A. Recovery of bitumen from Utah tar sands using ionic liquids. Energy & Fuels 2010;24(9):5081-5088.

[19] Williams P, Lupinsky A, Painter P. Recovery of bitumen from low-grade oil sands using ionic liquids. Energy & Fuels 2010;24(3):2172-2173.

[20] BinDahbag M, Hassanzadeh H, AlQuraishi A, Benzagouta M. Suitability of ionic solutions as a chemical substance for chemical enhanced oil recovery–A simulation study. Fuel 2019;242:368-373.

[21] Babadagli T. Dynamics of capillary imbibition when surfactant, polymer, and hot water are used as aqueous phase for oil recovery. Journal of colloid and interface science 2002;246(1):203-213.

[22] Karimi A, Fakhroueian Z, Bahramian A, Pour Khiabani N, Darabad JB, Azin R, et al. Wettability alteration in carbonates using zirconium oxide nanofluids: EOR implications. Energy & Fuels 2012;26(2):1028-1036.

[23] Ju B, Fan T. Experimental study and mathematical model of nanoparticle transport in porous media. Powder Technology 2009;192(2):195-202.

[24] Ju B, Fan T, Li Z. Improving water injectivity and enhancing oil recovery by wettability control using nanopowders. Journal of Petroleum Science and Engineering 2012;86:206-216.

[25] Yu W, Xie H. A review on nanofluids: preparation, stability mechanisms, and applications. Journal of nanomaterials 2012;2012:1-17.

[26] Maghzi A, Mohammadi S, Ghazanfari M, Kharrat R, Masihi M. Monitoring wettability alteration by silica nanoparticles during water flooding to heavy oils in

five-spot systems: A pore-level investigation. Experimental Thermal and Fluid Science 2012;40:168-176.

[27] Rahimi P, Gentzis T. The chemistry of bitumen and heavy oil processing. Practical advances in petroleum processing. Springer; 2006 :597-634.

[28] Lu R, Xu X, Yang J, Gao J. Reduction of total acid number of crude oil and distillate. Energy Sources, Part A 2007;29(1):47-57.

[29] Fong C, Wells D, Krodkiewska I, Hartley P, Drummond C. New role for urea as a surfactant headgroup promoting self-assembly in water. Chemistry of materials 2006;18(3):594-597.

[30] Sheng J. Investigation of alkaline–crude oil reaction. Petroleum 2015;1(1):31-39.

[31] BinDahbag M, Mohammadi M, Khalifi M, Aghajamali M, Zirrahi M, Hassanzadeh H. Efficiency of urea solutions in enhanced oil recovery. ACS Omega 2020, 5 (11): 6122-6129.

[32] CMG . Stars user guide-advanced processes & thermal reservoir simulator. 2018.

[33] Goda H, Behrenbruch P. Using a modified Brooks-Corey model to study oil-water relative permeability for diverse pore structures. *SPE Asia Pacific Oil and Gas Conference and Exhibition.* Society of Petroleum Engineers; 2004.

[34] CMG Group. CMOST user guide. Alberta; 2018.

[35] Halonen S, Kangas T, Haataja M, Lassi U. Urea-water-solution properties: density, viscosity, and surface tension in an under-saturated solution. Emission Control Science and Technology 2017;3(2):161-170.

[36] Azinfar B, Zirrahi M, Hassanzadeh H, Abedi J. Characterization of heavy crude oils and residues using combined gel permeation chromatography and simulated distillation. Fuel 2018;233:885-893.

[37] Heidaryan E. A note on model selection based on the percentage of accuracy-precision. Journal of Energy Resources Technology 2019;141(4): 045501.

CHAPTER 6: INJECTION OF HOT UREA SOLUTIONS AS A NOVEL PROCESS FOR HEAVY OIL RECOVERY – A PROOF-OF-CONCEPT EXPERIMENTAL STUDY*

6.1 Abstract

We report a proof-of-concept experimental study of hot urea solutions injection as a new recovery process to extract highly viscous oils. Eight flooding experiments were conducted to study the viability of hot urea solutions in displacing bitumen from cold sand packs. Three injection rates (4, 8, and 12 cm^3/min), four injection temperatures 453, 473/ 493, 513 K (180, 200, 220, and 240 ℃), and three urea solution concentrations (5, 10, and 15 wt%) were investigated. Another baseline experiment was conducted with fresh water for comparison with the urea solution scenarios. The results showed that the injection of hot urea solution into cold sand pack saturated with bitumen leads to a significant increase in the oil recovery due to the formation of in-situ water-in-oil emulsions. The results also reveal that the balance of the retention time and the amount of heat delivered to the sand pack leads to an optimum injection rate at which the oil recovery is improved considerably. Additionally, while the increment in injection temperature accelerates oil production, it decreases the ultimate oil recovery. These results might pave the way for improving the existing recovery techniques and introducing chemical in-situ oil recovery processes for reservoirs that are not currently exploitable using existing recovery techniques.

* BinDahbag, M., Zirrahi, M. and Hassanzadeh, H., 2021. Injection of hot urea solutions as a novel process for heavy oil recovery—A proof-of-concept experimental study. Journal of Industrial and Engineering Chemistry, 95, pp.244-251.

Keywords: Urea solution flooding; sand pack flooding; solvent-aided recovery; water-in-oil emulsion; viscous fingering; in-situ surfactants.

6.2 Introduction

Enormous resources of heavy oils are found in thin oil reservoirs that are not currently recoverable using existing technologies [1, 2]. Thermal recovery processes such as steam flooding, steam-assisted gravity drainage (SAGD), and cyclic steam stimulation (CSS) are the main methods that have been implemented to recover highly viscous heavy oils [3-5]. Many drawbacks such as the cost of steam generation, greenhouse gas emissions, excessive water treatment, and heat loss are associated with the current thermal recovery processes [6]. Co-injection of steam and solvents such as light hydrocarbons and non-condensable gases have been introduced to reduce the cost of steam generation and improve the efficiency of SAGD through solvent-aided processes [7, 8]. In these processes, both thermal and dilution effects are utilized to mobilize viscous oils. A significant volume of steam is injected into oil reservoirs and condenses at reservoir conditions. However, the potential impact of the aqueous phase has not been explored in the previous works [9]. In addition, there are significant heavy oil resources that are not currently exploitable using existing recovery methods such as SAGD and CSS. Only a few studies have investigated factors apart from viscosity reduction that influences the performance of bitumen recovery processes [10, 11]. It is evident that reducing the viscosity of the oleic phase is key to the success of the oil recovery processes. However, the role of the aqueous phase on the alteration of the mobility ratio of the displacing and displaced phases needs to be studied. Generally, the mobility of a phase is defined as the ratio of its effective permeability to its viscosity ($\lambda = k_{eff} / \mu$). The mobility ratio is defined as the ratio of the mobility of the

displacing aqueous phase to the mobility of the displaced oleic phase ($M = \lambda_{displacing} / \lambda_{displaced}$) [12]. In the water flooding process, the low mobility ratio is favorable. To achieve a favorable mobility ratio, either oleic phase viscosity should be reduced, or the aqueous phase viscosity should be increased [12]. In SAGD and CSS, as well as solvent-aided processes, the mobility ratio is typically improved via reducing the viscosity of the oleic phase.

This work seeks to synergize the reduction in viscosity of bitumen due to hot water flooding and the improvement in displacing phase viscosity due to the generation of favorable water-in-oil (W/O) emulsion capable of suppressing viscous fingering. A typical steam-oil-ratio (SOR) of 3 for steam-assisted gravity drainage (SAGD) recovery process implies that three barrels of water should be converted into steam to produce one barrel of bitumen. By comparison of energy required for hot water flooding and steam flooding processes at 493 K (220 ℃) reservoir temperature, hot water flooding requires only ~900 kJ/kg sensible heat energy [13]. Steam flooding process such as SAGD and CSS, however, requires ~1860 kJ/kg extra latent heat energy to be added to the sensible heat [14]. This reduction in energy consumption reduces energy intensity and reduce a significant amount of greenhouse gases emission. Furthermore, SAGD and CSS processes work successfully in thick reservoirs only where the thickness of the pay zone is more than 15 m [15]. Thin reservoirs with less than 10 m in thickness cannot be accessible with the conventional techniques due to high heat loss to overburden and understrata [16]. This work may pave the way for the recovery process to access 80% of heavy oil resources that are found in thin reservoirs [1].

Previously, we have shown that the presence of urea in the aqueous phase leads to the formation of favorable water-in-oil (W/O) emulsions at the displacement front and synergizes with the oil viscosity reduction leading to a more favorable mobility ratio and hence more efficient displacement [17, 18]. It has been proven that urea solution reacts with naphthenic acids found in bitumen at high temperatures to generate in-situ surfactants capable of emulsifying the oleic phase and generates water-in-oil (W/O) emulsions at the displacement front that can suppress viscous fingers and channeling [17]. The agglomerations of W/O emulsions grow over time, leading to their entrapment and clogging of the high mobility flow channels. This claim has been approved via simulating a previous work [19]. This phenomenon forces the aqueous phase to sweep the upswept areas that enhance the volumetric sweep efficiency [17]. The urea molecule consists of two amino groups (NH_2) joined by a double bond carbonyl functional group (C=O), and it melts at 460 K (133 °C). These functional groups give the basic nature to urea when its molecules dissolve in water to generate the urea solution [20]. Urea starts to decompose at 425 K (152 °C) to ammonia and isocyanic acid (HCNO), which in turn decomposes gradually to ammonia and carbon dioxide (CO_2) at high temperature and pressure conditions such as those encountered in thermal recovery processes [10, 21-23]. Both ammonia and carbon dioxide have proven to be effective in the enhanced oil recovery techniques [24-27]. The injection of urea solution into the reservoir could open the door to finding innovative new methods to dispose of carbon dioxide in the ground in a stable manner. Both urea and the generated ammonia are highly soluble in water and produce a basic solution that reacts with naphthenic acids found in oil to generate in-situ surfactants [10, 28]. The generation of the in-situ surfactants in the reservoir reduces the acidity of the oil, making it more

preferable for refineries and generates W/O emulsion, which is favorable for improving the volumetric sweep efficiency. Furthermore, flooding the reservoir with chemical solutions (i.e., urea solution, ionic solutions, CO_2) alters the wettability of the reservoir rock toward more water-wet due to the adsorption of polar charges found in these solutions to the actual charges on the rock surface [19, 29-32].

This work aims to study the impact of the generation of W/O emulsions on heavy oil recovery during the urea solution flooding of cold viscous oils. The generation of W/O emulsions can reduce the cost of oil production since it needs only the sensible heat, which is much lower than the energy required in steam-based processes that include both sensible and latent heats. With sensible heat only, the urea solution keeps the viscosity of W/O emulsion reasonably low such that it can be easily produced during the hot water flooding process due to the generation of W/O emulsions. Several sand pack urea solution flooding experiments, as a proof-of-concept, were conducted to displace cold viscous oil and study the effect of injection rate, injection temperature, and urea solution concentration on the recovery of highly viscous crude oil. In these experiments, homogeneous sand packs were prepared by packing Ottawa silica sand to mimic the actual reservoir. Certainly, these homogeneous sand packs do not completely represent the actual reservoir where the heterogeneous nature of rock properties prevails. Furthermore, well constraints in the actual field differ from lab-scale sand pack flooding experiments. However, the flooding experiments in a sand pack allow a better understanding of the oil recovery mechanisms.

6.3 Materials

The oleic phase used in sand pack flooding experiments is the Athabasca bitumen. The molecular weight, specific gravity, and °API gravity of this bitumen are 513 g/mol, 1.004,

and 9.44, respectively, and the oil viscosity at 423 K (150 °C) and 3.45 MPa is 29 cP. The freezing point depression technique was used to determine the molecular weight of the bitumen. The simulated distillation test (ASTM 7169) and the carbon number distribution, as well as the detailed thermophysical properties of this bitumen, have been reported elsewhere [33, 34]. The aqueous phases used in the flooding experiments were prepared by dissolving high purity crystals of urea provided by VWR Chemicals in deionized water. The porous media were prepared by packing a core holder with Ottawa silica sand (70 mesh size).

6.4 Experimental work

6.4.1 Sand pack flooding experimental procedure

1-D sand pack flooding experimental setup shown in Figure 6.1 was built to perform the flooding experiments. This setup consists of a horizontal stainless steel core holder packed with silica sands. The sand pack is pressurized axially to 6.9 MPa using a hydraulic hand pump to imitate the overburden pressure. The sand pack is flooded with CO_2 at 280 kPa inlet pressure for 20 min to remove the air from the porous media; then, it is vacuumed for one hour to ensure there is no air bubbles trapped in the sand pack during the saturation with water. The sand pack is fully saturated with water. Pore volume and porosity of the sand pack are calculated based on the volume of water imbibed into the sand pack. The barometric technique is used to measure the low-pressure drop along the sand pack at different flow rates ranging from 1 to 17 cm^3/min, and Darcy's law was applied to calculate the absolute permeability of the sand pack. Then, both the sand pack and the heavy oil accumulator are brought to 363 K (90 °C) using a VWR oven to mobilize the viscous heavy

oil and saturate the sand pack easily. The drainage process is started with an injection rate of 5 cm^3/min of oil until no further water is produced.

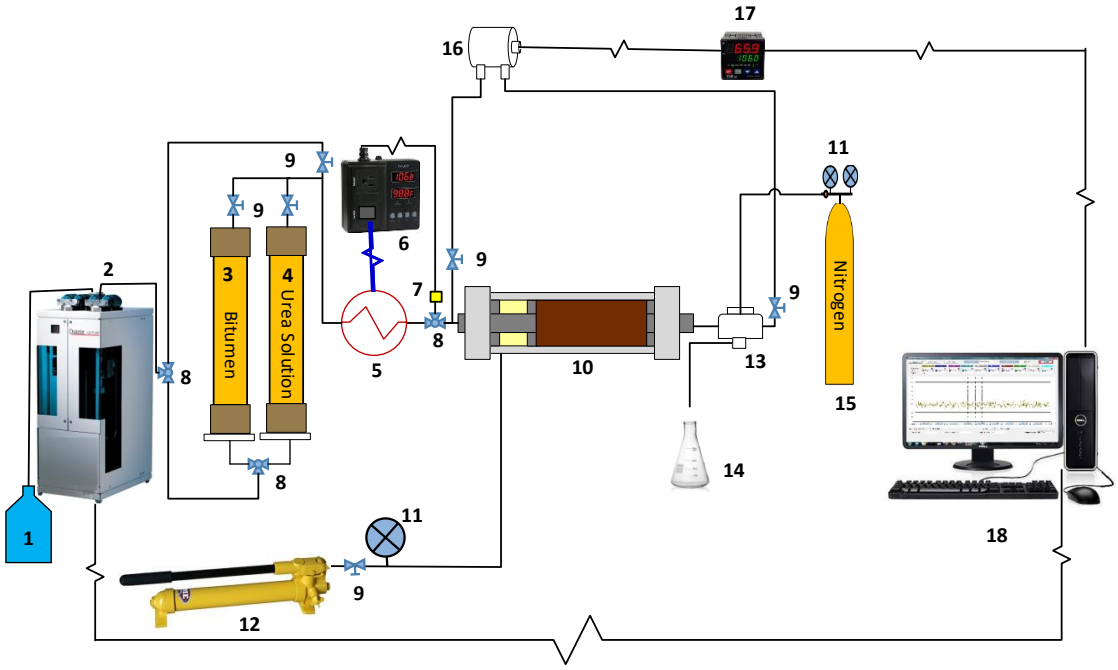

Figure 6.1. The schematic diagram shows the 1-D sand pack flooding experimental setup used for the flooding experiments. 1) distilled water, 2) QUIZIX pump, 3) heavy oil accumulator, 4) urea solution accumulator, 5) heat exchanger, 6) heat controller, 7) thermocouple, 8) three-way valve, 9) two-way valve, 10) axial sand pack core holder, 11) pressure gauge, 12) hand pump, 13) back pressure regulator, 14) graduated flask, 15) nitrogen cylinder, 16) pressure transducer, 17) SOLO data acquisition, 18) computer.

The hot sand pack is disconnected from the setup and opened from the top to drill a a connection hole with 0.8 cm in diameter through the center of the sand pack. Then, the sand pack is brought to room temperature (21 °C) overnight. The connection hole is then filled with clean silica sands and saturated with water. The connection hole allows connecting the injection and production ports during the flooding process to overcome the

immobility issue of viscous bitumen at room temperature. Figure 6.2 shows the sand pack after saturation with bitumen and creating a communication path between injection and production ports. Finally, the sand pack is flooded with urea solutions in different scenarios to study the effect of injection rate, injection temperature, and concentration of urea solution on oil recovery. In all experiments, the urea solution is injected indirectly into the sand pack via an external stainless-steel accumulator to protect the QUIZIX pump from corrosion. The pressure drop through the oil recovery stage is measured using a pressure transducer from Sensotec Company and recorded simultaneously every three seconds using SOLO 9696 data acquisition. A QUIZIX pump (QX6000) with accuracy ±0.001 cm^3/min is utilized to inject the fluids (water, bitumen, and urea solution) during the saturation and oil recovery stages. Urea solution is heated to the desired temperature using a heat exchanger before injecting it into the cold sand pack. It is worth noting that the sand pack is left uninsulated to imitate heat loss to the overburden and underburden strata. The pore pressure during the flooding process is kept higher than 3.44 MPa using a back-pressure regulator from Equilibar Company to avoid the generation of steam during the flooding experiments.

The flooding with urea solution is continued until a negligible oil rate is reached. In most of the flooding experiments, the pressure drops resulted from generating water-in-oil (W/O) emulsion in the sand pack tend to exceed the maximum limit of the pressure transducer. In order to protect the pressure transducer, the QUIZIX pump is paused several times during the urea solution flooding process. The produced emulsion is collected discretely in small samples ranging from 100 to 300 cm^3 based on the abundance of oil in the produced emulsion to obtain the recovery data as a function of time. The produced

bitumen volume is then used to calculate the cumulative oil recovery as a function of the pore volume injected of the urea solution.

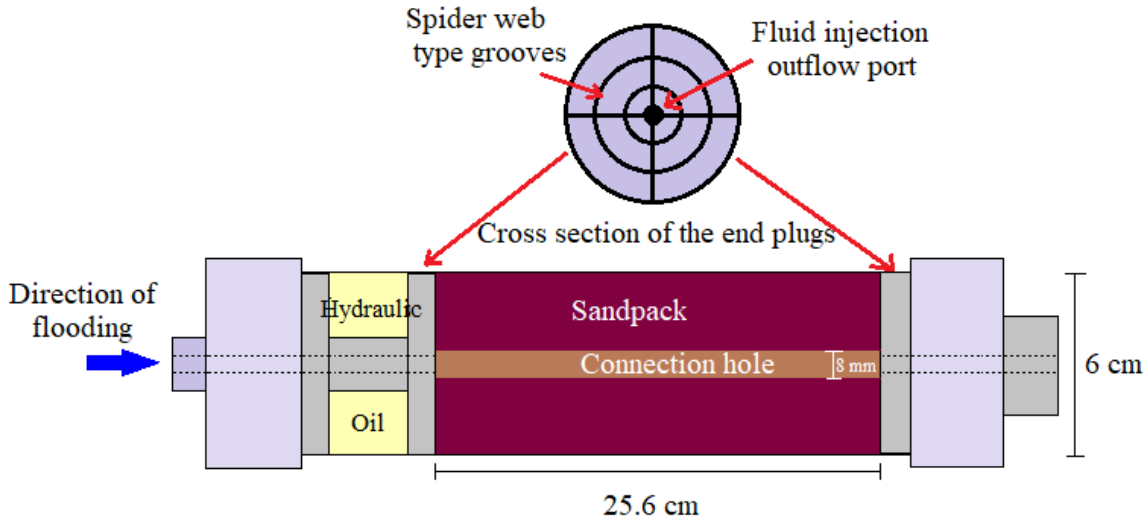

Figure 6.2. Schematic of the sand pack after saturation with bitumen and creating a communication hole between injection and production ports.

6.5 Results and discussion

Eight sand pack flooding experiments were conducted to investigate the effect of the injection rate, injection temperature, and urea solution concentration on oil recovery efficiency. Another flooding experiment was also conducted with fresh water and used as the baseline for comparison with the urea solution scenarios. The properties of the sand packs and the operating conditions of the experiments are shown in Table 6.1. In all flooding experiments, the displacing fluid (urea solution or freshwater) was injected at high temperatures into a sand pack maintained room temperature 294 K (21°C), and the effect of injection rate, injection temperature, and urea solution concentration were studied.

6.5.1 Effect of injection rate

In the first scenario (#1), the sand pack flooding was started with the injection of fresh water at an initial oil saturation of 0.895. The sand pack was flooded with nine pore volumes (PV) of hot liquid water at 493 K (220 ℃) at a flow rate of 8 cm^3/min. The injection of hot water was continued until a water cut of 98% was reached. The flooding results showed that oil production was started after the injection of two PV of hot freshwater. The oil recovery factor is gradually increased until recovery of 27% of the original oil-in-place (OOIP) was reached at nine PV injections, as shown in Figure 6.3. The low oil recovery is attributed to the lack of generation of W/O emulsion, which is evident from the low-pressure drop during the flooding experiment, as shown in Figure 6.3. The high fluctuation in the pressure drop curve is due to the high difference in viscosity of aqueous and oleic phases that generate ganglia of bitumen with diameters bigger than pore throat diameter leading to an instantaneous increment in pressure behind the front of the flow[35].

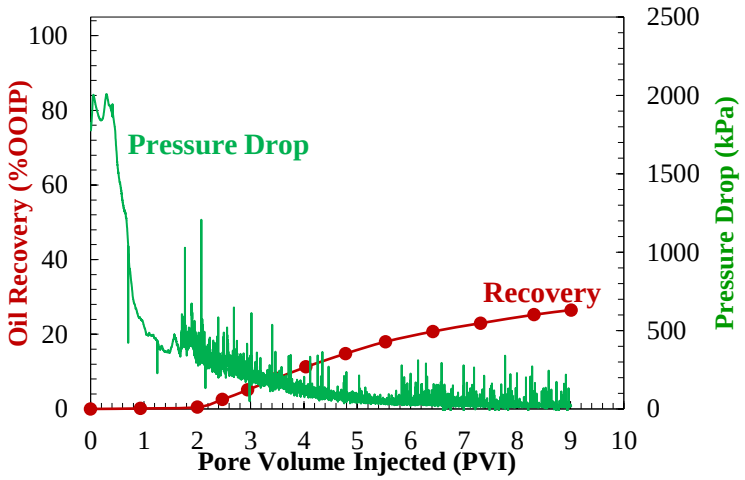

Figure 6.3. Oil recovery (-●-) and pressure drop (—) for hot water flooding at an injection rate of 8 cm^3/min at 493 K (220 ℃).

In the second experiment (#2), the sand pack with an initial oil saturation of 0.866 was flooded with 5.2 PV of 5 wt % hot liquid urea solution at 493 K (220 ℃) and an injection rate of 4 cm^3/min. The flooding process was continued until a water cut of 98% was achieved, and 43% of the original-oil-in-place was recovered, as shown in Figure 6.4. Similar to the hot water flooding scenario, oil production commenced after 1.8 PV of the injection process. However, injection of 5 wt % urea solution led to the formation of water-in-oil (W/O) emulsion, as evident in a sharp increase in pressure drop after injection of 1.8 PV of urea solution leading to higher oil recovery compared to the hot water flooding. The reaction of urea solution with naphthenic acids and generation of W/O emulsion have been verified by Fourier-Transform Infrared Spectroscopy (FTIR) technique, total acid number (TAN) measurements, and W/O emulsion viscosity measurements [17].

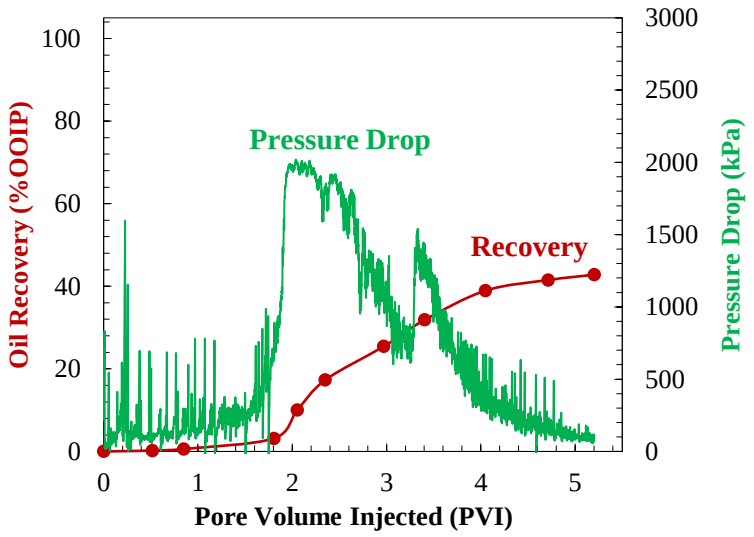

Figure 6.4. Oil recovery (–●–) and pressure drop (—) for 5 wt % hot urea solution flooding at an injection rate of 4 cm^3/min and 493 K (220 ℃).

In the next flooding experiment (#3), the sand pack at an initial oil saturation of 0.875 was flooded with 6.5 PV of 5 wt % hot urea solution at an injection rate of 8 cm^3/min, and 493 K (220 ℃). The flooding was continued until a water cut of 99% was reached, and 45% of the original oil place was recovered, as shown in Figure 6.5. The higher injection flow rate enhanced the formation of water-in-oil emulsion from the beginning of the flooding. The early formation of water-in-oil emulsion accelerated the production of oil considerably compared to the second experiment (injection rate of 4 cm^3/min).

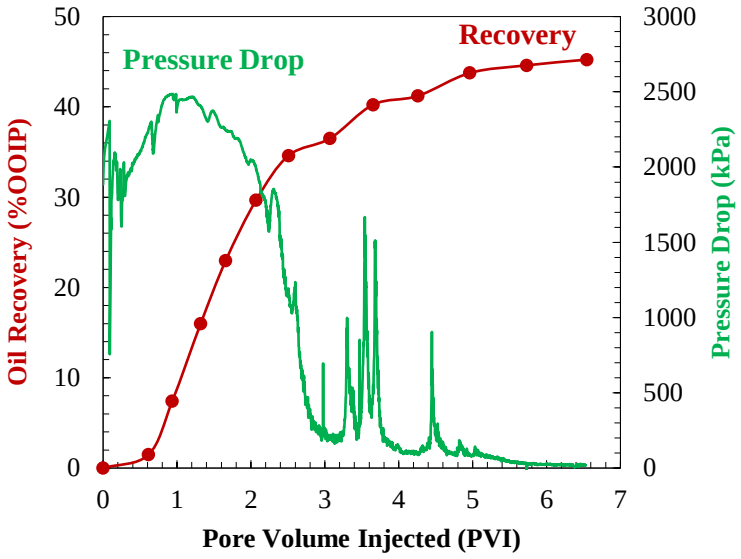

Figure 6.5. Oil recovery (—●—) and pressure drop (—) for the 5 wt% hot urea solution flooding at an injection rate of 8 cm^3/min and 493 K (220 ℃).

To further explore the role of injection flow rate, another flooding experiment (#4) was conducted by injecting a 5 wt % hot urea solution at a high injection rate of 12 cm^3/min and 493 K (220 ℃). The flooding process was continued for nearly nine pore volumes of the urea solution injection until a water cut of 97% was reached, and 37.4% of the original oil place was recovered. The results shown in Figure 6.6 reveal that while the water-in-oil emulsion was formed, it does not lead to faster oil recovery. This observation is due to the

fact that the retention time of the generated emulsion is not enough to allow aggregation of W/O emulsions agglomerates and subsequent clogging of the high mobility flow channels.

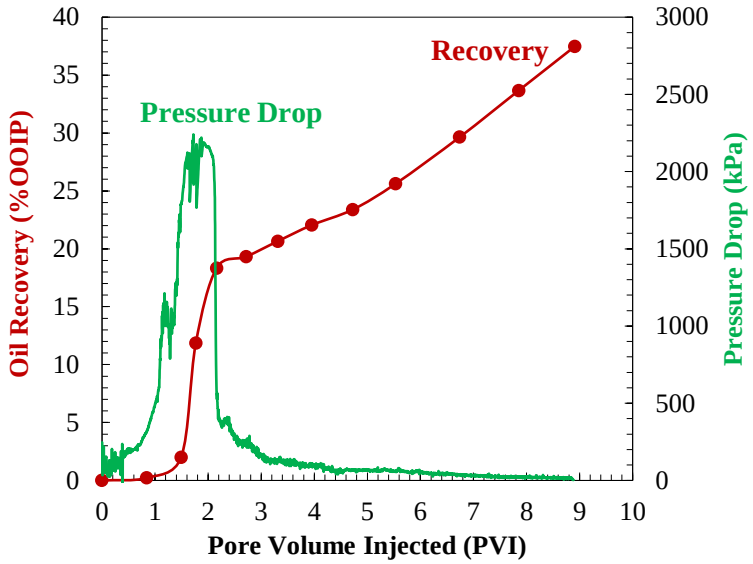

Figure 6.6. Oil recovery (–●–) and pressure drop (—) for the 5 wt% hot urea solution flooding at an injection rate of 12 cm^3/min and 493 K (220 ℃).

Figure 6.7 shows the effect of injection rate on recovery performance of 5 wt% urea solution flooding at 493 K (220 ℃). As shown, 8 cm^3/min is the optimum injection rate. The optimum observed is due to the balance between the heat transfer and the retention time of the generated water-in-oil emulsion in the sand pack. A higher injection rate (e.g., 12 cm^3/min) leads to a higher heat delivery. Simultaneously, it decreases the retention time of the generated water-in-oil emulsion, significantly leading to poor sweep efficiency.

On the other hand, the retention time is high at the low injection rate (4 cm^3/min), while the amount of heat delivered is low. It was observed that the effect of retention time of the in-situ generated emulsion is dominant in the acceleration of the oil recovery. At an intermediate injection rate, there is a balance leading to optimum oil recovery.

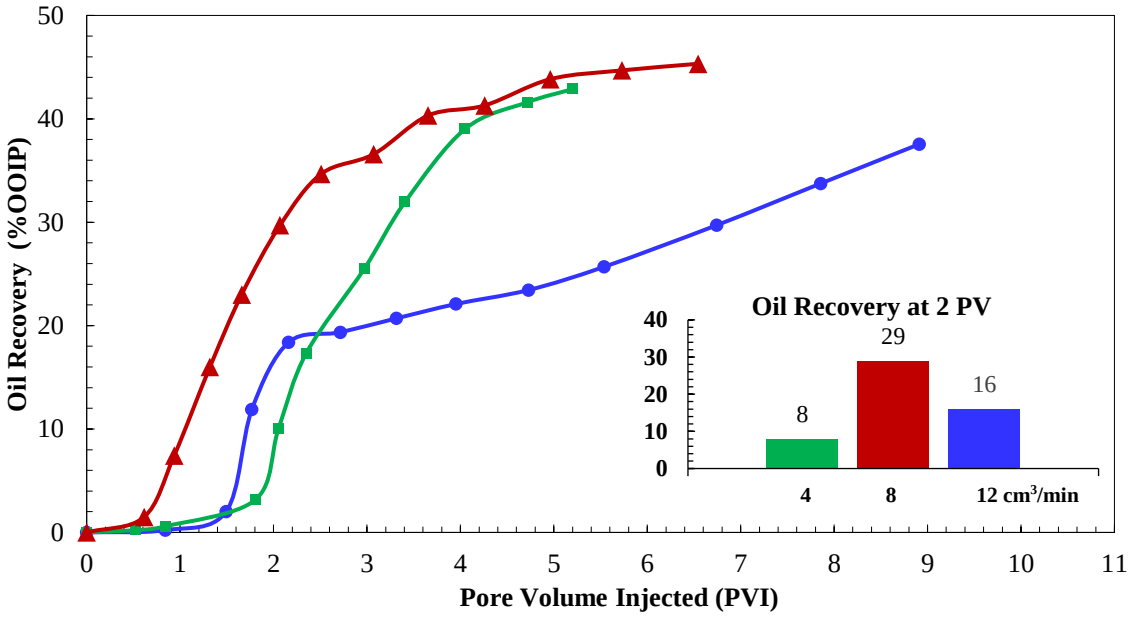

Figure 6.7. Oil recovery at different injection rates. (▬) 4 cm^3/min, (▲) 8 cm^3/min, and (●) 12 cm^3/min for 5 wt% urea solution injection at 493 K (220 °C).

6.5.2 Effect of injection temperature

In order to investigate the effect of temperature of the injected fluid on oil recovery, three additional experiments were conducted, and the results were compared with the third experiment (#3). A flooding experiment (#5) was conducted by injecting 5 wt% liquid urea solution at 513 K (240 °C) at an injection rate of 8 cm^3/min. The flooding was continued for seven pore volumes until a water cut of 98% is reached, and 49% of the original-oil-in-place was recovered. Similar to the third experiment, the early formation of water-in-oil emulsion was observed. The formation of emulsion accelerated the oil production and resulted in a more efficient displacement of bitumen, as shown in Figure 6.8. Another flooding experiment (#6) was carried out by flooding the sand pack with 5 wt% urea solution at an injection temperature of 473 K (200 °C) and an injection rate of 8 cm^3/min. The sand pack was flooded with 6.4 PV of urea solution to recover 49% of original-oil-in-

place with 99% final water cut, as shown in Figure 6.9. The results show that the ultimate oil recovery obtained from this experiment is close to the oil recovery achieved in the third experiment conducted at the same injection rate and injection temperature of 493 K (220 °C). The significantly higher pressure drops observed in this experiment (#6) is attributed to the higher viscosity of emulsions at lower temperatures. The last experiment (#7) in this category was conducted to explore the effect of lower injection temperature 453 K (180 °C). In this experiment, the sand pack was flooded with 5.5 PV of 5 wt% urea solution at an injection rate of 8 cm^3/min to extract 67% of the original-oil-in-place by reaching 99% water cut. The oil recovery was delayed for 1.6 PVI before it increases significantly through the next pore volume of injection, as shown in Figure 6.10. In addition, the maximum pressure drop was significantly higher compared to the other experiments at higher injection temperatures.

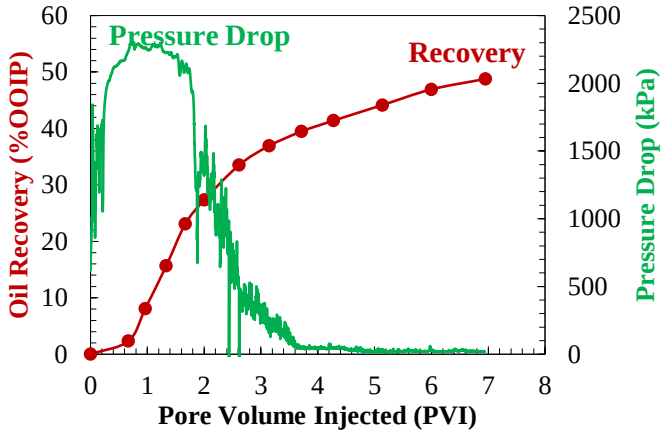

Figure 6.8. Oil recovery (—●—) and pressure drop (—) for the 5 wt% hot urea solution flooding at an injection rate of 8 cm^3/min and 513 K (240 °C).

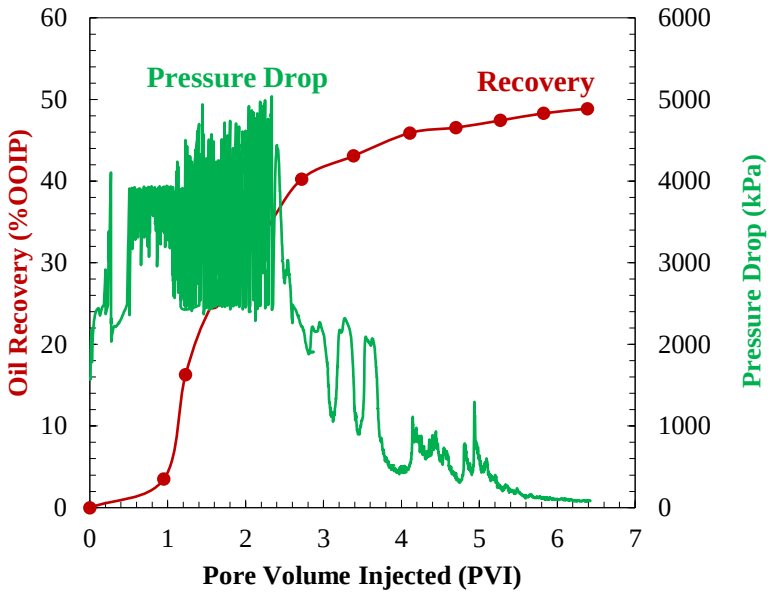

Figure 6.9. Oil recovery (—●—) and pressure drop (—) for the 5 wt% hot urea solution flooding at an injection rate of 8 cm^3/min and 473 K (200 ℃).

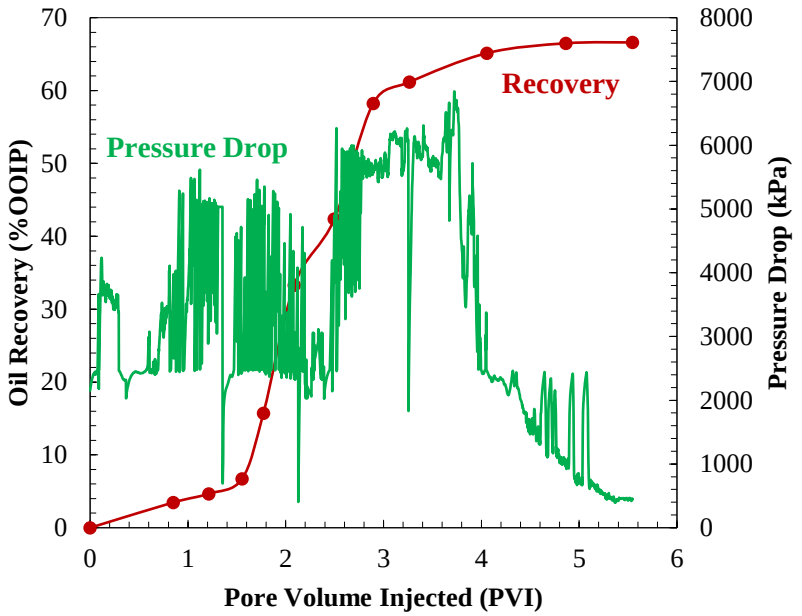

Figure 6.10. Oil recovery (—●—) and pressure drop (—) for the 5 wt% hot urea solution flooding at an injection rate of 8 cm^3/min and 453 K (180 ℃).

Figure 6.11 presents the effect of injection temperature on oil recovery performance of 5 wt% urea solution flooding at an injection rate of 8 cm^3/min. As shown, at higher temperatures 513 and 493 K (240 and 220 ℃), the oil recovery is accelerated initially, and the oil production starts to increase significantly at 0.6 PVI. However, for the lower temperatures 473 and 453 K (200 and 180 ℃), a delay in oil production is observed, and the oil recovery increased significantly at 1 and 1.6 PVI at 473 and 453 K (200 and 180 ℃), respectively. The delay in the oil recovery at low temperatures is attributed to less reduction in viscosity of oil resulted from lower delivery of heat compared to the high temperatures. On the other hand, flooding at low injection temperatures leads to higher ultimate oil recovery at higher pore volumes of injection. For instance, the injection of five pore volumes of urea solution at temperatures of 453 and 473 K (180 and 200 ℃) resulted in the recovery of 67 and 47% of the original-oil-in-place, respectively, compared to 44% oil recovery at 493 and 513 K (220 and 240 ℃). This additional oil recovery is attributed to the high viscosity of water-in-oil emulsion generated at lower temperatures, which suppresses viscous fingering more efficiently and forces the urea solution to sweep the unswept areas of the sand pack compared to higher temperatures. Besides, the high-pressure drop associated with flooding at lower temperatures confirms the high viscosity of the generated W/O emulsion [17]. This is evident in Figures 6.5, 6.8, 6.9, and 6.10, where the pressure drops are fluctuating at 2.3, 2.5, 4.0, and 6.0 MPa for 513, 493, 473, and 453 K (240, 220, 200, and 180 ℃), respectively. It is worth noting that lowering the injection temperature of the urea solution may not be the right choice to increase the oil recovery since a very high-pressure drop can be practically intolerable.

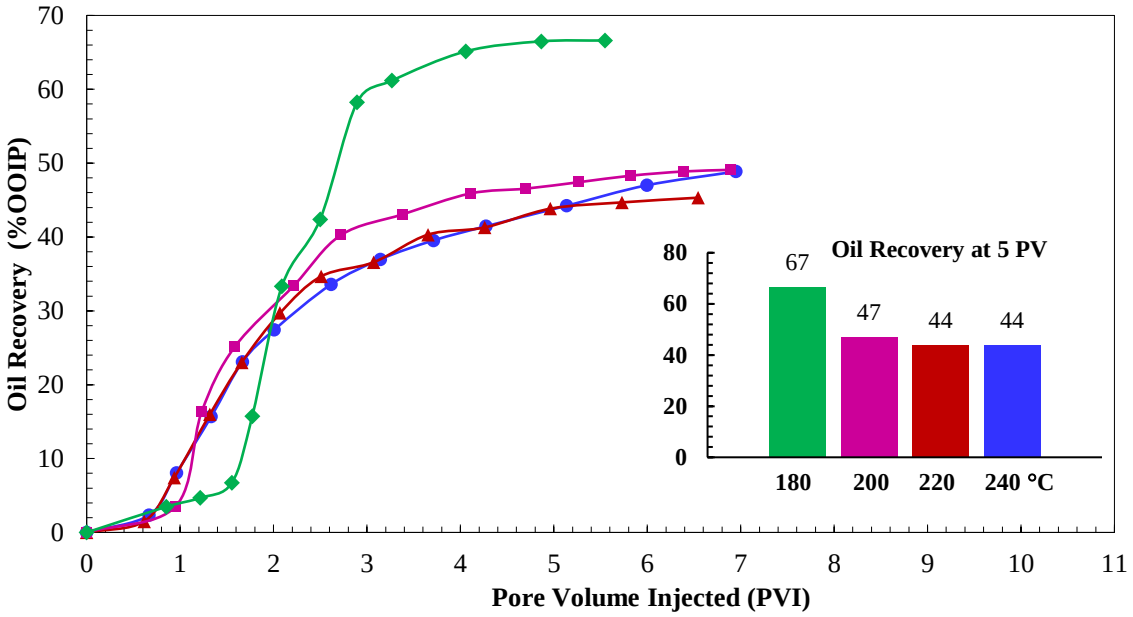

Figure 6.11. Oil recovery at different injection temperatures; (—◆—) 180 °C, (—■—) 200 °C, (—▲—) 220 °C, and (—●—) 240 °C for 5 wt% urea solution at 8 cm^3/min injection rate.

6.5.3 Effect of urea solution concentration

In the next two flooding experiments (#8 and #9), the effect of urea solution concentration on oil recovery efficiency was investigated. In the experiment (#8), the sand pack was flooded with a 10 wt% urea solution at 493 K (220 °C) and an injection rate of 8 cm^3/min. Five pore volumes of 10 wt% urea solution were injected until a water cut of 99% was reached, and 52% of the original-oil-in-place was recovered, as shown in Figure 6.12a. The results show that more than 50% of the original-oil-in-place was recovered by the end of the first three pore volumes of injection. However, in the case of a 5 wt% urea solution, it is necessary to inject more than six pore volumes to achieve the maximum oil recovery of 45%, as shown in Figure 6.5. The significant acceleration in the recovery of the oil is due to the formation of water-in-oil emulsion leading to more efficient displacement. In the next (and last) experiment (#9), the sand pack was flooded with 5 PV of 15 wt % urea

solution at 493 K (220 °C) and an injection rate of 8 cm^3/min. The flooding process was continued until a water cut of 99% was reached, and 73% of the original-oil-in-place was recovered, as shown in Figure 6.12b. The results reveal a significant increase in oil recovery compared to the previous cases of 5 and 10 wt% urea solutions.

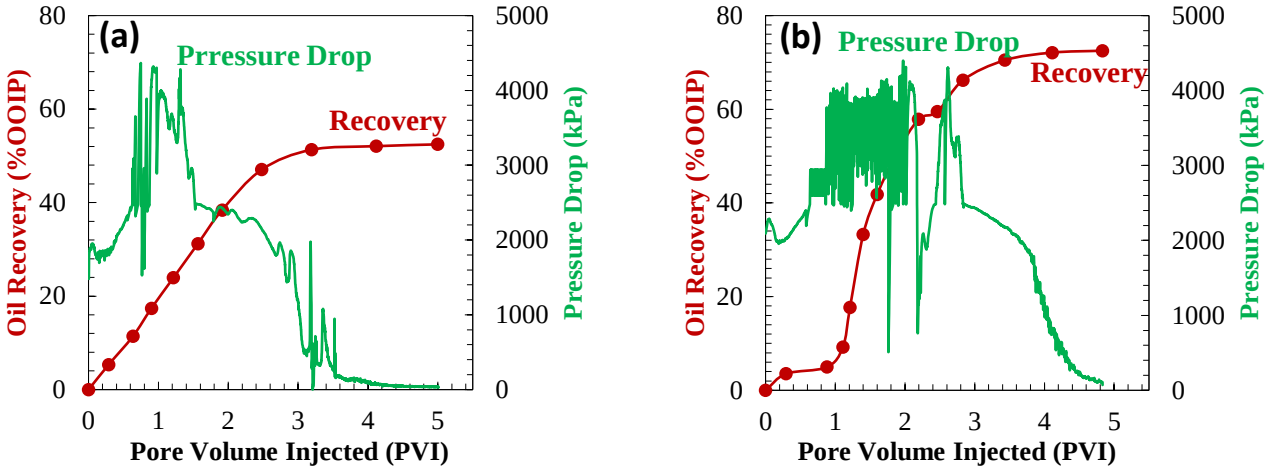

Figure 6.12. Oil recovery (—●—) and pressure drop (—) of a) 10 wt%, b) 15 wt% urea solutions injected at a flow rate of 8 cm^3/min and 493 K (220 °C).

Figure 6.13 shows the oil recovery factor for the three concentrations of urea solutions as well as the base case (hot water flooding experiment). It is seen that the water flooding experiment resulted in very low oil recovery due to the lack of the generation of water-in-oil emulsion responsible for the efficient displacement of the oil phase. Figure 6.13 reveals that the concentration of urea solution has a significant impact on the ultimate oil recovery as well as the acceleration of oil production. Unlike urea solutions, freshwater started recovering the oil gradually after injection of two pore volumes resulting in a final recovery of 27% OOIP after injection of nine pore volumes. As noted earlier, this poor efficiency is attributed to the incapability of freshwater to suppress viscous fingering despite the low

absolute permeability of this experiment (5.45 D). The lack of formation of W/O emulsion during the water flooding process allows freshwater to easily advance through the sand pack without displacing the oil, as indicated by the low-pressure drop shown in Figure 6.3.

On the other hand, urea solutions showed superiority in the efficiency of the oil recovery compared to freshwater, where the oil production commenced early during the first pore volume of injection of urea solution. As presented in Figure 6.12, 15 wt% urea solution recovered 54% of the original-oil-in-place at two PVI, whereas the lower concentrations (10 wt% and 5 wt%) recovered 40% and 29% original-oil-in-place, respectively. The results reveal that the presence of urea in the injected solution leads to the formation of W/O emulsion capable of suppressing viscous fingering despite the high absolute permeability (15.15 D) in case of flooding with 15 wt% urea solution, which is three times higher than absolute permeability of water flooding experiments (5.45 D) [17, 19].

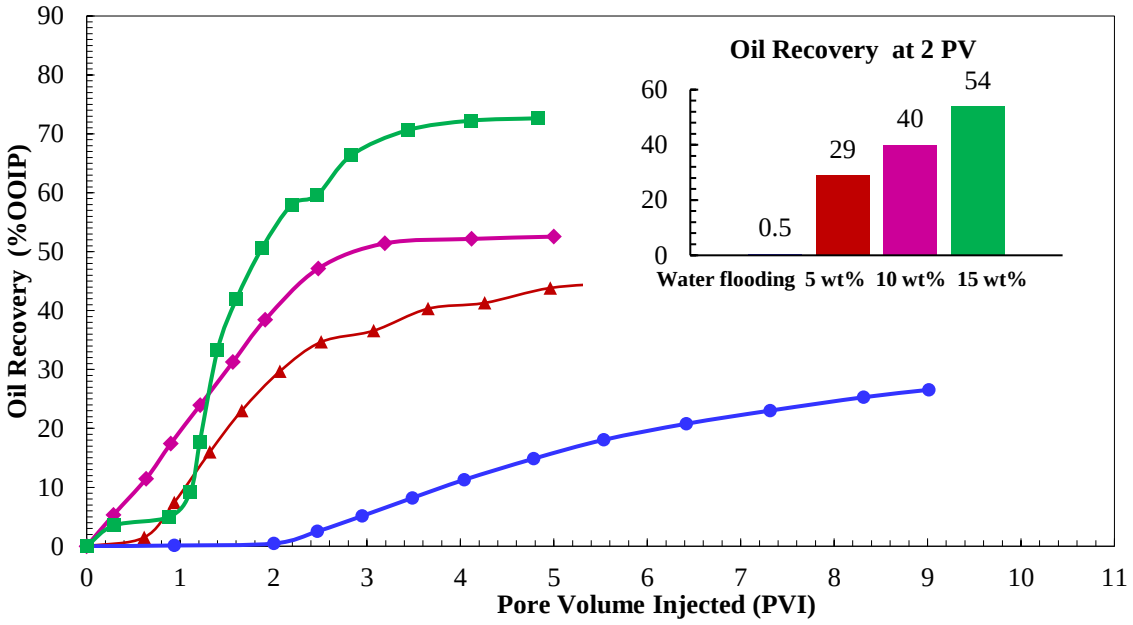

Figure 6.13. Oil recovery at different urea solution concentrations. (◆) water flooding, (▲) 5 wt% urea solution, (◆) 10 wt% urea solution, and (■) 15 wt% urea solution.

Table 6.1 The sand pack physical properties and experimental conditions of the conducted experiments.

Experiment #	Injected solution	Injection rate, cm^3/min	Temperature, °C	Sand pack length, cm	Pore volume, cm^3	Porosity, %	Absolute permeability, D	Initial oil saturation	Pore volume injected, PVI	Ultimate oil recovery, %OOIP
1	Water flooding	8	220	25.66	266.1	36.65	5.451	0.8951	9.00	26.50
2	5 wt % urea solution	4	220	26.05	269.2	36.56	10.315	0.8670	5.20	42.80
3	5 wt % urea solution	8	220	25.85	269.7	36.90	4.239	0.8755	6.54	45.23
4	5 wt % urea solution	12	220	25.95	268.5	36.60	10.266	0.8330	8.90	37.47
5	5 wt % urea solution	8	240	26.05	267.1	36.27	9.379	0.8860	6.90	48.77
6	5 wt % urea solution	8	200	26.14	268.5	36.89	4.040	0.8496	6.38	48.87
7	5 wt % urea solution	8	180	26.15	289.4	39.75	6.369	0.8955	5.54	66.60
8	10 wt % urea solution	8	220	25.65	279.5	38.54	12.748	0.9330	5.00	52.45
9	15 wt % urea solution	8	220	25.55	267.9	37.08	15.155	0.9200	4.80	72.50

6.6 Summary and Conclusion

Heavy oil recovery techniques such as steam-assisted gravity drainage (SAGD) and solvent-aided processes rely heavily on viscosity reduction. In these techniques, a significant volume of steam is injected into heavy oil reservoirs. The injected steam condenses and transfers its latent heat to the oil sands leading to the mobilization of viscous bitumen. Co-injection of solvent has also been practiced to reduce steam consumption and improve the recovery process. In this work, we conducted proof-of-concept experiments to demonstrate the viability of the utilization of urea solutions to improve oil displacement by

hot water flooding. In this process, the urea solution reacts with naphthenic acids found in oil to generate in-situ surfactants leading to the formation of water-in-oil emulsions. The formation of water-in-oil emulsion results in a more efficient displacement of oil and, thus, more efficient recovery. To further study this idea, we have conducted nine flooding experiments with urea solutions and freshwater to study the effect of injection rate, injection temperature, and urea solution concentration on the recovery of bitumen from cold sand packs. The following conclusion can be drawn from this study.

1. Injection of hot urea solution into heavy and viscous oil reservoirs improves the oil recovery efficiency significantly compared to freshwater due to its capability to generate water-in-oil emulsions responsible for suppressing viscous fingers and clogging high mobility flow channels.
2. The injection rate significantly affects the oil recovery efficiency. An optimum injection rate balances the heat delivery to the heavy oil and the retention time of the in-situ generated water-in-oil emulsions leading to higher oil recovery.
3. The higher injection temperature of the urea solutions accelerates oil production. However, it significantly decreases the ultimate oil recovery due to the reduction in retention time and lower viscosity of the water-in-oil emulsion associated with the flooding at high temperatures.
4. Urea solution concentration plays a significant role in the ultimate oil recovery, as well as the acceleration of oil production. More than 54% of the original oil place (OOIP) was produced after injecting two pore volumes of 15 wt% urea solution compared to 40% and 29% of the OOIP for 10 and 5 wt% urea solutions, respectively.

6.7 References

[1] Adams D. Experiences with waterflooding Lloydminster heavy-oil reservoirs. Journal of Petroleum Technology 1982;34(08):1,643-1,650.

[2] Takahashi A, Torigoe T. Oil sands reservoir characterization in Athabasca, Canada. *International Petroleum Technology Conference*. International Petroleum Technology Conference; 2008.

[3] Meldau R, Shipley R, Coats K. Cyclic gas/steam stimulation of heavy-oil wells. Journal of Petroleum Technology 1981;33(10):1,990-1,998.

[4] Butler R. Steam-assisted gravity drainage: concept, development, performance and future. Journal of Canadian Petroleum Technology 1994;33(02):44-50.

[5] Wu Z, Huiqing L, Wang X, Zhang Z. Emulsification and improved oil recovery with viscosity reducer during steam injection process for heavy oil. Journal of industrial and engineering chemistry 2018;61:348-355.

[6] You N, Yoon S, Lee C. Steam chamber evolution during SAGD and ES-SAGD in thin layer oil sand reservoirs using a 2-D scaled model. Journal of Industrial and Engineering Chemistry 2012;18(6):2051-2058.

[7] Zirrahi M, Hassanzadeh H, Abedi J, Moshfeghian M. Prediction of solubility of CH_4, C_2H_6, CO_2, N_2 and CO in bitumen. The Canadian Journal of Chemical Engineering 2014;92(3):563-572.

[8] Sabet N, Hassanzadeh H, Abedi J. Selection of efficient solvent in solvent-aided thermal recovery of bitumen. Chemical Engineering Science 2017;161:198-205.

[9] Sheng J. Enhanced oil recovery field case studies. Gulf Professional Publishing; 2013.

[10] Guo E, Jiang Y, Gao Y, Shen D, Zhigang C, Yu P. A New Approach to Improve Recovery Efficiency of SAGD. *SPE Middle East Oil & Gas Show and Conference.* Society of Petroleum Engineers; 2017.

[11] Erpeng G, Hongyuan W, Oilfield L, Youwei J, Yongrong G, Junhui S. Experimental study of urea-SAGD process. *SPE EOR Conference at Oil and Gas West Asia.* Society of Petroleum Engineers; 2018.

[12] Ahmed T. Principles of waterflooding. 2001.

[13] Water - Specific Heat. 2020. Engineering ToolBox; 2004.

[14] Water - heat of vaporization; 2010. Available from: https://www.engineeringtoolbox.com/water-properties-d_1573.html. [Accessed July 7, 2021].

[15] Zhao D, Wang J, Gates I. Optimized solvent-aided steam-flooding strategy for recovery of thin heavy oil reservoirs. Fuel 2013;112: 50-59.

[16] Gates I. Solvent-aided steam-assisted gravity drainage in thin oil sand reservoirs. Journal of Petroleum Science and Engineering 2010;74(3-4):138-146.

[17] BinDahbag M, Mohammadi M, Khalifi M, Aghajamali M, Zirrahi M, Hassanzadeh H. Efficiency of urea solutions in enhanced oil recovery. ACS Omega 2020;5(11):6122-6129.

[18] BinDahbag M, Zirrahi M, Hassanzadeh H. Solubility and liquid density of ammonia/Athabasca bitumen mixtures at temperatures up to 463 K: Measurements and modeling. Journal of Chemical & Engineering Data 2019;64(8):3592-3597.

[19] BinDahbag M, Al-Gawfi A, Hassanzadeh H. Suitability of hot urea solutions for wettability alteration of bitumen reservoirs–Simulation of laboratory flooding experiments. Fuel 2020;272:117713.

[20] Sheng J. Investigation of alkaline–crude oil reaction. Petroleum 2015;1(1):31-39.

[21] Wang J, Hu Y, Cai Y, Zhao C, Zhu L, Zhao C, et al. Influence of urea-SCR system parameters on NOx conversion rate and liquid film. Energy Sources, Part A: Recovery, Utilization, and Environmental Effects 2019:1-14.

[22] Schaber P, Colson J, Higgins S, Dietz E, Thielen D, Anspach B, et al. Study of the urea thermal decomposition (pyrolysis) reaction and importance to cyanuric acid production. American laboratory 1999;31(16):13-21.

[23] Gargurevich I. Aqueous urea decomposition reactor: reaction modeling and scale up. Journal of Chemical Engineering & Process Technology. 2016;7 (2): 1000289.

[24] Southwick J, Van den E, Van Rijn C, Van Batenburg D, Boersma D, Svec Y, et al. Ammonia as alkali for alkaline/surfactant/polymer floods. SPE Journal 2016;21(01):10-21.

[25] Le van S, Chon B. Effects of salinity and slug size in miscible CO_2 water-alternating-gas core flooding experiments. Journal of industrial and engineering chemistry 2017;52:99-107.

[26] Lee Y, Kim S, Wang J, Sung W. Relationship between oil production and CO_2 storage during low-salinity carbonate water injection in acid carbonate reservoirs. Journal of Industrial and Engineering Chemistry 2020, 88: 215-223.

[27] Zeng Y, Farajzadeh R, Biswal S, Hirasaki G. A 2-D simulation study on CO_2 soluble surfactant for foam enhanced oil recovery. Journal of Industrial and Engineering Chemistry 2019;72:133-143.

[28] Lu R, Xu X, Yang J, Gao J. Reduction of total acid number of crude oil and distillate. Energy Sources, Part A 2007;29(1):47-57.

[29] Ehrlich R, Hasiba H, Raimondi P. Alkaline waterflooding for wettability alteration-evaluating a potential field application. Journal of Petroleum Technology 1974;26(12):1,335-1,343.

[30] BinDahbag M, AlQuraishi A, Benzagouta M. Efficiency of ionic liquids for chemical enhanced oil recovery. Journal of Petroleum Exploration and Production Technology 2015;5(4):353-361.

[31] BinDahbag M, Al Quraishi A, Benzagouta M, Kinawy M, Al Nashef I, Al Mushaegeh E. Experimental study of use of ionic liquids in enhanced oil recovery. Journal of Chemical Engineering & Process Technology 2014;4(165): 1000165.

[32] Yekeen N, Padmanabhan E, Thenesh A, Sevoo L, Kamalarasan A, Kanesen L, et al. Wettability of rock/CO_2/brine systems: A critical review of influencing parameters and recent advances. Journal of Industrial and Engineering Chemistry 2020(88):1-22.

[33] Zirrahi M, Hassanzadeh H, Abedi J. Experimental and modeling studies of MacKay River bitumen and water. Journal of Petroleum Science and Engineering 2017;151:305-310.

[34] Azinfar B, Zirrahi M, Hassanzadeh H, Abedi J. Characterization of heavy crude oils and residues using combined gel permeation chromatography and simulated distillation. Fuel 2018;233:885-893.

[35] Avraam D, Payatakes A. Flow regimes and relative permeabilities during steady-state two-phase flow in porous media. Journal of Fluid Mechanics 1995;293:207-236.

CHAPTER 7: CONCLUSION AND RECOMMENDATIONS

7.1 Summery

In this study, the solubility of ammonia in Athabasca bitumen was measured at the vapor-liquid equilibrium condition. The liquid phase density of ammonia saturated-bitumen was also measured. Several 1-D sand pack flooding experiments were conducted on heated sand packs at 423 K (150 ℃) to investigate the bitumen recovery mechanism. Supporting experiments such as IFT measurements, emulsion viscosity measurements, TAN measurements, and FTIR measurements were implemented on recovered bitumen to prove the generation of in situ surfactants through the flooding process. A series of complementary 1-D sand pack flooding experiments of hot urea solutions injection into cold sand packs (at room temperature) were conducted to design and optimize the injection rate, injection temperature, and urea solution concentration. Furthermore, fine grid numerical simulations were conducted to model the 1-D sand pack flooding experiments to obtain relative permeability curves and confirm the improvement in wettability alteration through history matching the experimental oil recovery data.

7.2 Conclusion

The findings of this study can be summarized as follows:

- The solubility of ammonia in bitumen and the density of ammonia saturated-bitumen have been measured accurately and modeled by the Peng-Robinson equation of state (PR-EoS). The binary interaction coefficient between ammonia and bitumen was tuned to fit the experimental solubility data with an AARD of 8.537%. A linear temperature-dependent volume shift parameters of ammonia were tuned to fit the experimental density data of ammonia saturated-bitumen with an AARD of 0.218%. The generated

data finds application in reservoir simulation of the solvent-aided thermal recovery process.

- The flooding experiments of urea solutions in heated sand packs at 423 K (150 ℃) showed an acceleration in the oil recovery due to generating W/O emulsion highlighting the synergy between the reduction in viscosity of bitumen and suppression of the viscous fingering due to emulsifying the oil phase. The in-situ surfactants generated from reacting urea solutions with naphthenic acids form a high viscosity W/O emulsion, which creates a more stable displacement front weakening the viscous fingering effect.
- The high temperature decomposes urea into ammonia and CO_2. Meanwhile, the basic nature of the ammonia solution (ammonium hydroxide) is the main factor responsible for the interaction of ammonia with naphthenic acids found in the bitumen through generating the in situ surfactants.
- Interfacial tension measurements revealed a noticeable reduction in the IFT of the bitumen/aqueous phase in the presence of urea in the aqueous phase solution. In addition, total acid number (TAN) measurements verified a significant reduction in (TAN) of the treated bitumen. The basic nature of urea solutions helps to reduce the TAN of bitumen and improves the quality of bitumen for refineries.
- The analysis of the FTIR measurements showed the reaction of carboxylic acids found in bitumen with the aqueous ammonia solutions that led to the formation of amide functional group and, consequently, the formation of amide surfactants.
- The flooding with urea solutions improves the oil recovery efficiency significantly due to altering the rock wettability toward more water wet, which leads to detaching oil

efficiently from the rock surfaces. The alteration in the wettability of rock toward more water-wet is reflected in the oil relative permeability endpoints obtained from the numerical simulation results.

- Hot water flooding of viscous oils dramatically suffers from the viscous fingering phenomenon through the recovery of bitumen and heavy crude oils due to the considerable difference in the viscosity of oleic and aqueous phases. However, the addition of urea into the aqueous phase reduces the viscous fingering effect and delays the water breakthrough by stabilizing the displacement front with a stable W/O emulsion. The convex shape of the oil relative permeability curves obtained from the numerical simulation results demonstrates the channeling and viscous fingering phenomena.
- The hot urea solution flooding into cold sand pack (at room temperature) reveals that the high and low injection rates negatively affect oil recovery efficiency. Therefore, obtaining the optimum value of the injection rate is an essential point in oil recovery. The optimum injection rate balances the heat delivery to the cold oil sands and the retention time of the generated water-in-oil emulsion in the sand pack leading to higher oil recovery.
- The higher injection temperature of the urea solutions accelerates oil production at the beginning of flooding since more thermal energy transfers into the sand pack. However, it significantly decreases the ultimate oil recovery due to the reduction in the urea solution retention time and lower viscosity of the W/O emulsion associated with the flooding at high temperatures.

- Urea solution concentration plays a vital role in the ultimate oil recovery and the acceleration of the oil production process. The higher the concentration of urea solution, the higher the ultimate oil recovery by injecting fewer pore volumes of urea solution.

7.3 Recommendation for future work

Based on the work conducted and results obtained in this study, future research could continue to explore the following areas:

- Although the solubilities of urea in pure aliphatic (i.e., heptane) and aromatic (i.e., benzene) hydrocarbons are very low as reported in the literature, it is better to measure the solubility of urea in real crude oil so that an accurate fluid model valid for use in the simulation studies can be developed.
- The in situ surfactants generated should be investigated in more detail to better understand essential parameters such as the type and order of chemical reaction, reaction rate, activation energy, and the stoichiometric coefficients of reacting and produced components. These parameters are essential to include the chemical reaction responsible for generating surfactants in the simulation model.
- To better understand the mechanism of oil recovery by urea solution flooding, the decomposition kinetics of urea into ammonia and carbon dioxide at high temperature and high pressure conditions needs to be investigated. This investigation will shed light on the role of ammonia and carbon dioxide in oil recovery efficiency.
- The emulsification mechanism at the displacement front has not been fully understood yet. Therefore, conducting sand pack flooding experiments using a pre-

prepared emulsion with known oil concentration and known oil droplet size will help in determining the effect of O/W emulsion on diverting and restricting the water phase flow through the flooding process.

- Sand pack flooding experiments should be extended to a 3-D physical model, which will significantly help determine the optimum flooding and possible scaling to field conditions.
- The experimental and history matching results should be extended via optimization with numerical simulation to find application in designing a new in situ recovery process for bitumen recovery from oil sands.